Laboratory Simulation and Evaluation of Aerosol Particles Penetration, Deposition and Removal Processes in Sheltering Houses Equipped with Ventilation Systems

Wenlu Wang

京都大学

KYOTO UNIVERSITY

Laboratory Simulation and Evaluation of Aerosol Particles Penetration, Deposition and Removal Processes in Sheltering Houses Equipped with Ventilation Systems

2020

Wenlu Wang

Advisor: Minoru Yoneda

Lab of Environmental Risk Analysis

Department of Environmental Engineering

Graduation School of Engineering

Abstract

Chapter 1. Introduction

This chapter introduces the background of the accident at the Fukushima Daiichi Nuclear Power Plant and its impacts on the surrounding air. In addition, the objectives and the structure of this research are also introduced.

Chapter 2. A Review of Research on Aerosol Particles Penetration from Outdoor to Indoor

In this chapter, the referred properties of aerosol particles of this thesis are introduced. Moreover, literatures concerning the research progress of aerosol penetration are reviewed.

Chapter 3. Simulation and Evaluation of Sheltering Efficiency of Houses Equipped with Ventilation Systems

Experiments in this chapter investigate various elements that may affect the penetration factor, categorize particles (especially for UFPs) by the penetration characteristics for universal household sliding windows, reveal the most effective sheltering configuration for houses in air pollution emergencies, and compare the differences between the completely ideal state (uncharged/neutralized) and the actual situation through the particle charging state. The results illustrate that a high air exchange rate corresponds to a high penetration factor, and the concentration difference between outdoor and indoor affects ventilation efficiency. For universal household sliding windows, frames made of plastic coupled with an air exchange rate less than or equal to $1.20\ \mathrm{h}^{-1}$ can prevent particle penetration more effectively in air pollution emergencies. As the external particles gradually disperse and the concentration decreases, a ventilation system with a large air exchange rate may effectively purify the indoor air. However,

UFPs of less than 69 nm are able to undergo penetrate in a large amount, especially when the air exchange rate is lower than 1.20 h^{-1}. Therefore, effective housing sheltering is still a challenge if the external source is primarily UFPs. The laboratory results of this work provide a reference for emergency evacuations and indoor air quality improvements when environmental air pollution accidents and extreme weather occur.

Chapter 4. Determination of the Optimal Penetration Factor for Evaluating the Invasion Process of Aerosols from a Confined Source Space to an Uncontaminated Area

Due to the outbreak and spread of COVID-19, SARS-CoV-2 has been proven to survive in aerosols for hours. To evaluate the invasion process of virus-containing aerosols from a confined source space to an uncontaminated area, based on the work in chapter 3 and a widely used concentration model, four numerical calculations of the penetration factor are proposed in this chapter. A theoretical time-correction P_{est} was applied to a size-dependent P_{avg} by proposing a correction coefficient r, and the error analysis of the real-time $P(t)$ and the derived P_d were also performed. The results indicated that P_{avg} supplied the most stable values for laboratory penetration simulations. However, the time-correction is of little significance under current experimental conditions. $P(t)$ and P_d are suitable for rough evaluation under certain conditions due to the inevitability of particles detaching and re-entering after capture. The proposed optimal P value and the error analysis could help provide insight into the penetration mechanism, and can also provide a rapid and accurate assessment method for preventing and controlling the spread of the epidemic.

Chapter 5. A Review of Indoor Particles: Behavior and Ventilation Technology

In this chapter, the behaviors of indoor particles, including deposition and coagulation, and the research progress of that under ventilation is reviewed.

Chapter 6. Assessment of Air Purification Effect in Sheltering Houses Equipped with Ventilation Systems after Air Pollution Incidents

A key issue in the later stage of an environmental emergency is indoor air purification. This chapter investigates a reasonable ventilation strategy for indoor air purification in the later stage of an air pollution accident. Using a closed test chamber to simulate a sheltering house with a ventilation system, the deposition rates of aerosol particles were measured under both ideal and non-ideal conditions. Additionally, the actual turbulence state can be inferred by querying the optimal K_e in the β-K_e diagram proposed by this work. The main removal mechanism for particles within the range of 53.3–371.8 nm at an air exchange rate less than 1.19 h^{-1} is deposition. A ventilation system based on a high-power exhaust pump causes a large turbulence, which results in the resuspension of particles outside the cumulative mode range with a 'sudden drop' in the deposition rate. In the later stage of an air pollution accident or in the case where outdoor particles do not contribute indoors, turning off other stirrers and fans and increasing the AER value of the ventilation system to more than 1.19 h^{-1} can achieve the desired air purification effect. This study provides a reference to improve the indoor air quality in the event of an air pollution accident. It also provides effective information for general household air purification. Additionally, it can support the construction of shelters in areas and countries prone to air pollution accidents or floating dust/hazy weather.

Chapter 7. Conclusions and Perspectives

The main findings and limitations of this study are summarized and emphasized.

Contents

Chapter 4. Determination of the Optimal Penetration Factor for Evaluating the Invasion Process of Aerosols from a Confined Source Space to an Uncontaminated Area

Chapter 5. A Review of Indoor Particles: Behavior and Ventilation Technology

Chapter 6. Assessment of Air Purification Effect in Sheltering Houses Equipped with Ventilation Systems after Air Pollution Incidents

Chapter 7. Conclusions and Perspectives

Appendix

Chapter 1. Introduction

1.1 Research background

On March 11, 2011 at 2:46 p.m., a Pacific earthquake of 9.0-magnitude occurred in the northeast region of Japan, with a focal depth of 24 km. Epicenter-initiated slips spread slowly along plate boundaries due to an inter-plate earthquake. When it reached the Japanese trench in the direction of the ground, the gap of the Japanese trench in some locations became larger, reaching tens of meters. This large displacement near the seabed is thought to have caused a huge tsunami. The earthquake motion and the caused tsunami result in enormous damage to the regions from Tohoku to Kanto of Japan (Fig. 1).

Fig.1 A Pacific earthquake of 9.0-magnitude occurred in the northeast region of Japan at 2:46 p.m. on March 11, 2011 [1]

One of the damages caused by the Great East Japan Earthquake was Fukushima Daiichi Nuclear Power Plant accident [2]. The Nuclear Power Plant comprised six separate boiling water reactors originally designed by General Electric (GE) and maintained by the Tokyo Electric Power Company (TEPCO)

(Fig. 2). Due to the tsunami caused by the earthquake, all power supplies at TEPCO's Fukushima Daiichi Nuclear Power Station were lost, the reactor pressure vessel was damaged at Unit 2, the buildings at Units 1 and 3 were severely damaged by the explosion of hydrogen generated in the reactor, and Unit 4 was not operating due to the periodic inspection. In addition, radioactive substances such as radioactive iodine, cesium, and strontium were released into the environment in large quantities because of the damage of Unit 3 [3].

Fig. 2 This Geo-Eye satellite image shows the nuclear reactors (labeled) at the Fukushima Daiichi plant after the earthquake and tsunami hit northeastern Japan [4].

After the accident occurred in Fukushima Daiichi nuclear power plant on March 2011, the radioactive cloud containing high concentrations of radioactive substances outflows, the state and Fukushima went into a big panic because of lack of intelligence, coupled with the continuous occurrence of unexpected

accidents. Evacuation to houses is recommended as an emergency measure against radiation. However, the amount of exposure during indoor evacuation has not yet been accurately ascertained. The main reason is that the reduction effect of indoor exposure caused by indoor evacuation is affected by various factors. At that time, the government adopted improper methods of refuge, resulting in the death of hundreds of patients and the elderly. Others have pointed out that children are vulnerable to radioactive iodine, there may be more thyroid cancer patients in the future. To provide accidents similar to nuclear power plants and factories that use toxic chemicals, emergency evacuation plan is the current urgent and important issues. When toxic gas is approaching, people are not sure how they should choose, mobile refuge in the car even in case of traffic jams or staying in the house waiting for the gas passing and dispersed. There is no exact data for supporting its decision, such as invasion rate of toxic substances in the outdoor air to indoor air or adsorption rate of toxic chemicals to the floor or walls inside houses. Also, there is no accurate analysis in nuclear power plant accident in Chernobyl. In order to ensure the safe operation of nuclear power plants in the future and process of various kinds of toxic substances on the chemical plant, these data are needed for safety evaluation. In addition, the results also can provide references to evasive action of residents in some countries against high concentration of $PM_{2.5}$ in the outdoor air. All these data and work mentioned above are highly desired.

1.2 Research objective

Based on the background of the accident at the Fukushima nuclear power plant, similar accidents have occurred frequently in various regions of the world. For example, chemical leakage or explosion during transportation and storage, or air pollution caused by extreme weather, such as floating dust or haze. Pollutant plumes containing aerosol particles enter houses through building cracks, fans or tubes during migration and diffusion. These particles are suspending in indoor air

or depositing on the ground, walls, and roofs, increasing exposure risks for residents sheltering in houses. It has reported that people spend more than 90% of their lives indoors, and the time would be much more during the epidemic.

The series of experiments and work in this thesis are conducted for environmental emergency related to air pollution. Firstly, the processes from outdoor particles penetration, deposition and removal were simulated by conducting experiments using a test chamber equipped with a ventilator. Hereafter, various factors that may affect the value of penetration factor were investigated; four numerical calculations of the penetration factor were proposed to evaluate the invasion process of aerosols from a confined source space to an uncontaminated area; and deposition rate under ideal and non-ideal conditions were discussed and querying method was further proposed for rough inferring turbulence status. Finally, the most effective sheltering configuration of houses in air pollution emergencies, the optimal penetration factor for evaluating the invasion process of virus-containing aerosols, and a reasonable ventilation strategy for indoor air purification in the later stage of an air pollution accident were given.

1.3 Research structure

There are 7 chapters in this study, the structure is shown in Fig. 3.

Chapter 1

Introduction

Chapter 2

A Review of Research on Aerosol Particles Penetration from Outdoor to Indoor

- ⊙ Properties of aerosol particles
- ⊙ Review on the research progress of penetration factor

Chapter 5

A Review of Research on Indoor Behavior and Removal Technology of Aerosol Particles

- ⊙ Indoor behavior of aerosol particles
- ⊙ Review on the research progress of deposition rate
- ⊙ Review on the research progress of indoor ventilation

Chapter 3

Simulation and Evaluation of Sheltering Efficiency of Houses Equipped with Ventilation Systems

- ⊙ Effect from different AERs
- ⊙ Effect from charging state
- ⊙ Effect from particle concentrations and size
- ⊙ Effect from household windows

Chapter 4

Determination of the Optimal Penetration Factor for Evaluating the Invasion Process of Virus-Containing Aerosols from a Confined Source Space to an Uncontaminated Area

- ⊙ Correction coefficient r value and its time limit
- ⊙ The estimated indoor concentration at an estimated P value
- ⊙ Selection of the optimal penetration factor

Chapter 6

Assessment of Air Purification Effect in Sheltering Houses Equipped with Ventilation Systems after Air Pollution

- ⊙ Determination of the application scope of AER
- ⊙ Size-resolved deposition rate under ideal conditions
- ⊙ Total concentration with time
- ⊙ Size-resolved deposition rate under non-ideal

Chapter 7

Conclusions and Perspectives

Fig. 3 Research Structure

5

References

[1] UM to Fukushima: Japan's triple disaster explained.
https://www.missoulacurrent.com/outdoors/2017/06/montana-japan-
tsunami-earthquake/?print=print

[2]気象庁:平成 23 年東北地方太平洋沖地震の概要, 第 133 号（オンライ
ン、2019. 1. 22）.
https://www.jma.go.jp/jma/kishou/books/gizyutu/133/ABSTJ.pdf

[3] 東京電力: 福島第一原子力発電所事故（オンライン、2019. 1.22）.
https://www.ene100.jp/fukushima

[4] Timeline of Events at Japan's Fukushima Nuclear Reactors.
https://www.livescience.com/13294-timeline-events-japan-fukushima-
nuclear-reactors.html

Chapter 2. A Review of Research on Aerosol Particles Penetration from Outdoor to Indoor

2.1 Properties of aerosol particles

2.1.1 Definition of aerosols

The term 'aerosol' was firstly used to describe an aero-solution, clouds of microscopic particles in air in 1920. Similar to the term 'hydrosol', a colloid system with water as the dispersed medium [1], primary aerosols contain particles introduced directly into the gas; secondary aerosols form through gas-to-particle conversion [2].

An aerosol is a two-phase system. It is generally defined as a collection of solid or liquid particles suspended in a gas. They are usually able to stabilize for at least a few seconds or even a year or more under certain circumstances. The particle size ranges from about 0.002 μm to greater than 100 μm. There are many types of airborne microscopic particles classified according to physical form and how they were generated: resuspended soil particles, smog generated by electricity generation, particles formed by photochemistry, salt particles formed by ocean spray, and atmospheric clouds of water droplets or ice particles. There are also various common phenomena, such as dust, smoke, mist, haze, fog, fume, cloud and smog. Aerosols not only affect visibility and climate, but also our health and life quality [2]. In this study, salt particles with particle size of less than 542 nm formed by spray was analyzed.

2.2.2 Particle size and concentrations

Particle size has a major influence on aerosol behavior. All properties of aerosol particles are strongly dependent on the particle size, and changes in particle size will affect the particles' behavior and even its mechanism of action. In addition, the general properties can also be estimated by integrating over the

size distribution [2]. Therefore, understanding how aerosol characteristics change with particle size is the basis for aerosol research.

There are some common measures of aerosol concentration. Where, the most common one for environmental health and effect is mass concentration, which is defined as the mass of particulate matter per unit volume, with the most common units as $\mu g/m^3$; Also, number concentration is another one commonly used in aerosol science, presenting for the number of particles per unit volume, and its unit is number/ cm^3 or number/ m^3. In this study, number concentration with the unit as number/ cm^3 was used due to the output unit of instrument for measurement.

2.2 Review on the research progress of aerosol penetration

The increasing pollution of the atmospheric environment and the frequent occurrence of extreme weather have caused much concern. Since outdoor particles entering houses would cause harm to the health of residents, scientists have done plenty of research on aerosols. It is generally believed that there are three mechanics for outdoor particles entering the indoor, (1) natural ventilation. Residents are used to opening windows or doors to let air flow into the room, so as to replace indoor air and improve the indoor environment. In this mode, the air flow is mainly affected by the natural wind speed; (2) infiltration. External pollutant particles enter the building pipes, exhaust fans or the cracks between doors, windows and walls then pollute the indoor environment; and (3) Forced ventilation. For those buildings equipped with forced ventilation systems, turning on the forced ventilator to allow the outdoor air to be purified to a certain degree through the filter device then enter the room can discharge the indoor polluted air. However, the filter device cannot completely remove all the pollutants in the outdoor air, resulting in the indoor environment is polluted. Research on indoor particles originating from outdoors began in the last century. Related research initially focused on penetration by natural ventilation and infiltration; since the

development of ventilation systems in recent years, penetration by mechanical ventilation has begun to receive attention (Fig.1). And Since natural ventilation is uncontrolled, this study mainly introduces infiltration and forced ventilation.

Research progress of aerosol penetration mechanics
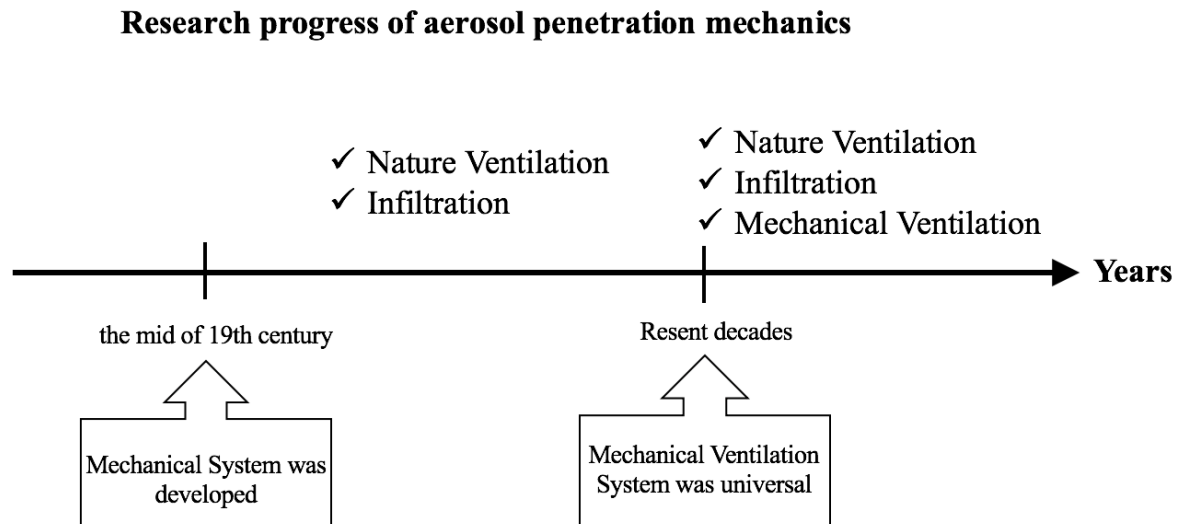
Fig. 1 Research progress of aerosol penetration mechanics

2.2.1 Aerosol penetration under infiltration

Infiltration is a mechanic of introducing outdoor air into a building, usually unintentionally through cracks in building envelopes and the use of doorways [3]. Due to accidental, the air entering the building is not purified, and it is unideal. Therefore, improving indoor air quality by reducing infiltration is one of the efficient methods. In addition, infiltration is caused by wind, the negative pressure of buildings and the effect of air buoyancy. Due to the uncontrollability of wind and air buoyancy, HAVC designers usually properly pressurize buildings to allow outdoor air to enter more than exfiltration for dramatical reduction of infiltration. Additionally, sealing the envelops in buildings is another way. Therefore, the research related to infiltration focused on the cracks in building envelopes.

Three main deposition mechanisms are existing in the penetration process through cracks: gravitational setting, Brownian diffusion, and inertial impaction. Based on the original theory, penetration through cracks has been investigated in

field [4-9], in chambers [10-13] and has been improved in theory [14-15]. Compared with laboratory simulation experiments, the conditions of the field experiment are very close to the actual situation, but the uncontrollability of the conditions will bring fluctuations to the data, resulting in deviations; While simulating in the laboratory chamber, the cracks in building envelopes typically are assumed at an ideal state, such as rectangular slots, smooth surface. And actually, the roughness of the building materials, such as brick, cement and wood, may hinder penetration of particles.

Liu and Nazaroff (2001) firstly presented modeling calculations, which provided important insight into the expected values of pollutant penetration and the factors that affect them [14]. They considered three types of common cracks in buildings, straight-through, L-shaped, and double-bend (Fig. 2). The penetration of ozone depends on the geometry of the crack, as well as its reactivity with the crack surface. Penetration is complete for reaction probabilities less than 10^{-5} and crack heights greater than 1 mm. Building envelope in reality can effectively remove pollutants, but the current leakage path of pollutants cannot be completely predicted.
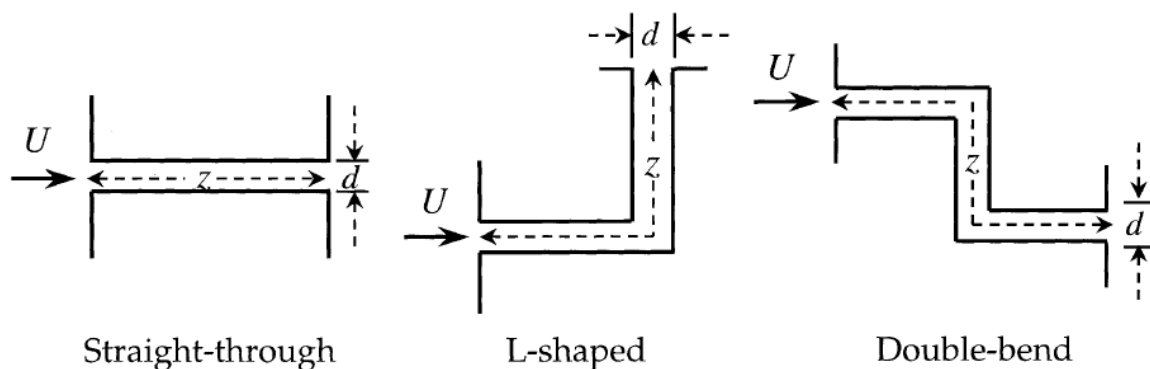

Fig. 2. Configuration of three types of idealized cracks through building envelopes

Hereafter, they presented the experimental results of the penetration of particles through cracks in building envelopes [11]. They prepared rectangular slits by using seven common building materials (aluminum, brick, concrete,

plywood, mahogany wood, pine wood and particle board), and extracted air from the slits by applying a certain pressure difference. The results showed that when the particle size is greater than 0.1 μm, the penetration factor of the rough surface is higher than that of the smooth surface; and the result is reversed for the particle size between 0.1 and 1 μm.

Lai et al. (2012) studied the penetration of fine particles with particle sizes of 20 to 500 nm in straight, smooth and rough cracks under four different pressures of 2 to 8 Pa [16]. The results show insensitivity to the roughness level. In addition, in the case of low-pressure difference, rough cracks are more conducive to the deposition of small particles than smooth cracks.

Chen et al. (2012) proposed a method for predicting the particle penetration factor of actual buildings [17]. Based on the American Society of Heating, Refrigeration, and Air-Conditioning Engineers (ASHRAE) Handbook, the method estimated the geometry of cracks in the building envelope, and also considering the impact of inertial collisions, while the effect of gravity leakage on vertical leakage is ignored. Through field test verification, particles with a diameter in the range of 0.5 to 6 μm corresponding to the penetration factor of 0.2 to 1, the experimental data of the penetration factor is in good agreement with the predicted data. In addition, air exchange rate is an important factor that affects particles passing through cracks in real buildings. For an actual building with a high air exchange rate (for example, 1 ACH), the inertial collision of coarse particles has a significant effect on the penetration factor, but the effect of the ratio of the horizontal crack area to the vertical crack area is negligible; additionally, the effective air leakage area coefficient can affect the penetration factor to a certain extent.
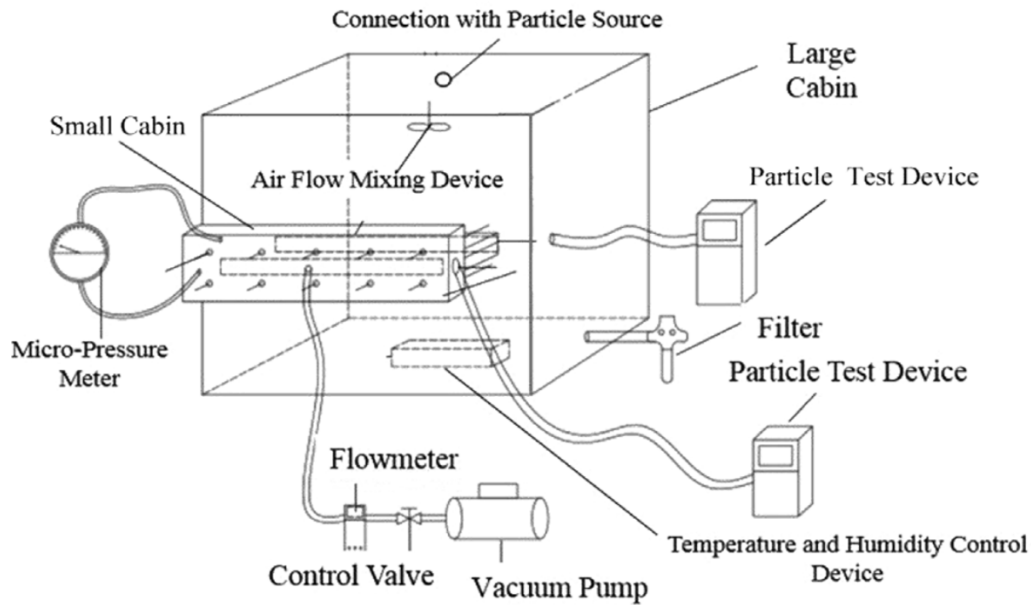
Fig. 3 Schematic diagram of experimental system

The most relevant work for the current study was Lv et al. (2018) which conducted an experimental platform to quantitatively analyze the main factors affecting the penetration coefficient and then proposed a semi-empirical formula (Fig.3) [13]. These factors contain crack sizes, pressure difference (ΔP), particle sizes (d_p), temperature (T) and relative humidity (RH). The results showed when the crack height (H) is 1 mm, the penetration coefficient of PM_1 and $PM_{2.5}$ does not change significantly with the pressure difference within a certain range, but when the crack height (H) is 0.25 mm, it has significant linear relationship. And a net displacement is existing under the action of gravity and Brownian diffusion. When the crack height (H) is approach to or less than the maximum of the value, the penetration coefficient is proportional to the crack height (H) but inversely proportional to the crack length; otherwise the change is insignificant. The penetration coefficient decreases as the particle size increases, while T and RH have no effect on the penetration process of particles in the crack. Additionally, considering the material roughness made the accuracy of the proposed model significantly improved.

2.2.2 Aerosol penetration under forced ventilation

Indoor ventilation is necessary for a resident to live a healthy and comfortable life in a house. In Japan, most areas have a subtropical humid climate- humidity in summer is easy to cause mold problems, while dust and viruses are easily floating in the dry air in winter. In response, Japanese law requires the introduction of systematic ventilation (24-hour ventilation) to ensure good indoor air quality and avoid sick building syndrome [18]. Fig. 4 presents the main components of a ventilation system. Inlet vent in Fig. 4(a), inside of which there is a filter, can purify the outdoor air then bring it into the indoor; outlet vent in Fig. 4(b) usually is installed in the ceiling, which can collect polluted indoor air; ventilator in Fig. 4(c) discharges those collected air outdoors; and the operation panel in Fig. 4(d) can be used for manual control.
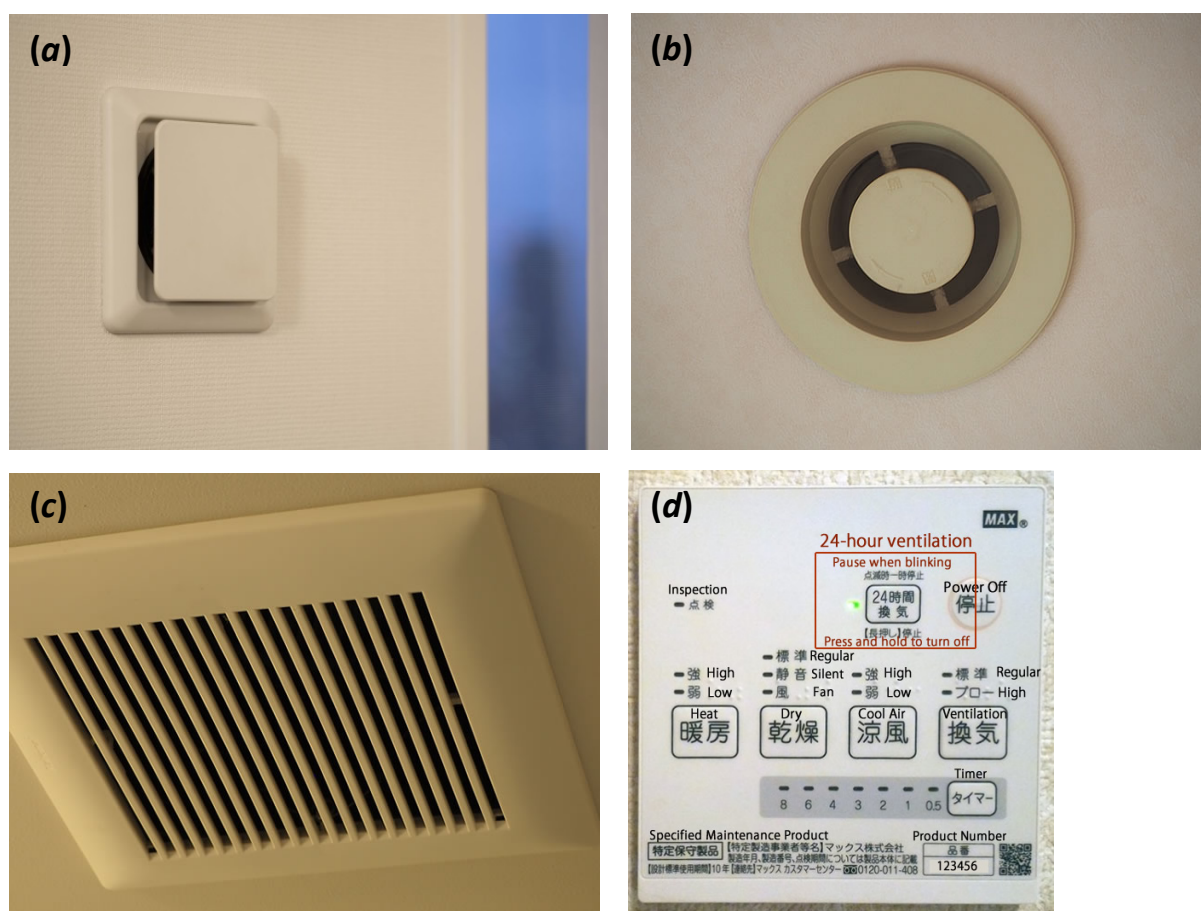
Fig. 4 The main components of the ventilation system. (a) Inlet vent, (b) outlet vent, (c) ventilator and (d) operation panel

Ventilation system collects dust efficiently and purifies indoor air to some extent (Fig. 5). However, pressure drop and concentration difference between indoor and outdoor caused by mechanical ventilation and severely polluted outdoor air may result in pollutant particles entering the indoor. Additionally, the filter in outlet vent of the ventilation system is not able to trap all types of particles, leading to increased indoor air pollution.
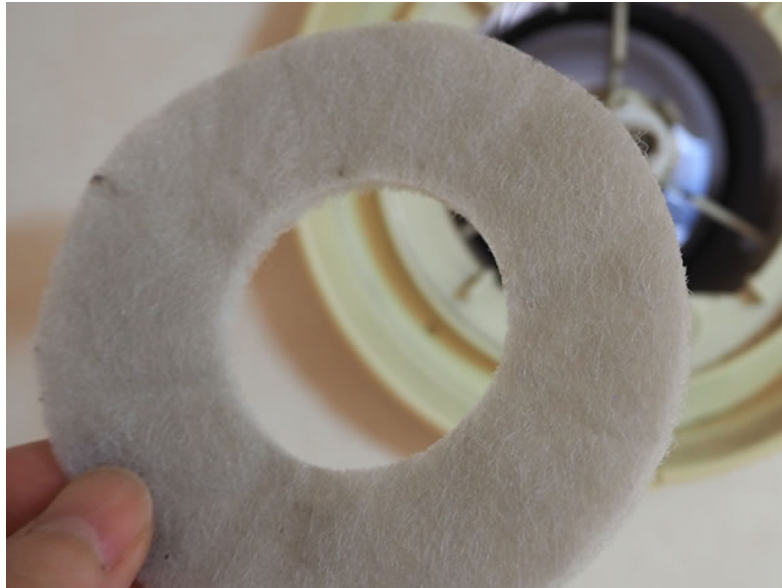
Fig. 5 A used filter

However, the research at present on mechanical ventilation concentrated in field test using real houses equipped with a real ventilation system, and such kind of research is mostly carried out in North America because of the universal use of house ventilation systems [19-21]. Therefore, the adverse effects caused by mechanical ventilation is only carried out in recent years but still relatively limited due to the limited use of ventilation systems available for experiments.

The research initially on mechanical ventilation usually use application models and empirical data to investigate indoor particles from outdoor sources, and ventilation rates can also be queried and classified from the literature based on building types [22-23].

Chen and Zhao (2011) published a review summarizing and analyzing three parameters that reflect the relationship between indoor and outdoor particles, I/O

ratio, infiltration factor and penetration factor [24]. Among them, the I/O ratio is affected by many factors, which has little significance for revealing the relationship between indoor and outdoor particles; the infiltration factor can eliminate the influence of indoor sources, but it cannot effectively reflect the particle penetration mechanism; and the penetration factor is the optimal parameter for revealing particle conditions between indoor and outdoor.

Chen et al. (2016) investigated indoor and outdoor particles in mechanically ventilated and air-conditioned buildings (ACMV) during and after the 2013 Haze in Singapore (Fig. 6) [25]. The results indicated that the haze can increase the concentration of indoor particles with a size of 0.3 -2.5 μm. Air conditioners and mechanical ventilation systems equipped with MERV 7 filters can effectively prevent outdoor particles from entering the building. But in extraordinary situations such as haze, it is still difficult to keep people from being exposed to high concentrations indoors.
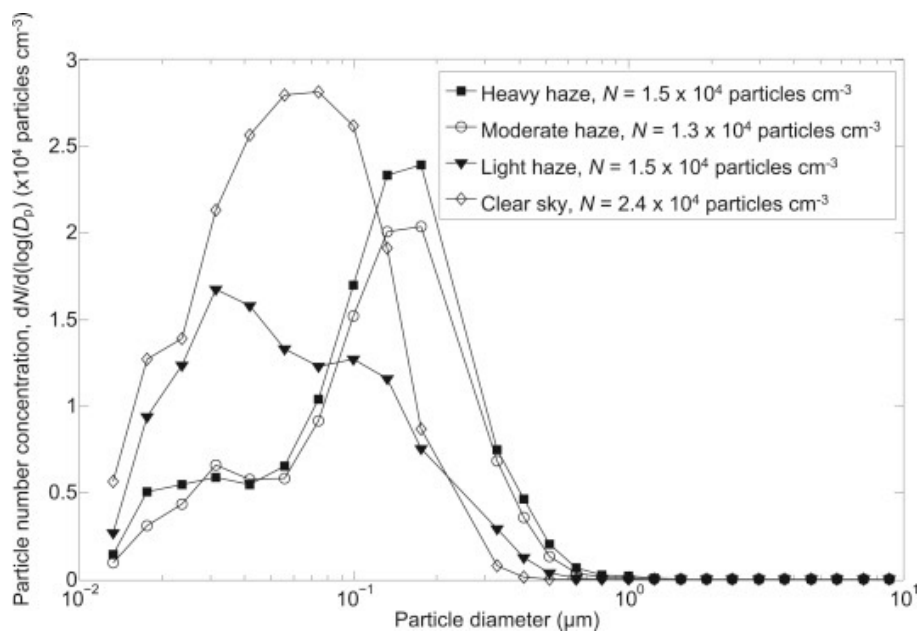
Fig. 6 Particle size distribution indoors using ACMV equipped with a MERV 7 filters. The particle size distribution ranged mainly from 0.3 to 1.0 μm with a certain degree of attenuation and hysteresis. The moderate correlation of particles in the range of 1.0-2.5 μm was observed while there was no correlation for particles larger than 2.5 μm

Miller et al. (2017) selected four buildings equipped with mechanical ventilations in two cities of the United States to measure ultrafine (0.055-0.1 m)

and fine (0.1-0.7 m) particulate matter (PM) in indoor and outdoor [26]. The results show that, in addition to urban PM differences and seasonal differences (summer is higher than autumn), night infiltration increases the indoor ultrafine PM concentration, while the exposure time in the nighttime increases on weekends when HVAC is not used. In addition, when the HVAC system is turned on, the correlation of ultra-fine PM is higher; and the AMS data indicates that there is a loss of particulate phase nitrate. Therefore, it is necessary to improve the filtration of mechanically ventilated buildings.

The latest research by Shi and Li (2020) proposed the mathematical relationship between the mechanical ventilation rate (MV-ratio) and the initial air infiltration rate (INF-ratio) [27]. In this regard, the minimum MV-ratio was calculated for buildings with multilayer windows to achieve a zero-infiltration rate, and they also analyzed the influential factors and laws. The conclusion is that the minimum ratio between the MV-ratio and the INF-ratio (reaching zero infiltration) depends on the window width-to-height ratio, the vertical spacing between the windows and the number of window layers (Fig. 7).
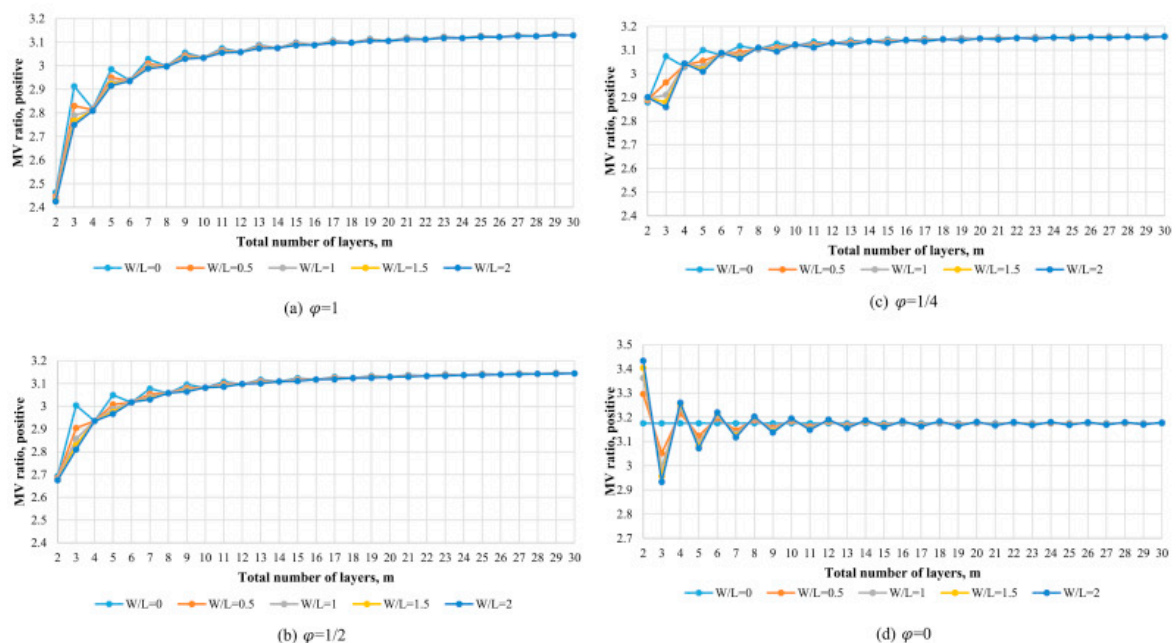
Fig. 7 The specific law curves - Influential factors of MV-ratio

References

[1] George, H., Aerosols. 1984.

[2] William, C. H., Aerosol technology: properties, behavior, and measurement of airborne particles. 1999.

[3] Fundamentals volume of the ASHRAE Handbook, Ch. 27, ASHRAE, Inc., 2005

[4] Thatcher, T.L. and Layton, D.W., 1995. Deposition, resuspension, and penetration of particles within a residence. Atmos. Environ., 29 (1995) 1487-1497.

[5] Abt, E., Suh, H.H., Catalano, P.J., Koutrakis, P., 2000. Relative contribution of outdoor and indoor particle sources to indoor concentration. Environ. Sci. Technol., 34 (2000) 3579-3587.

[6] Koponen, I.K., Asmi, A., Puhto, K., Kulmala, M. Indoor air measurement campaign in Helsinki, Finland 1999 e the effect of outdoor pollution on indoor air. Atmos. Environ., 35 (2001) 1465-1477.

[7] Zhu, Y.F., Hinds, W.C., Krudysz, M., Kuhn, T., Froines, J., Sioutas, C., Penetration of freeway ultrafine particles into indoor environments. J. Aerosol Sci., 36 (2005) 303-322.

[8] Guo, H., Morawska, L., He, C. and Gilbert, D. Impact of ventilation scenario on air exchange rates and on indoor particle number concentration in an airconditioned classroom. Atmos. Environ., 42 (2008) 757-768.

[9] Xu, B., Liu, S. and Zhu, Y. Ultrafine particle penetration through idealized vehicle cracks. J. Aerosol Sci., 41 (2010) 859-868.

[10] Mosley, R.B., Greenwell, D.J., Sparks, L.E., Guo, Z., Tucker, W.G., Fortmann, R., Whitfield, C. Penetration of ambient fine particles into the indoor environment. Aerosol Sci. Technol., 34 (2001) 127-136.

[11] Liu, D.-L., Nazaroff, W.W. Particle penetration through building cracks. Aerosol Sci. Technol., 37 (2003) 565-573.

[12] Jeng, C. J., Kindzierski, W. B., Smith, D.W. Particle penetration through rectangular shaped cracks. J. Environ. Eng. Sci., 5 (2006) S111-S119.

[13] Lv, Y., Wang, H., Wei, S., Wu, T., Liu, T., Chen, B. The experimental study on indoor and outdoor penetration coefficient of atmospheric fine particles. Build. Environ., 132 (2018), pp. 70-82.

[14] Liu, D.-L., Nazaroff, W. W. Modeling pollutant penetration across building envelopes. Atmos. Environ., 35 (2001) 4451–4462

[15] Tian, L., Zhang, G., Lin, Y., Yu, J., Zhou, J., Zhang, Q. Mathematical model of particle penetration through smooth/rough building envelop leakages. Build. Environ., 44 (2009) 1144–1149.

[16] Lai, A. C.K., Joanna, L.S., Fung, M. Li, Leung, K.Y. Penetration of fine particles through rough cracks. Atmos. Environ., 60 (2012) 436-443

[17] Chen, C., Zhao, B. Zhou, W., Jiang, X., Tan, Z. A methodology for predicting particle penetration factor through cracks of windows and doors for actual engineering application. Build. Environ., 47 (2012), 339-348.

[18] Living guide in Tokyo. RISE Corp. https://living.rise-corp.tokyo/house-ventilation-systems/

[19] Russell, M., Sherman, M. and Rudd, A. review of residential ventilation technologies. HVAC&R Research., 13 (2007) 325-348.

[20] Sherman, M. H. and Walker, I. S. Measured air distribution effectiveness for residential mechanical ventilation. HVAC&R Research, 15 (2009) 211-229.

[21] Sherman, M. H., Logue, J. M., and Singer, B. C. Infiltration effects on residential pollutant concentrations for continuous and intermittent mechanical ventilation approaches, Indoor Environ., 17 (2011) 159-173.

[22] Riley, W., McKone, T. E., Lai, A. C. K., Nazaroff., W. W. Indoor particulate matter of outdoor origin: importance of size-dependent removal mechanisms. Environ. Sci. Technol., 36 (2002) 2, 200-207

[23] Nazaroff, W. W. Indoor particle dynamics. indoor Air, 14 (2004) 175–183

[24] Chen, C. and Zhao, B. Review of relationship between indoor and outdoor particles: I/O ratio, infiltration factor and penetration factor. Atmos. Environ., 45 (2011) 275-288.

[25] Chen, A., Cao, Q., Zhou, J., Yang, B. Chang, W., Nazaroff, W.W. Indoor and outdoor particles in an air-conditioned building during and after the 2013 haze in Singapore. Build. Environ., 99 (2016) 73-81.

[26] Miller, S. L., Facciola, N. A. Toohey, D. and Zhai, J. Ultrafine and Fine Particulate Matter Inside and Outside of Mechanically Ventilated Buildings. Int. J. Environ. Res. Public Health, 14 (2017) 128.

[27] Shi, Y. and Li, X. Effect of mechanical ventilation on infiltration rate under stack effect in buildings with multilayer windows. Build. Environ., 170 (2020) 106594.

Chapter 3. Simulation and Evaluation of Sheltering Efficiency of Houses Equipped with Ventilation Systems

3.1 Introduction

Previous reports have demonstrated that diverse particles with aerodynamic diameters ranging from 20 to 3000 nm can intrude into a house [1-2]. Indoor particles originate from two sources. One is generated indoors such as cooking, smoking, house decoration, and human activities [3-9]. The other comes from the outdoor environment by penetrating cracks or slits in the structure [10-15]. As people spend a lot of time indoors [16-19], both indoor and outdoor particles influence the indoor exposure of the human body.

When an air pollution or extreme weather event occurs, a contaminant cloud or gas stream containing a high pollutant concentration is generated. This enters into indoor space through the cracks or gaps of an architectural structure and not only threatens the indoor air quality, but also adversely affects human health.

A person's home is typically the primary choice for sheltering. In this case, one of the most relevant parameters to determine the effectiveness of house sheltering is the penetration factor (P), which is used to characterize the fractional particles in the infiltrating airflow that penetrate the wall gaps in the building envelope. Many studies have referenced the P value, including those involving field tests [10,13,20-25], experimental model tests [26-30], and theoretical simulation analysis [31-34]. Previous studies tend to focus on the following areas: refinement of the effect of slits dimensions on particles penetration [1,35-38], determination of the outdoor-to-indoor relationship [21-24,39-40], and discussions on the effect of AER and P value under various house sealing conditions [1,38]. Mosley et al. (2001) [1] set up a chamber with two compartments using gypsum board walls and a ceiling. Three kinds of rectangular crack apparatuses were embedded in the middle wall for the determination. They

chose 3004 Emery oil, KCl, and incense to simulate the indoor entry of ambient fine particles through horizontal slits. However, they did not consider the particle charging state. Instead the effect was determined from the relevant characteristics of cracks (size, particle concentration, pressure difference, etc.). Real building components such as window frame materials were not considered but the effect from mixing fan speed was included.

Liu and Nazaroff (2003) also simulated the penetrating process. They focused on building envelopes (size and materials) and the effect of the pressure difference. Their chamber only had one compartment coupled with a rectangular crack apparatus. Consequently, the indoor particle concentration was not considered. In this case, the ventilation efficiency and degree of air purification were not identified.

In summary, most of the literature focuses on the penetration dynamics from an outdoor to an indoor environment. Setting the characteristics of the gaps or cracks remains a hot issue. However, few reports are concerned about the effects of the particle properties themselves such as an increased concentration and the charging state. Moreover, the introduction of forced ventilation systems into new residential houses, differences in household window frame materials, and the difference between laboratory evaluations and actual situations may affect the penetration factor results.

Air emergencies like explosions and chemical leakage, or extreme weather events such as sandstorms and haze, have a high probability of occurrence in certain countries and regions of the world. Such events would gravely impact human health, even if most people sheltered indoors at the time of the incident. In this regard, the corresponding research to simulate a common residential house and the surrounding environment using a test chamber and assessing the effectiveness of housing sheltering is highly desirable.

This study investigates various elements that may affect the P value, categorizes particles (especially for UFPs) by the penetration characteristics for

universal household sliding windows, reveals the most effective sheltering configuration for houses in air pollution emergencies, and compares the differences between the completely ideal state (uncharged/neutralized) and the actual situation through the particle charging state. The laboratory results of this work provide a reference for emergency evacuations and indoor air quality improvements when environmental air pollution accidents and extreme weather occur. The results in this work will further provide a way to solve related problems in accident-prone areas.

3.2 Methodology

3.2.1 Chamber System Description

Fig. 1(a) illustrates the chamber system used to study particles activities. The main test body in Fig. 1(b) was developed to simulate a common residential house and its surrounding environment. The structure was fully enclosed and made of acrylic resin. The test chamber was composed of outdoor and indoor compartments, which each had an inner size of 1.01m×0.80m×0.80m and were separated by a test body including a custom-designed, moisture-proof and airtight wall and a household sliding window with two panes (see as Fig. A.$_1$). The window in this experiment is customized to the universal household type (semi-external type with angle integrated frame), and the wall is a unitary structure that has undergone a good sealing treatment, so that the cracks exist only between the two sliding panes and between the wall and window. In this study, the window was kept closed at all times; the window frame materials were changed to aluminum or plastic according to experimental conditions, and both frames have the same specifications. In addition, particles in the two compartments could be collected to measure the concentration of suspended particles in real time through small holes, and AER could be controlled by an exhaust pump out of the right part. In this experiment, each compartment had a household fan with a fixed speed

installed. The left fan mixed the particles evenly to form the overall contamination of the external environment, while the right fan mixed carbon dioxide (CO_2) gas before introducing outdoor particles.
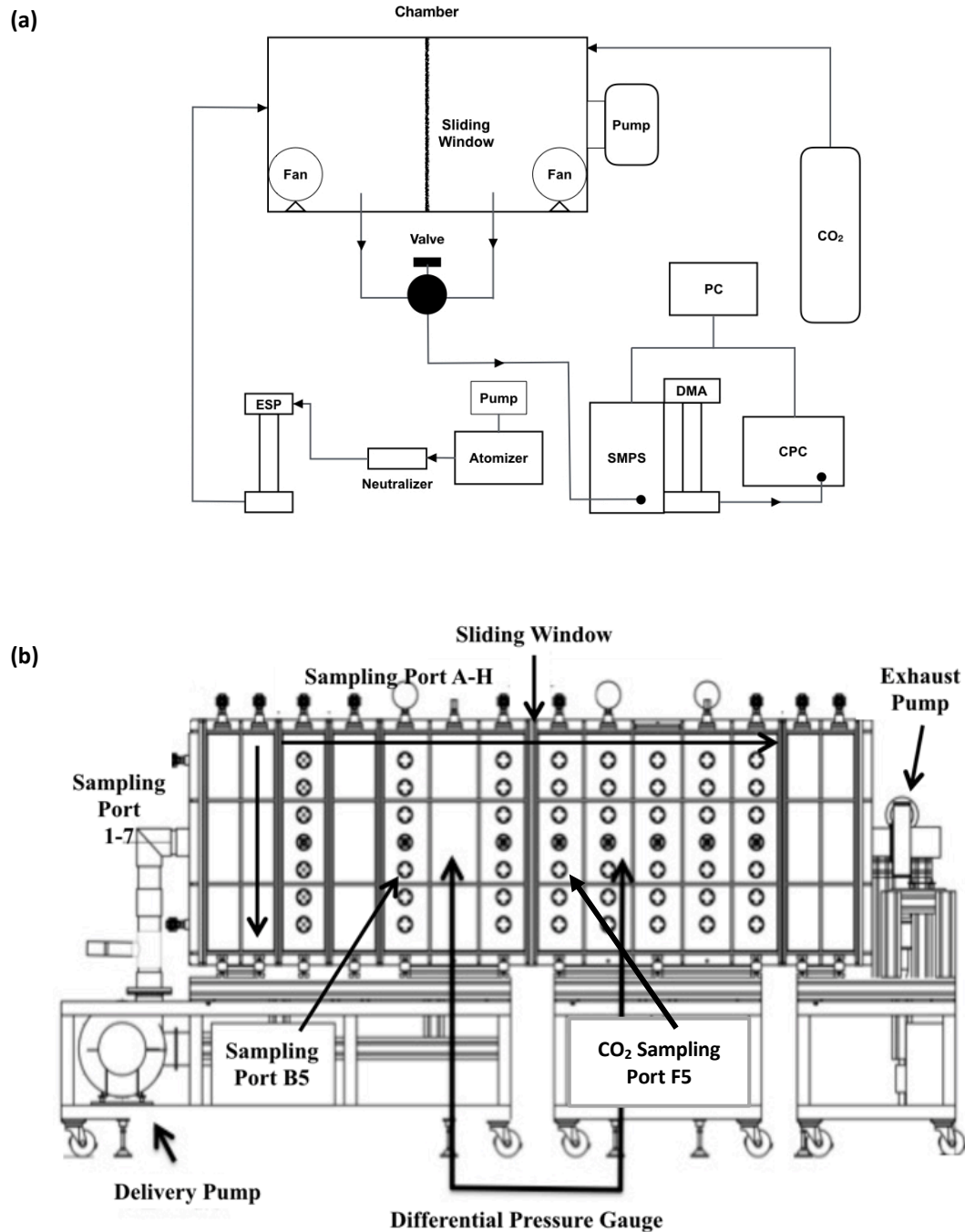
Fig. 1. Chamber system: (a) schematic of the chamber system and (b) diagram of the test chamber.

3.2.2 Experimental Method and data analysis

As shown in Fig. 1 (a), aerosol particles were injected into the outdoor compartment until a desired concentration was reached. Then, CO_2 was introduced into the indoor compartment. After being uniformly mixed by fans, the ventilation system with an operated AER was turned on, and the measurement of particles and CO_2 simultaneously were started. Hereafter, the particles in the outdoor space penetrated through cracks of window and wall, and CO_2 in the indoor chamber decayed with time due to the presence of an AER.

Here, a sodium chloride (NaCl) aqueous solution with a mass concentration of 10% (w/w) or 0.1% (w/w) was sprayed onto poly-dispersed particles ranging from 69 nm to 514 nm and 21 nm to 217 nm by a 6-jet atomizer (TSI model 3706) respectively. A radioactive neutralizer is widely used in aerosol studies to neutralize electrostatic charge of the particles and to impart a bipolar equilibrium charge distribution on particles for size classification using a differential mobility analyzer (DMA) [42-46]. Such particles were defined as neutralizing particles whose activity exhibited the effects of electrostatic forces. Similarly, an electrostatic precipitator (ESP, Self-product) was connected to remove the surface charge from the neutralized particles prior to entering the outdoor compartment. Such particles are referred to as uncharged particles and are typically simulated in the laboratory without considering the electrostatic force. Additionally, particle generation stopped when their initial total number concentration in the outdoor compartment reached around 1.0×10^4 particles/cm^3. Then the concentration of poly-dispersed particles was measured with a scanning mobility particles sizer (SMPS, TSI model 3082: sample flow 0.30L/min, sheath flow 3.00L/min, size range 17-542 nm) and electrically classified by DMA. An ultrafine condensation particle counter (CPC, TSI model 3776) was configured to detect the concentration of particles in the chamber. During the measurement, the concentrations of the two compartments in real-time, C_{out} and C_{in}, respectively,

were measured by switching the valve every minute for 36 minutes. That is, C_{out} was only measured for odd minutes while C_{in} was only determined for even minutes.

The decay of the CO_2 concentration is commonly used to confirm the actual AER. In this study, the full ranged-value of the operated AER was set as 0.16 h^{-1}, 0.30 h^{-1}, 0.70 h^{-1}, 1.07 h^{-1}, 1.20 h^{-1}, 1.50 h^{-1}, 2.00 h^{-1}, or 3.00 h^{-1}. The decay of the CO_2 concentration (ppm) during the time Δt, $\Delta C_{CO_2}(t)$, is well approximated by an exponential equation,

$$\Delta C_{CO_2}(t) = e^{-a\Delta t} \tag{1}$$

Where, $\Delta C_{CO_2}(t)$ is a variable and has already deducted the part that leaked into the outdoor compartment in real time. And a is AER (h^{-1}), which is an important factor that influences the penetration behaviors of particles through cracks in real buildings [41] and reflects the relationship between the operated AER and its measured value (hereinafter referred to as 'actual AER' or 'AER').

After obtaining the results and regularity of the penetration factor, the representative particle size range and the AER value were selected to analyze the change rate of the particles concentration over time of the two compartments. Hence, the cause of the change of the penetration factor and the role of the ventilation system were explored. The size range of 69–100 nm, 100–200 nm, 200–300 nm, 300–500 of 10% (w/w) and 21–69 nm, 69–100 nm, 100–200 nm of 0.1% (w/w), and averaged actual AER were used for data analysis. These size scopes covered UFPs and FPs below 514 nm. Crossovers in the same range (69–100 nm and 100–200 nm) for both concentrations (10% and 0.1%) were used to discuss the effects of the particles concentration and charging state. Meanwhile, the three kinds of AER values represented the flow settings of the entire experiment.

3.2.3 Estimation Methods

This study assumed that the sheltering house (indoor compartment) was well sealed, the entire process lacked indoor sources, and the particles were in suspension or sedimentation after entering. Additionally, particle resuspension was neglected since the test chamber was cleaned by filtered air before each experiment [47]. Meanwhile, the possibility that the outdoor particles contained in the filtered air penetrating through cleaning or ventilation can be ignored due to lack of target particles in the experimental environment. Thus, the contaminant cloud or airflow passing through the crack from the outside (outdoor compartment) was the only path. The process was in a steady state, and the P value was derived from the mass balance equation [40,48],

$$dC_{in}/dt = aPC_{out} - aC_{in} - kC_{in} \tag{2}$$

which is described as,

$$P = \frac{a+k}{a} \frac{C_{in}}{C_{out}} \tag{3}$$

All P values in this work were calculated by Eq. (3), where the first term ($\frac{a+k}{a}$) is determined by a given AER value and the empirical value k. And the second term, I/O ratio, indicates the relationship between indoor and outdoor 36-minute averaged concentrations.

In this equation, k is the deposition rate. It is generally believed that the k values can be acquired in two ways: experimental determination and model estimation. As expressed as Eq. (4) and Eq. (5), the k value can be determined experimentally using the decay method when particle generation is terminated [49].

$$C(t) = C(0)exp\,(-\lambda t) \tag{4}$$

where, $\lambda = a + k$ (5)

In the case where the particles continuously penetrate from the outside, the indoor particle concentration does not decrease monotonically with time. At the

same time, the use of the ventilation system largely influences the concentration. Therefore, the concentration decay method cannot obtain the k value.

Assuming no resuspension during the process, the deposition rate k has a negligible impact on C_{in} in the steady state [1, 50]. Thus, the formula describing the deposition rate k was approximated by Okuyama et al. (1986) as [26, 51]

$$k = \left(\frac{S_T}{V_T}\right)\left(\frac{D}{\delta}\right) + \frac{u_t}{H} \tag{6}$$

where, $\delta = 2.884D^{\frac{1}{3}}$ cm $\tag{7}$

$$D = \frac{C_c \kappa T}{3\pi\mu d_p} \text{ cm}^2/\text{s} \tag{8}$$

$$u_t = \frac{C_c(\rho_p - \rho_f)d_p^2 g}{18\mu} \text{ cm/s} \tag{9}$$

$$C_c = 1 + K_n\left[1.165 + 0.483 exp(-\frac{0.997}{K_n})\right] \tag{10}$$

$$K_n = \frac{2\lambda_m}{d_p} \tag{11}$$

As the above equations demonstrate, k is a function of d_p under the steady state and depends on d_p regardless of the concentration or other conditions (Fig. 2). Eq. (6) was employed as the final model to estimate the k value in this study.
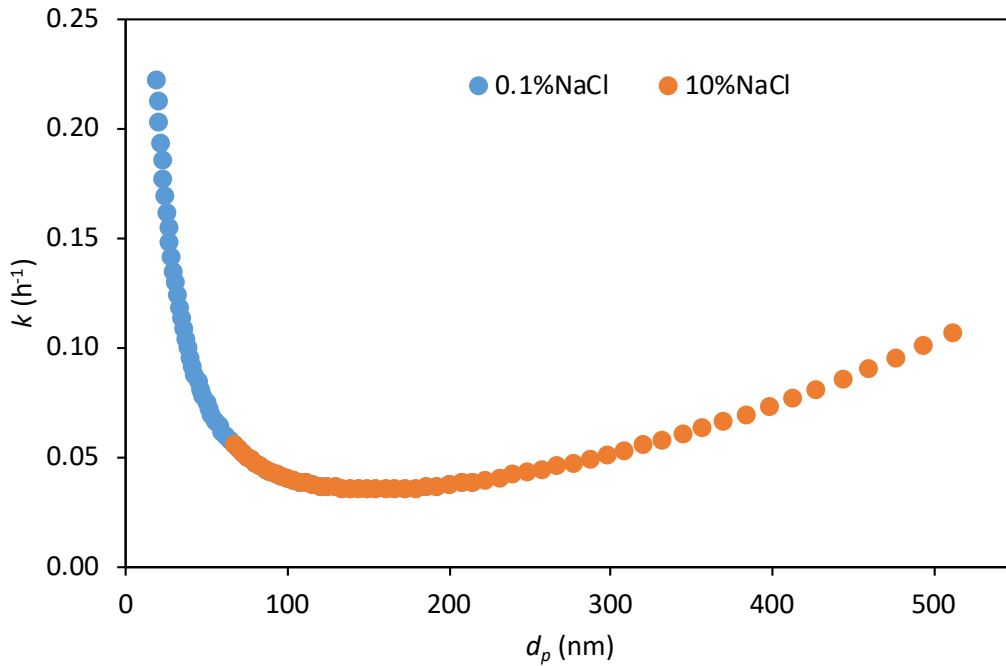
Fig. 2. Deposition rate k as a function of diameter d_p

For the change rate of concentration with time, including the growth rate and decay rate, a monotonically increasing (decreasing) region can be fitted with the least squares and compared to the absolute value of the slope. It can be also determined by the ratio of the difference of the highest value and time as

$$the\ change\ rate\ of\ concentration\ with\ time\ (cm^3/t) = \frac{C_{max} - C_{min}}{\Delta t} \quad (12)$$

In this experiment, the second method was used to analyze the non-monotonic areas while reflecting real-time ventilation efficiency. In addition, the decay method (Eq. (4)) was used to calculate the decay portion, and the results of the exponential regression were used to characterize the removal mechanism and the method application.

3.2.4 Quality Control and Measurement Uncertainty

The temperature of the laboratory, where the test chamber was located, was kept at 25 °C year-round, and there was no obvious turbulence interference in the external environment. To ensure the quality, the test chamber was cleaned by turning on a delivery pump outside of the outdoor compartment until the concentrations of both compartments were less than 5.0 particles/cm^3 (see Fig. 1). Additionally, the measurement errors due to the mixing differences and instrument drift were reduced by multiple measurements under the same conditions. After the calculation, the errors of the final P value with respect to the concentration change and the charging state were typically less than 5%. The maximum error was 9%, and the measurement error of the P value with respect to the slit material comparison was less than 3%. For AER, the error from stability of CO_2 gas and instrument drift was less than 11%, but the maximum was 21%.

3.3 Results and discussion

3.3.1 AERs

Table 1 shows the calibration result of AERs. Corresponding to the operated values, the actual averaged AERs were used for data analysis in similar conditions and measurements in this work.

Table 1

Operated AER and actual averaged AER

Operated AER (h^{-1})	0.16	0.30	0.70	1.07	1.20	1.50	2.00	3.00
Actual averaged AER (h^{-1})	0.31	0.46	0.85	1.20	1.37	1.79	2.43	3.70

3.3.2 Penetration factor

3.3.2.1 Effect from different AERs

Fig. 3 (a)–(b) compare the size-dependent P with particle concentration at 10% with d_p from 69 nm to 514 nm and at 0.1% with d_p from 21 nm to 217 nm respectively. Using the same d_p of the two concentrations ranging from 69 nm to 217 nm, Fig. 3 (c) gives the P value changes with the averaged AER and correlation between the relevant factors. Generally, a high AER corresponds to a high P and tends to remove indoor particles. In the case where the initial C_{out} is fixed, the concentration difference (around 1.0×10^4 particles/cm^3 in this work) between indoor and outdoor 'squeezes' particles through the cracks more easily, increasing the P value.

In terms of C_{in}, when AER equals to 0.31 h^{-1} (a < 1.20 h^{-1}), the curve is slowly monotonically increasing because C_{out} is much larger than C_{in} and infiltration is the primary mechanism (see Fig. A.$_2$ (b) and Fig. A.$_3$ (b)), which is consistent with the result of 0.71 h^{-1} by Yamamoto et al. (2010) [52]. Beginning from 1.20 h^{-1}, the maintenance segment appears in the C_{in} curve after a period of growth (See Fig. A.$_2$ (d) and Fig. A.$_3$ (d)). In this case, the growth rate becomes large, and the concentration between the two compartments tend to balance. It should

be noted that the trend of the change in C_{in} is represented by three distinct segments when AER exceeds 1.20 h^{-1}: (1) Growth. This may be because a large amount of outdoor particles penetrate indoors due to a large concentration difference at which time infiltration is dominant; (2) Maintenance. After a certain time (12–14 m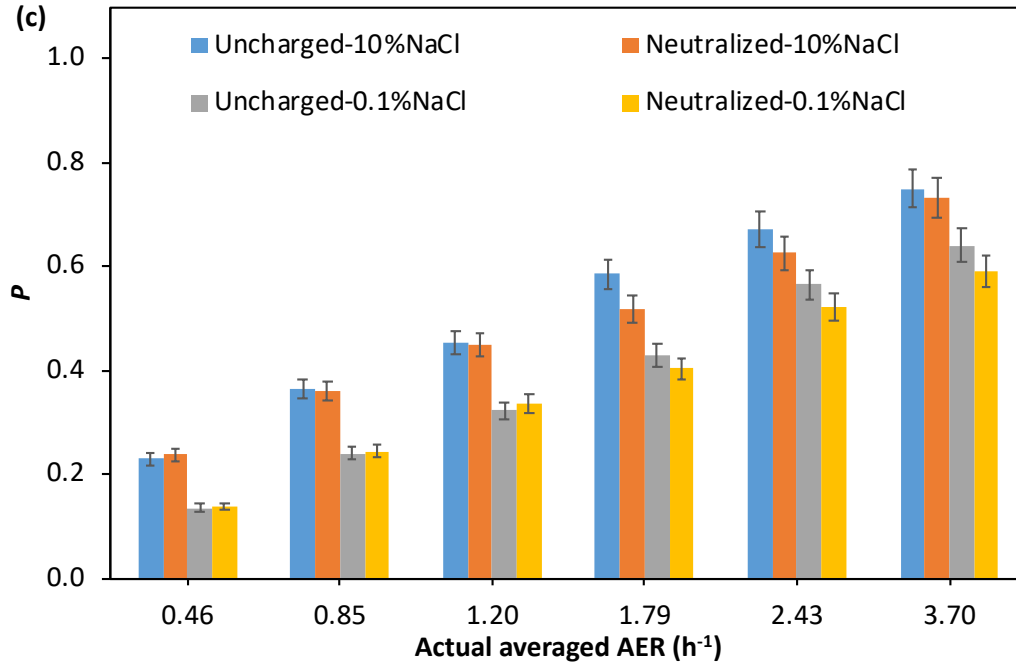in in this experiment), the concentration difference between the inner and outer compartments gradually decreases until it reaches an equilibrium. (3) Decline. Once balanced, mechanical ventilation starts to dominate. The indoor concentration starts to show a declining trend toward zero, while the decrease in particle concentration in the outdoor compartment lead to a decrease in infiltration. When outdoor concentration is lower than indoor concentration, a higher AER can force the ventilation system to remove the indoor particles effectively, so that the ventilation system can play a main role in purifying the indoor environment when AER exceeds 1.20 h^{-1}. Therefore, segment (3) can only be seen in Fig. A.$_2$ (f) and Fig. A.$_3$ (f) (a=3.70 h^{-1}). Otherwise, 'a high AER corresponds to a high P' means that the risk of a large amount of outdoor particles infiltrating into the room increases if there is a high concentration in the outdoor space.

This research used the decay method to analyze the decline segments (10% concentration with last 22 minutes and 0.1% concentration with last 24 minutes). Regardless of the particle size range, the exponential decay rate is less than the AER value (a=3.70 h^{-1}=0.062 min^{-1}). Hence, the removal mechanism is mainly mechanical ventilation, and the decay method is not suitable to estimate deposition rate k. Instead, a model simulation of deposition rate k was chosen. It can also be inferred that when AER is much larger than k, the indoor particle concentration increases and the retention time becomes extremely short, the k value can be ignored. In this extreme case, P value can be roughly estimated as

$$P \approx \frac{C_{in}}{C_{out}} = I/O \text{ ratio} \tag{13}$$

(a)

Legend:
- ▲ Uncharged-0.31 h⁻¹
- ✳ Uncharged-1.20 h⁻¹
- ● Uncharged-3.70 h⁻¹
- ✕ Neutralized-0.31 h⁻¹
- ■ Neutralized-1.20 h⁻¹
- + Neutralized-3.70 h⁻¹

(b)

Legend:
- ▲ Uncharged-0.31 h⁻¹
- ✳ Uncharged-1.20 h⁻¹
- ● Uncharged-3.70 h⁻¹
- ✕ Neutralized-0.31 h⁻¹
- ■ Neutralized-1.20 h⁻¹
- + Neutralized-3.70 h⁻¹

(69, 0.08)
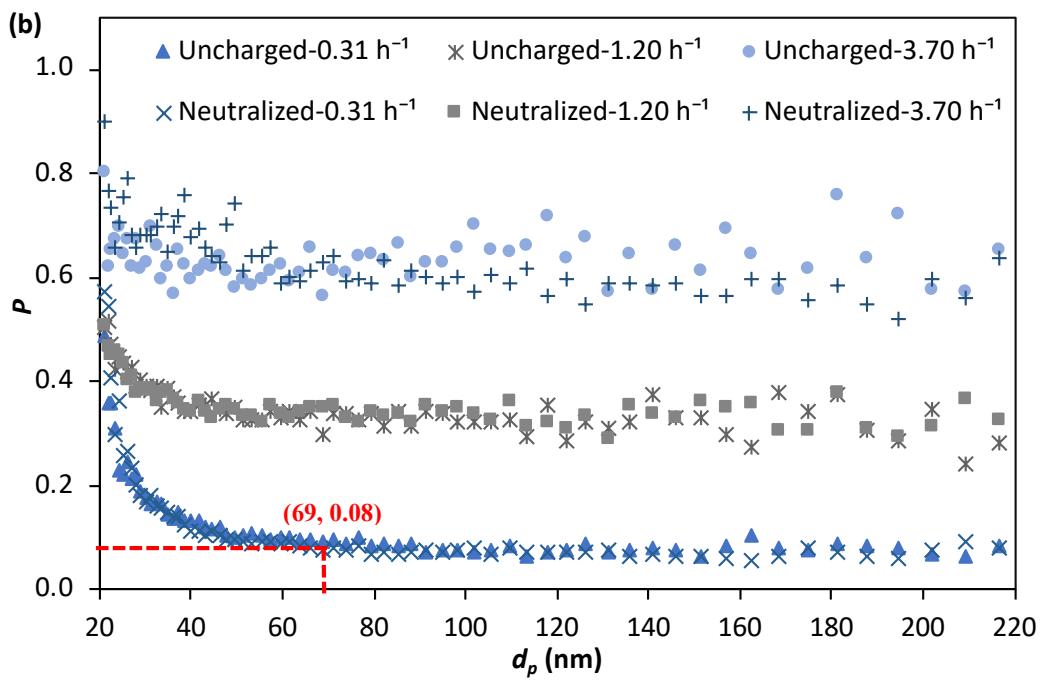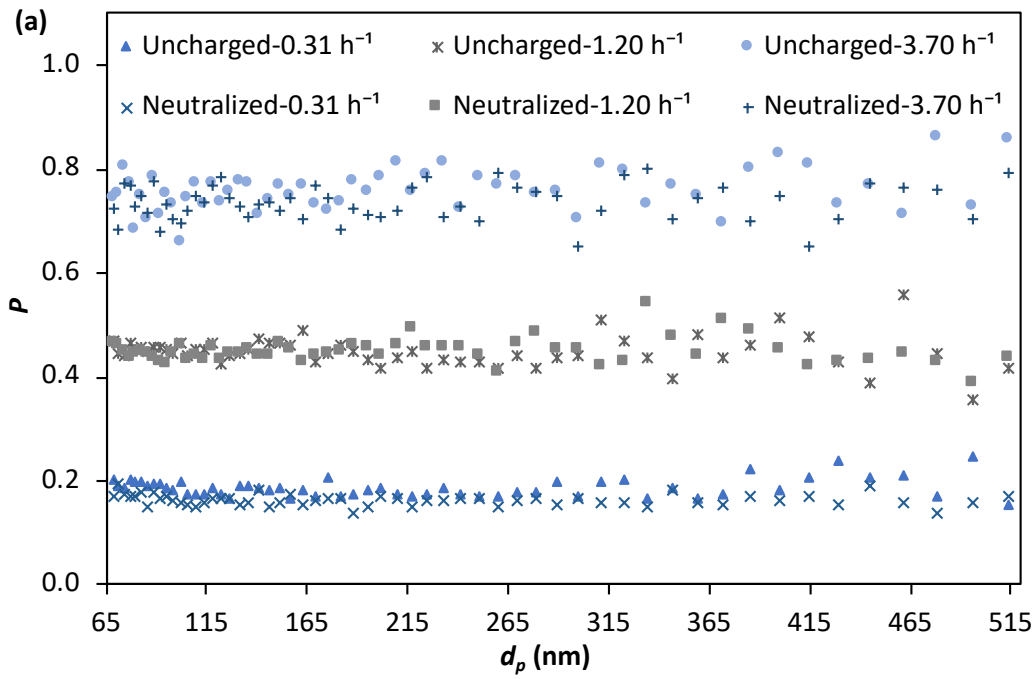
Fig. 3. P value change by d_p/ averaged AER: (a) particle concentration at 10% with d_p from 69 nm to 514 nm, (b) particle concentration at 0.1% with d_p from 21 nm to 217 nm, and (c) P value changes with the actual averaged AER and the correlation between the relevant factors (d_p from 69 nm to 217 nm).

Table 2

(a) Change rate of the concentration over time (outdoor compartment)

Averaged AER (h^{-1})	0.31		1.20		3.70	
Charging state	Uncharged	Neutralized	Uncharged	Neutralized	Uncharged	Neutralized
10% (w/w)	36-minute average concentration decay rate (particles/$cm^3 \cdot$min)					
69-100 nm	1.3	2.4	6.4	5.7	5.0	6.6
100-200 nm	2.1	3.1	4.2	5.8	7.1	11.0
200-300 nm	0.9	2.1	1.7	2.8	6.2	10.6
300-500 nm	0.5	1.2	0.5	1.0	3.6	6.7
0.1% (w/w)	36-minute average concentration decay rate (particles/$cm^3 \cdot$min)					
21-69 nm	2.8	2.9	5.7	5.9	7.6	4.0
69-100 nm	1.2	2.7	2.0	3.3	6.5	8.0
100-200 nm	0.7	1.4	0.7	1.4	2.5	6.3

32

(b) Change rate of concentration over time (indoor compartment)

Averaged AER (h^{-1})	0.31		1.20		3.70					
Averaged AER(min^{-1})	0.005		0.020		0.062					
Charging state	Uncharged	Neutralized	Uncharged	Neutralized	Uncharged	Neutralized	Uncharged	Neutralized	Uncharged	Neutralized
Indoor (10%) (nm)	Growth rate 36-minute-average (cm^3/min)				Growth rate First 14-minute-average (cm^3/min)		Decay rate Last 22-minute-average (cm^3/min)		Decay rate Last 22-minute-averaged λ(min^{-1})	
69-100	0.2	0.7	2.9	2.6	4.3	5.7	2.0	2.7	0.045	0.058
100-200	0.4	1.0	2.1	2.8	6.5	10.3	3.0	4.5	0.051	0.051
200-300	0.3	0.5	1.0	1.4	6.4	9.0	3.2	4.1	0.058	0.052
300-500	0.2	0.2	0.3	0.5	4.5	6.5	2.1	2.8	0.062	0.049
Indoor (0.1%) (nm)	Growth rate 36-minute-average (cm^3/min)				Growth rate First 12-minute-average (cm^3/min)		Decay rate Last 24-minute-average (cm^3/min)		Decay rate Last 24-minute-averaged λ (min^{-1})	
21-69	0.6	0.7	2.9	2.9	8.7	5.8	1.7	1.1	0.026	0.027
69-100	0.6	0.9	1.8	2.6	8.1	9.4	1.5	1.6	0.025	0.022
100-200	0.2	0.6	0.5	1.0	3.5	6.4	0.7	0.9	0.025	0.021

3.3.2.2 Effect from charging state

Particle charging state influences P. As shown in Fig. 3 (c), when AER is less than or equal to 1.20 h^{-1}, all the P values of the uncharged particles from 10% (w/w) NaCl are higher than those of the neutralized ones, the exception being the group data of 0.46 h^{-1} due to the slight differences in respective AER values. For the 0.1% (w/w) particles, the P value of the neutralized particles is slightly higher than the uncharged particles, except for 0.31 h^{-1}. When AER is less than or equal to 1.20 h^{-1}, the two kinds of particles have similar P values. As shown in Table 2 (b), uncharged particles from 21–69 nm provided by 0.1% (w/w) NaCl have similar growth rates as the neutralized ones when AER is less than or equal to 1.20 h^{-1} (uncharged as 0.6 cm^3/min and neutralized as 0.7 cm^3/min when AER is 0.31 h^{-1}; Both uncharged and neutralized are 2.9 cm^3/min when AER is 1.20 h^{-1}). The two kinds of particles at the other sizes also have similar growth rates.

Because the particles are easily affected by other factors such as real-time changes in the AER values during the measurements, the influence of the charging state on the P value is minimal when AER is less than or equal to 1.20 h^{-1} (see Table $A_{.1}$).

Significant features occur when AER exceeds 1.20 h^{-1} (see Fig. 3 (c)). The P value of the uncharged particles is higher than that of the neutralized ones. That is, the uncharged particles are more susceptible to penetration, whereas the neutralized particles may be affected by the electrostatic force, hindering penetration. Linked with the result of change rate of indoor concentration over time in Table 2, the growth rate and the decay rate of uncharged particles increases a lot when d_p is less than 69 nm (uncharged as 8.7 cm^3/min compares with neutralized as 5.8 cm^3/min), while for neutralized particles, d_p values more than 69 nm clearly dominate, indicating that they are more susceptible to the external force provided by mechanical ventilation. In addition to the resistance caused by particle charges, the increases in particle size result in more particles being deposited in the crack due to the diffusion effect and gravitational settling. This lowers the P value [38], so that the P values of uncharged particles are greater than that of neutralized particles when AER is more than 1.20 h^{-1}.

Considering the complexity of the particle charging state in ambient air, laboratory simulations may overestimate the penetration factor of the actual atmosphere but underestimate the ventilation efficiency if only uncharged particles are used as the particle source. Conversely, the simulation experiment will underestimate the penetration factor and overestimate the effectiveness of the ventilation system using neutralized particles as the sole source.

3.3.2.3 Effect from particle concentrations and size

P value change by particle concentration with the same d_p from 69 nm to 217 nm in Fig. 3 shows that a 10% particle concentration exhibits a higher P than a 0.1% particle concentration regardless of charging state (P value as 0.24, 0.45

and 0.74 for 10% compares with 0.14, 0.33 and 0.62 for 0.10 % at an AER of 0.46 h^{-1}, 1.20 h^{-1}, 3.70 h^{-1}, respectively). Generally, a high concentration means that both the number of particles per unit volume and particle size are large and corresponding inertial increases the possibility of intrusion to some extent. Meanwhile, particles provided by 0.1% (w/w) solution are easily captured by window cracks due to increasing deposition caused by the diffusion effect. Most Literature had illustrated that the P values for UFPs are usually small due to the effect of Brownian diffusion [50]. However, compared with these results, Mosley and Whitfield (2002) estimated the natural AER to be the lowest one as 0.20 h^{-1}, and the P value of particles below 50 nm increased slightly with the decreased d_p [53]. Similarly, Vette et al (2010) reported the same phenomenon of particles below 30 nm in the case of doors and windows and heating, ventilation and cooling (HVAC) system being turned off [54].

In this work, a tangential guide is introduced for a clearer view with the tangential point (d_p, P) as (69, 0.08) in Fig. 3 (b), P value increases sharply as d_p gradually decreases from 69 nm, and the smaller the AER, the more obvious the phenomenon. With respect to d_p below 69 nm, diffusion effect by ventilation system is usually small due to a small AER (like 0.31 h^{-1}). The P value would be large accordingly because of a large concentration difference. As the AER increases to more than 1.20 h^{-1} (e.g. a=3.70 h^{-1}), the hindrance from the diffusion effect tends to stabilize the behavior of these small particles. Additionally, Fig. A.$_4$ (a) and Fig. A.$_4$ (c) demonstrate that 0.1% (w/w) solution provides 21-217 nm particles with peaks between 40-70 nm, indicating that the external source is mainly UFPs. Meanwhile, the I/O ratio at an AER of 0.31 h^{-1} represents a higher infiltration for d_p less than 40 nm than for other sizes. When the AER increases to 3.70 h^{-1}, the size distribution of particle concentration in the external environment is significantly lower than that at other AERs. Table 2 also gives the same trend with size ranged from 21 nm to 69 nm. The decay rate of outdoor concentration and the growth rate of indoor concentration are both higher,

suggesting that the particles in this range are easy to penetrate. Therefore, when the initial concentration of the outdoor particles is fixed, the AERs affect the penetration, removal characteristics and the external environment to some extent, and this effect is remarkable as the AER value increases. On the other hand, it reveals the experimental limitation of using a non-constant external source over time at a high AER. That is, the results of this work are only for a short-term evaluation. This differs from the experiments and assessments in most literature, which usually identified common features by hours, days or years.

In addition, the use of fan mixing has been reported. For particles with an AER aerodynamic diameter in the range of 100 to 2000 nm, the mixing fan rate has a negligible effect on the deposition rate k [1]. The particle sizes in this study (21–514 nm) are mostly contained in this range. Alongside the easy-penetration-character of particles less than 69 nm, this provides evidence that deposition rate k is not the main removal mechanism and the mixing fan rate has a minimal impact on the penetration process. This is also the reason why this study uses the penetration factor to explore the sheltering efficiency of houses.

3.3.2.4 Effect from household windows

This experiment was performed using a universal household sliding window. Two different frame materials (aluminum and plastic) were used. All other specifications were the same. To eliminate the influence of charge, mixed uncharged particles were selected as the research object. At the same time, the averaged AER values less than or equal to 1.20 h^{-1} were used to reduce the impact of external forces caused by the ventilation system.

For the two different materials, aluminum has high electric conductivity and plastic supplies electrostatic force by friction. In this section, the observed-d_p (40 nm) can be seen instead of the selected tangential point d_p (69 nm), and the d_p may vary with other factors such as semi-external areas of the window, cracks materials, etc. Linked with the division of UFPs in section 3.2.3, full ranged

diameters (21 nm-514 nm) can be further divided according to the effect from two kinds of window frame materials on the P value: (1) $d_p > 200$ nm. As shown in Fig. 4 (a), particles of this range tend to penetrate the aluminum frame due to their inertia effect and the concentration difference between the indoor and outdoor compartments, while electrostatic force caused by friction between the particles and plastic frame hinders the penetration behavior. However, when the AER increases to 1.20 h^{-1}, the plastic frame displays a higher P value, indicating that mechanical ventilation begins to function; (2) 40nm (69 nm) < d_p < 200 nm. For particles of this range in Fig. 4 (b), concentration difference plays the main role for passing through the aluminum frames, while diffusion effect supplies a resistance; (3) d_p < 40 nm (69 nm). Particles with observed-d_p less than 40 nm correspond to a significantly high P, especially for plastic frame window (as shown in Fig. 4 (b)). Particles of less than 40 nm (69 nm) have a large specific surface area and can be in sufficient contact with and rubbed against the surface of the window frame, thereby easily generating electrostatic charges. The rubbed plastic surface will further attract tiny particles of less than 40 nm, while the rubbed particles will stay on the plastic surface due to the opposite charges. When these tiny particles accumulate to a certain amount, they will accelerate passing through the window cracks due to collision and repulsion with each other. The AER applied by the indoor ventilation system enhances this effect. It may also be relevant with the structure of household sliding windows. The sliding properties make the window less affected by airflow, but the feature of the semi-external type results in the large area of the window body contacting the outdoor particles, and the size of the cracks may allow the particles below 40 nm (69 nm) to pass (see Fig. A.[1]). Additionally, the Wilcoxon signed rank test results of P values along with AER changes illustrate that both UFPs and FPs have significant differences in the penetration characteristics of the two window frame materials except for UFPs at the AER of 1.20 h^{-1} (Table 3).
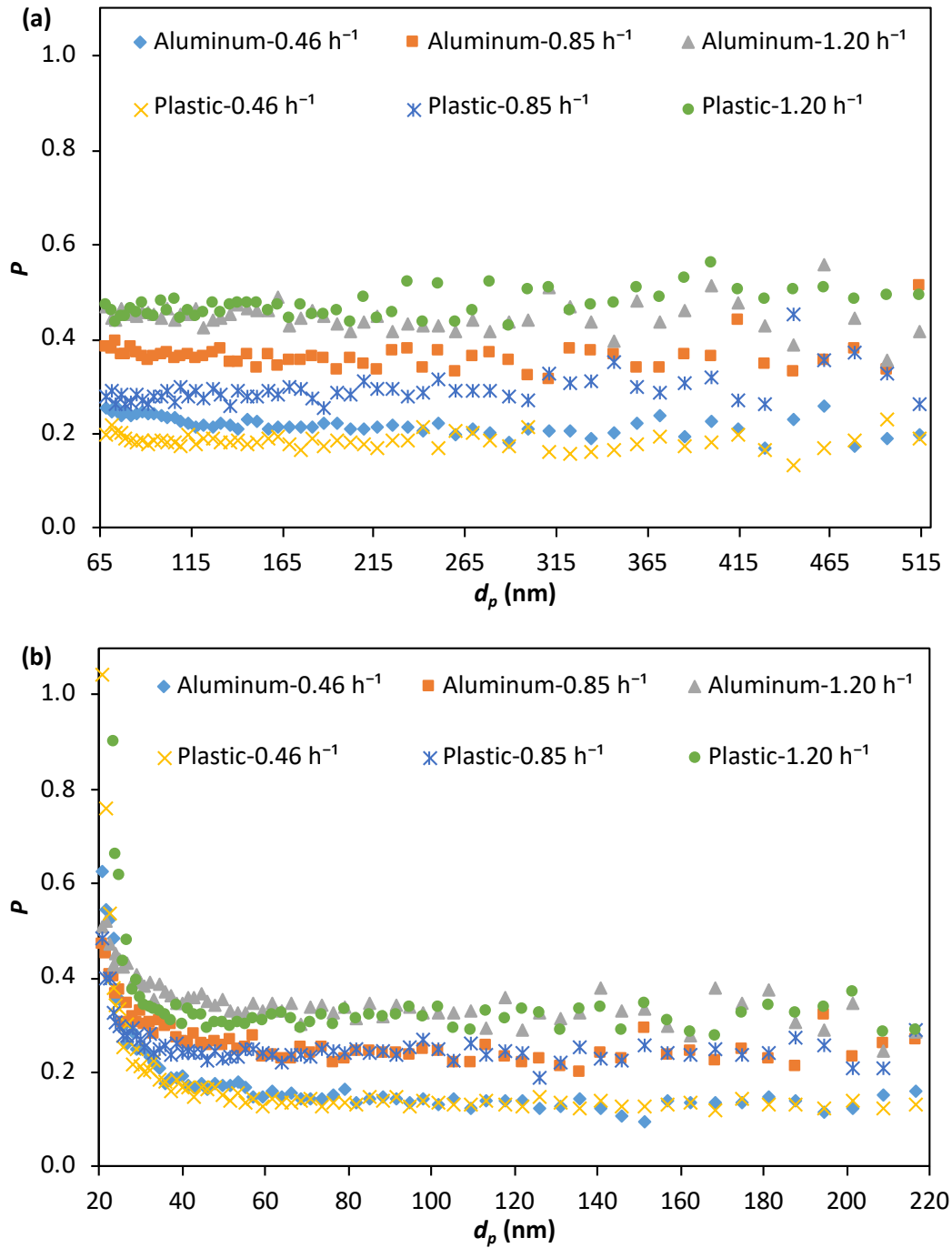
Fig. 4. Effect of window frame materials (Plastic& Aluminum) on the P value change as a function of d_p/ averaged AER: (a) particle concentration at 10% with d_p from 69 nm to 514 nm and (b) particle concentration at 0.1% with d_p from 21 nm to 217 nm.

Table 3

Effect of AER on the penetration factor using two kinds of window frame materials (n=45)

Averaged AER	Mean of Penetration factor		SD of Penetration factor		Median of Penetration factor		Result	
UFPs∈ [21,100) nm	plastic	Aluminum	plastic	Aluminum	plastic	Aluminum	P-Value of Wilcoxon signed rank test	
0.46 h^{-1}	0.23	0.25	0.17	0.11	0.19	0.24	1.03E-05	<0.001***
0.85 h^{-1}	0.27	0.32	0.05	0.06	0.26	0.30	1.92E-11	<0.001***
1.20 h^{-1}	0.50	0.40	0.43	0.05	0.35	0.39	0.16	-
FPs∈ [100,514] nm	plastic	Aluminum	plastic	Aluminum	plastic	Aluminum	P-Value of Wilcoxon signed rank test	
0.46 h^{-1}	0.18	0.21	0.02	0.02	0.18	0.22	8.97E-10	< 0.001 ***
0.85 h^{-1}	0.30	0.36	0.03	0.03	0.29	0.36	7.01E-10	< 0.001 ***
1.20 h^{-1}	0.48	0.45	0.03	0.03	0.48	0.44	1.09E-06	< 0.001 ***

3.4 Conclusion

This study experimentally investigates the relationship between air exchange rate, charging state, particle concentration and size, slit material, and penetration factor, indicates the best house sheltering configuration in an emergency situation, and compares the differences between the ideal state (fully charged or not at all) to the actual situation through the particle charging state. Within the scope of this work, the following conclusions are drawn:

1. In the case where the outdoor concentration is fixed initially, it decays over time, while the trend of the change in indoor concentration is represented by three distinct segments if air exchange rate exceeds 1.20 h^{-1} due to the concentration difference between outdoor and indoor.

(1) When the outdoor concentration is higher than the indoor one, a high air exchange rate usually corresponds to a high penetration factor regardless

of charging state, indicating the increased risk of a large amount of outdoor particles infiltrating into the room;

(2) When the outdoor concentration is similar to the indoor one, concentration change is insignificant;

(3) When the outdoor concentration is less than the indoor one, the ventilation system can play a major role in purifying the indoor environment.

2. For universal household sliding windows, in the case where the external source is mainly UFPs and an air exchange rate is lower than 1.20 h^{-1}, particles smaller than 69 nm are able to undergo penetration due to a large concentration difference between indoor and outdoor, while particles ranged from 69nm to 100 nm tends to capture because of the large diffusion effect. Electrostatic force by friction between plastic cracks and particles and the special structure of the window may enhance the penetration.

3. Laboratory simulations may overestimate the penetration factor but underestimate the ventilation efficiency if the source is only uncharged particles. Conversely, using charged particles as the sole source underestimates the penetration factor and overestimates the effectiveness of the ventilation system.

4. In air pollution emergencies, the external concentration is higher than the interior. In terms of total concentration, window frames made of plastic coupled with an air exchange rate less than or equal to 1.20 h^{-1} can prevent most particles from penetrating. As the external particles gradually disperse and the concentration decreases to less than that indoors, increasing air exchange rate of the ventilation system may be an effective method to purify indoor air. However, effective housing sheltering is still a challenge if the external source is mainly UFPs.

References

[1] R. B. Mosley, D. J. Greenwell, L. E. Sparks, Z. Guo, W. G. Tucker, R. Fortmann, C. Whitfield, Penetration of Ambient Fine Particles into the Indoor Environment, Aerosol Sci. Technol.34 (1) (2001)127-136.

[2] J. Thornburg, D. S. Ensor, C. E. Rodes, P. A. Lawless, L. E. Sparks, R. B. Mosley, Penetration of Particles into Buildings and Associated Physical Factors. Part I: Model Development and Computer Simulations, Aerosol Sci. Technol. 34 (3) (2001) 284-296.

[3] L. A. Wallace, F. Wang, C. Howard-Reed, A. Persily, Contribution of gas and electric stoves to residential ultrafine particle concentrations between 2nm and 64nm: Size distributions and emission and coagulation rates, Environ. Sci. Technol. 42 (2008) 8641-8647.

[4] C. R. He, L. D. Morawska, J. Hitchins, D. Gilbert, Contribution from indoor sources to particle number and mass concentrations in residential houses, Atmos. Environ. 38 (2004) 3405-3415.

[5] C. M. Long, H. H. Suh, P.J. Catalano, P. Koutrakis, Using time- and size-resolved particulate data to quantify indoor penetration and deposition behavior, Environ. Sci. Technol. 35(2001) 2089-2099.

[6] L. A. Wallace, Ultrafine particles from a vented gas clothes dryer, Atmos. Environ. 39 (2005) 5777-5786.

[7] W. Szymczak, N. Menzel, L. Keck, Emission of ultrafine copper particles by universal motors controlled by phase angle, J. Aerosol Sci. 38 (2007) 520-531.

[8] B. K. Coleman, H. Destaillats, A. T. Hodgson, W. W. Nazaroff, Ozone consumption and volatile byproduct formation from surface reactions with aircraft cabin materials and clothing fabrics, Atmos. Environ. 42 (2008) 642-654.

[9] C. J. Weschler, Ozone's impacton public health: Contributions from indoor exposures to ozone and products of ozone-initiated chemistry, Environ. Health Perspect. 114 (2006) 1489-1496.

[10] D. Rim, L. Wallace and A. Persily, Infiltration of Outdoor Ultrafine Particles into a Test House, Environ. Sci. Technol. 44 (2010) 5908-5913.

[11] M. L. Pereira, G. Graudenz, A. Tribess, L. Morawska, Determination of particle concentration in the breathing zone for four different types of office ventilation systems, Build. Environ. 44 (2009) 904-911.

[12] L. Wallace, Indoor particles: a review, J Air Waste Manag Assoc 46 (2) (1996) 98-126.

[13] E. Abt, H. H. Suh, P. Catalano, P. Koutrakis, Relative contribution of outdoor and indoor particle sources to indoor concentrations, Environ. Sci. Technol. 34 (17) (2000) 3579-3587.

[14] R. Allen, T. Larson, L. Sheppard, L. Wallace, L. J. S. Liu, Use of real-time light scattering data to estimate the contribution of infiltrated and indoor-generated particles to indoor air, Environ. Sci. Technol. 37 (16) (2003) 3484-3492.

[15] L. Wallace, R. Williams, A. Rea, C. Croghan, Continuous weeklong measurements of personal exposures and indoor concentrations of fine particles for 37 health-impaired North Carolina residents for up to four seasons, Atmos. Environ. 40 (3) (2006) 399-414.

[16] P. L. Jenkins, T. J. Phillips, E. J. Mulberg, S. P. Hui, Activity Patterns of Californians - Use of and Proximity to Indoor Pollutant Sources, Atmospheric Environment Part a-General Topics 26 (12) (1992) 2141-2148.

[17] J. Robinson, WC. Nelson, National human activity pattern survey data base, Research Triangle Park, NC: USEPA; 1995.

[18] N. E. Klepeis, W. C. Nelson, W. R. Ott, J. P. Robinson, A. M. Tsang, P. Switzer, J. V. Behar, S. C. Hern, W. H. Engelmann, The National Human Activity Pattern Survey (NHAPS): a resource for assessing exposure to

environmental pollutants, J Expo Anal Environ Epidemiol 11 (3) (2001) 231-252.

[19] T.L. Thatcher, D.W. Layton, Deposition, resuspension, and penetration of particles within a residence, Atmos. Environ. 29 (1995) 1487-1497.

[20] C. Y. H. Chao, M. P. Wan, E.C.K. Cheng, Penetration coefficient and deposition rate as a function of particle size in non-smoking naturally ventilated residences, Atmos. Environ. 37 (2003) 4233-4241.

[21] S. E. Chatoutsidou, L. Mašková, L. Ondráčková, J. Ondráček, M. Lazaridis, J. Smolík, Modeling of the aerosol infiltration characteristics in a cultural heritage building: The Baroque Library Hall in Prague, Build. Environ. 89 (2015) 253-263.

[22] T. Hussein, Indoor-to-outdoor relationship of aerosol particles inside a naturally ventilated apartment − A comparison between single-parameter analysis and indoor aerosol model simulation. Science of The Total Environment. 596-597 (2017) 321-330.

[23] Y. J. Hu, L. J. Bao, C. L. Huang, S. M. Li, P. Liu, E. Y. Zeng, Exposure to air particulate matter with a case study in Guangzhou: Is indoor environment a safe haven in China? Atmos. Environ. 191 (2018) 351-359.

[24] B. Mølgaard, J. Ondráček, P. Šťávová, L. Džumbová, M. Barták, T. Hussein, J. Smolík, Migration of aerosol particles inside a two-zone apartment with natural ventilation: A multi-zone validation of the multi-compartment and size-resolved indoor aerosol model, Indoor and Built Environment. 23 (5) (2013) 742-756.

[25] S. Shi, C. Chen, B. Zhao, Air infiltration rate distributions of residences in Beijing, Build. Environ. 92 (2015) 528-537.

[26] K. Okuyama, Y. Kousaka, S. Yamamoto, T. Hosokawa, Particle loss of aerosols with particle diameters between 6 and 2000 nm in stirred tank, J. Colloid Interface Sci. 110 (1986) 214-223.

[27] G. P. Fotou, S. E. Pratsinis, A Correlation for Particle Wall Losses by Diffusion in Dilution Chambers, Aerosol Sci. Technol. 18 (2) (1993) 213-218.

[28] S. Lewis, Solid particle penetration into enclosures, J. Hazard Mater. 43 (1995) 195–216.

[29] D. L. Liu, W.W. Nazaroff, Particle penetration through building cracks, Aerosol Sci. Technol. 37 (2003) 565-573.

[30] F. Tavakoli, S. K. Mitra, J. S. Olfert, Aerosol penetration in microchannels, Journal of Aerosol Science 42 (5) (2011) 321-328.

[31] J. Bouilly, K. Limam, C. Beghein, F. Allard, Effect of ventilation strategies on particle decay rates indoors: An experimental and modelling study, Atmos. Environ. 39 (27) (2005) 4885-4892.

[32] L. Tian, G. Zhang, Y. Lin, J. Yu, J. Zhou, Q. Zhang, Mathematical model of particle penetration through smooth/rough building envelop leakages, Build. Environ. 44 (6) (2009) 1144-1149.

[33] X. Gao, X.K. Wang, Correlation study on air change rate and particle penetration coefficient though building envelope, Heat. Vent. Air Cond. 46 (2016) 14-19.

[34] C. E. Anderson Jr, Analytical models for penetration mechanics: A Review, International Journal of Impact Engineering. 108 (2017) 3-26.

[35] D. L. Liu, W.W. Nazaroff, Modeling pollutant penetration across building envelopes, Atmos. Environ. 35 (2001) 4451-4462.

[36] C. Chen, B. Zhao, A modified Brownian force for ultrafine particle penetration through building crack modeling, Atmos. Environ. 170 (2017), 143-148.

[37] A. Li, T. Ren, C. Yang, W. Lv, F. Zhang, Study on particle penetration through straight, L, Z and wedge-shaped cracks in buildings, Build. Environ. 114 (2017) 333-343.

[38] Y. Lv, H. Wang, S. Wei, T. Wu, T. Liu, B. Chen, The experimental study on indoor and outdoor penetration coefficient of atmospheric fine particles, Build. Environ. 132 (2018) 70-82.

[39] H. Bennett, P. Koutrakis, Determining the infiltration of outdoor particles in the indoor environment using a dynamic model, J. Aerosol Sci. 37 (6) (2006) 766-785.

[40] D. Rim, L. A. Wallace, A. K. Persily, Indoor Ultrafine Particles of Outdoor Origin: Importance of Window Opening Area and Fan Operation Condition, Environ. Sci. Technol. 47 (4) (2013) 1922-1929.

[41] C. Chen, B. Zhao, W. Zhou, X. Jiang, Z. Tan, A methodology for predicting particle penetration factor through cracks of windows and doors for actual engineering application, Build. Environ. 47 (2012) 339-348.

[42] M. Adachi, D. Y. H. Pui, B. Y. H. Liu, Aerosol Charge Neutralization by a Corona Ionizer, Aerosol Sci. Technol. 18 (1) (1993) 48-58.

[43] D. Covert, A. Wiedensohler, L. Russell, Particle charging and transmission efficiencies of aerosol charge neutralizers, Aerosol Science and Technology 27 (2) (1997) 206-214.

[44] J. H. Ji, G. N. Bae, J. Hwang, Characteristics of aerosol charge neutralizers for highly charged particles, J. Aerosol Sci. 35 (11) (2004) 1347-1358.

[45] M. Alonso, F. J. Alguacil, Particle Size Distribution Modification During and After Electrical Charging: Comparison between a Corona Ionizer and a Radioactive Neutralizer, Aerosol and Air Quality Research 8 (4) (2008) 366-380.

[46] A. Nicosia, L. Manodori, A. Trentini, I. Ricciardelli, D. Bacco, V.Poluzzi, L. Di Matteo, F. Belosi, Field study of a soft X-ray aerosol neutralizer combined with electrostatic classifiers for nanoparticle size distribution measurements, Particuology 37 (2018) 99-106.

[47] C. Liu, J. Yang, S. Ji, Y. Lu, P. Wu, C. Chen, Influence of natural ventilation rate on indoor PM2.5 deposition, Building and Environment, 144 (2018) 357-364.

[48] W. E. Wilson, D. T. Mage, L. D. Grant, Estimating separately personal exposure to ambient and nonambient particulate matter for epidemiology and risk assessment: Why and how, Journal of the Air & Waste Management Association 50 (7) (2000) 1167-1183.

[49] W. C. Lee, J. M. Wolfson, P. J. Catalano, S. N. Rudnick, P. Koutrakis, Size-Resolved Deposition Rates for Ultrafine and Submicrometer Particles in a Residential Housing Unit, Environ. Sci. Technol. 48 (17) (2014) 10282-10290.

[50] C. Chen, B. Zhao, Review of relationship between indoor and outdoor particles: I/O ratio, infiltration factor and penetration factor, Atmos. Environ. 45 (2011) 275-288.

[51] J. H. Kim, G. W. Mulholland, S.R. Kukuck, D. Y. H. Pui, Slip Correction Measurements of Certified PSL Nanoparticles Using a Nanometer Differential Mobility Analyzer (Nano-DMA) for Knudsen Number From 0.5 to 83, J Res Natl Inst Stand Technol. 110 (1) (2005) 31-54.

[52] N. Yamamoto, D. G. Shendell, A. M. Winer, J. Zhang, Residential air exchange rates in three major US metropolitan areas: results from the Relationship Among Indoor, Outdoor, and Personal Air Study 1999-2001, Indoor Air. 20 (1) (2010) 85-90.

[53] R.B. Mosley, C. Whitfield, The influence of building features on air exchange rate and particle penetration, Proceedings: Indoor Air. (2002) 856-861.

[54] A. F. Vette, A. W. Rea, P. A. Lawless, C. E. Rodes, G. Evans, V. R. Highsmith, L. Sheldon, Characterization of Indoor-Outdoor Aerosol Concentration Relationships during the Fresno PM Exposure Studies, Aerosol Science and Technology. 34(1) (2010) 118-126.

Chapter 4. Determination of the Optimal Penetration Factor for Evaluating the Invasion Process of Aerosols from a Confined Source Space to an Uncontaminated Area

4.1 Introduction

The global outbreak of coronavirus disease (COVID-19) has seriously endangered the health and safety of all human beings. Scientists have conducted extensive research on the Severe Acute Respiratory Syndrome Coronavirus 2 (SARS-CoV-2), referring to transmission dynamics [1-3], removal technology [4], and climate factor [5]. Correia et al. (2020) pointed out that improper use of the ventilation system could aggravate the spread of the virus [6]. Doremalen et al. (2020) experimentally generated SARS-CoV-2-containing aerosols with a diameter of less than 5 μm, and illustrated that SARS-CoV-2 can survive and be infectious in aerosols for hours, in some cases even days on surfaces [7]. Moreover, it is well known that coronavirus is more likely to exist in confined and poorly ventilated spaces. In this case, aerosols can carry or combine with viruses into an uncontaminated area under certain ventilated conditions. However, the most effective evaluation method for aerosols penetrating from the polluted area or the source area to the unpolluted space is still not clear.

In recent decades, the fate of aerosols penetrating from outdoor has received widespread attention from scientists due to the direct relationship with human health [8-12]. Related penetration research is usually carried out in two ways: field measurement and laboratory simulation. Field experiments are always conducted in real buildings such as school classrooms, dormitories, and offices [13-22], while a test chamber or a building brick is usually used as the object to simulate the indoor or outdoor environment in laboratory simulations [22-27]. The difference between laboratory simulation and field testing is a greater control

of the conditions in a laboratory setting. Additionally, the change in concentration of aerosols is one of the basic characteristics in the penetration process. Based on the law of mass balance, Thatcher et al (2003) had represented the indoor concentration over time "t" as [28],

$$\frac{\partial C_{in}}{\partial t} = a \cdot [P \cdot C_{out} - C_{in}] - k \cdot C_{in} + G + S + F + K + H \tag{1}$$

where, C_{in} and C_{out} are the indoor and outdoor particle concentrations (cm^{-3}), a is air exchange rate (AER) (h^{-1}) associated with ventilation system, k is the rate of particles deposition loss onto interior surfaces (h^{-1}), while P is the penetration factor. G, S, F, K and H represent the particle generation from the indoor source, particles for dissociation/vaporization, the formation of new particles due to chemical reactions, the particles for coagulation and for hygroscopic growth (cm^{-3} h^{-1}), respectively.

For the source, concentrations, size of particles and the experimental conditions used in most simulations, it is assumed that the effects of dissociation/vaporization (S), new chemical formation (F), coagulation (K) and hygroscopic growth (H) are avoided in the analysis. If the study only focuses on the single penetration process, the indoor source (G) also has no significance. In this case, Eq. (1) is simplified to the expression with parameter a, k and P, as

$$dC_{in}/dt = aPC_{out} - aC_{in} - kC_{in} \tag{2}$$

Similarly, assuming that the particle flow passing from the outdoor compartment is the only path under ideal conditions, the outdoor particle concentration in a confined space could be affected by the air exchange rate "a" of the indoor compartment and the deposition rate "k" of outdoor particles. Therefore, the outdoor particle concentration over time can be expressed as,

$$dC_{out}/dt = -aP_0C_{out} - kC_{out} \tag{3}$$

It is assumed that a certain number of particles tend to penetrate from the outdoor compartment at time "t" under the action of a ventilator, but only a portion enters the indoor compartment while the rest is trapped by the sash gap.

In this case, "P_0" represents the total proportion of the particles participating in the penetration at a certain AER "a". If those trapped particles do not detach and re-enter the outdoor compartment, P_0 can be estimated as 1.

A review of the literature shows that the portion of "P" entering the indoor compartment can be defined as follows: the parameter P, associated with infiltration airflow, denotes the fraction of outdoor particles passing through building cracks, leakage paths and window openings [29-31]. In Eq. (2), "a" and "k" are the only influencing factors, and the equilibrium solution ($dC_{in}/dt = 0$) is derived as,

$$P = \frac{a+k}{a} \frac{C_{in}}{C_{out}}$$ (4)

In the experiments of penetration simulations in recent decades, Eq. (4) is widely used for quantification of the particle penetration through building cracks. Thornburg et al (2001) reported penetration factor using this equation, and C_{in} and C_{out} were described as the time average of the indoor and outdoor concentrations [29]; Rim et al (2013) mentioned in the derivation that the equation was for the particle size category [31]; while other literatures defaulted the P value to the size-resolved one [14, 32, 33]. However, there is little reference to the optimal method for determining the P value.

Recently, our group performed penetration simulations for emergency evacuation [27]. A fully enclosed chamber used aerosols with a size range of 69-500 nm to simulate the penetration process from outdoor to indoor. This range can represent some fine particles and ultra-fine particles (FPs/ UFPs) in accidents or extreme weather related to air pollution. As the particles gradually pass through the window under a set AER, the indoor concentration may increase, maintain or decrease, while the outdoor concentration continues to decline. In the previous experiment in Chapter 3, the initial outdoor concentration of each test changed over time, that is, a stable and continuous particle source could not be provided. This is also the limiting factor for laboratory simulations. Therefore, two

questions require further discussions: (1) "is the parameter P of Eq. (4) without a time attribute suitable for the case where the concentration changes in a confined source space?" and (2) "what is the optimal P value?".

Based on the aforementioned properties of SARS-CoV-2 regarding its ability to survive in aerosols for hours, FPs/ UFPs may carry or combine with SARS-CoV-2 and then penetrate into uncontaminated areas together. To evaluate the invasion process of aerosols from a confined source space to an uncontaminated area, based on the previous work in Chapter 3 and the widely used concentration model Eq. (2)-Eq. (4), this study will thus be (1) proposing four numerical calculations of penetration factor, the size-dependent P_{avg}, the time-corrected P_{est}, the real-time $P(t)$, and the direct-derived P_d; (2) comparing and evaluating the observed indoor concentrations and the estimated ones; and (3) selecting the optimal P value for penetration process. The proposed optimal P value and the error analysis could help provide insight into the penetration mechanism, and can also provide a rapid and accurate assessment method for preventing and controlling the spread of the epidemic.

4.2 Methodology

4.2.1 Experimental basis

Based on the previous work on penetration simulation for emergency evacuation in Chapter 3, Fig. 1 gives the schematic of the whole experimental system, including a simulation system and a measurement system. A fully enclosed chamber as the main body of the simulation system was conducted in the laboratory (laboratory environment has insignificant influence on the test chamber). The chamber contains two parts, an outdoor compartment (left) and an indoor compartment (right), with each inner size of 1.01 m × 0.80 m × 0.80 m. The two parts are divided by a household sliding window, which is kept closed during the measurement. In the measurement system, polydisperse sodium

chloride particles with a mass concentration of 10% are sprayed into the outdoor compartment by a 6-jet atomizer (TSI model 3706). The full size range of the particles, ranging from 69 nm to 500 nm with a peak range of 100-300 nm according to size distribution characteristics, imitate virus-containing aerosols in this range. They passed through a silicone desiccant, a neutralizer (Am241, 3MBq), and an electrostatic precipitator (ESP, prepared in laboratory). Running the test for 36 minutes displays a concentration change of the two compartments in time distribution by a scanning mobility particles sizer (SMPS, TSI model 3938) and an electrostatic classifier (TSI model 3082) with a long differential mobility analyzer (DMA, TSI model 3081A); meanwhile, the series of real-time concentrations corresponding to indoor (each even-minute, that is, 2, 4, 6…32, 34, 36 min) and outdoor (each odd-minute, that is, 1, 3, 5…31, 33, 35 min) are recorded by an ultrafine condensation particle counter (CPC, TSI model 3776). Additionally, particle concentration accuracy is $\pm$ 10 % and sizing accuracy is 1 % at 100 nm for 10:1 sheath / aerosol flow ratio (sheath flow and aerosol flow are 3.0 L / min $\pm$ 2.0 % and 0.3 L / min $\pm$ 1.5 % as of reading, respectively). Fig. 2 shows the photos of the experiment.

In this study, the outdoor compartment simulates a closed source space filled with virus-containing aerosols, where a certain amount of particles (around 1.0×10^4 cm^{-3}) are introduced at the initial moment; while the indoor compartment with an initial concentration close to zero simulates an uncontaminated room. Due to the particle flow gradually passing through the crack and entering the indoor compartment while the ventilation system is in operation, the series of the indoor and the outdoor concentrations recorded at every time "t" reported in Chapter 3 exhibits a tendency for continuous attenuation [27]. The AER of the ventilation system was controlled from 0.31 h^{-1} to 3.70 h^{-1}, where 0.31 h^{-1}, 1.20 h^{-1} and 3.70 h^{-1} were selected for discussion according to their penetration properties. These experimental concentrations are named as "observed

concentration(s)" in this study as a basis for judging proposing calculation methods.
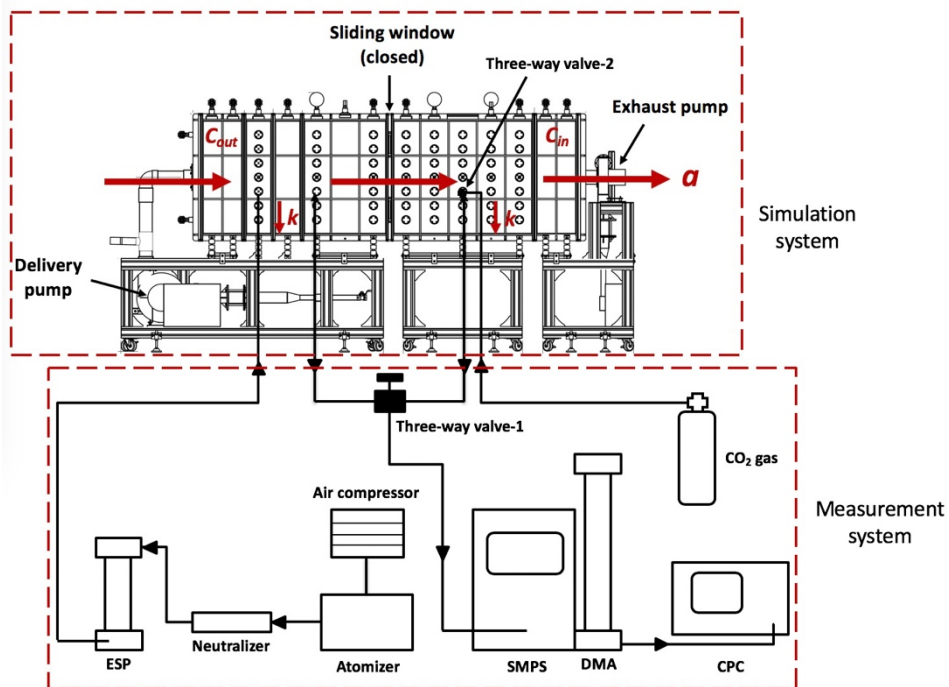
Fig. 1 Experimental system for penetration simulation

Fig. 2 Experimental photos. (a) the test chamber in simulation system (delivery pump and exhaust pump are not mentioned) and (b) CPC and SMPS with DMA in measurement system.

4.2.2 Numerical calculation of penetration factor

Assuming C_{in}(t) and C_{out}(t) as the real-time indoor and outdoor concentrations for instantaneous calculation, respectively, and P(t) as the real-time value of

penetration factor at time t, or P_{avg} representing the average penetration factor for a short-term evaluation, Eq. (4) can be expressed as,

$$P(t) = \frac{a+k}{a} \frac{C_{in}(t)}{C_{out}(t)} \qquad (5)$$

and

$$P_{avg} = \frac{a+k}{a} \frac{C_{in,avg}}{C_{out,avg}} \qquad (6)$$

where, $C_{in,avg}$ and $C_{out,avg}$ are the time-averaged concentrations for each particle size. $P(t)$ is "time-dependent/ size-averaged" penetration factor of the indoor compartment, that is, the penetration factor corresponds to the total concentration per minute at the average diameter. P_{avg} is "size-dependent/ time-averaged" penetration factor of the indoor compartment, representing the penetration factor corresponding to the average concentration of 36 minutes at each particle size. However, P_{avg} is a size-dependent parameter without a time property. Therefore, the theoretical value P_{est} is introduced for time correction in this study.

In case of $C_{in} \neq 0$, $C_{in}(0)$ and $C_{out}(0)$ represent for the initial conditions. Therefore, by integrating Eq. (2) and Eq. (3), the real-time concentrations at t time can be obtained as follows,

$$C_{in}(t) = [P_{est}aC_{out}(0)t + C_{in}(0)] \cdot e^{-(a+k)t} \qquad (7)$$

$$C_{out}(t) = C_{out}(0) \cdot e^{-(aP_0+k)t} \qquad (8)$$

Considering the continuous change in concentration from 0 to T time, then

$$C_{in}^T = \left(\frac{1}{t}\right) \int_0^t C_{in}(t) \, dt \qquad (9)$$

$$\left(\frac{1}{t}\right) \int_0^t C_{in}(t) \, dt = \frac{\{1-[1+(a+k)t]e^{-(a+k)t}\}}{(a+k)^2 t} \cdot P_{est}aC_{out}(0) - \frac{1-e^{-(a+k)t}}{(a+k)t} \cdot C_{in}(0) \qquad (10)$$

$$C_{out}^T = \left(\frac{1}{t}\right) \int_0^t C_{out}(t) \, dt \qquad (11)$$

$$\left(\frac{1}{t}\right) \int_0^t C_{out}(t) \, dt = \frac{1-e^{-(a+k)t}}{(a+k)t} \cdot C_{out}(0) \qquad (12)$$

Combined Eq. (6), Eq. (10) and Eq. (12),

$$P_{avg} = \frac{a+k}{a} \cdot \frac{C_{in}^T}{C_{out}^T} \qquad (13)$$

$$\frac{a+k}{a} \cdot \frac{C_{in}^T}{C_{out}^T} = \left\{\frac{1-[1+(a+k)t]e^{-(a+k)t}}{1-e^{-(a+k)t}}\right\} \cdot P_{est} - \frac{a+k}{a} \cdot \frac{C_{in}(0)}{C_{out}(0)} \tag{14}$$

Here, defined the item "$\frac{1-[1+(a+k)t]e^{-(a+k)t}}{1-e^{-(a+k)t}}$" involving in the parameters "a" "k" and "t" as "correction coefficient r", then

$$r = \frac{1-[1+(a+k)t]e^{-(a+k)t}}{1-e^{-(a+k)t}} \tag{15}$$

so,

$$P_{est} = \frac{1}{r} \cdot \left[P_{avg} + \frac{a+k}{a} \cdot \frac{C_{in}(0)}{C_{out}(0)}\right] \tag{16}$$

In case of C_{in} =0,

$$P_{est} = \frac{1}{r} \cdot P_{Avg} \tag{17}$$

To search for an approximation close to the expected value, a simple equation is visually derived from the ratio of Eq. (7) and Eq. (8) (assumed P_0 = 1) to directly estimate the penetration factor,

$$P_d = \frac{1}{at} \cdot \left[\frac{C_{in}(t)}{C_{out}(t)} - \frac{C_{in}(0)}{C_{out}(0)}\right] \tag{18}$$

Here, P_d represents a time series of approximate values over 36 minutes.

In case of $C_{in}(0)$ =0, Eq. (18) changes to

$$P_d = \frac{1}{at} \cdot \frac{C_{in}(t)}{C_{out}(t)} \tag{19}$$

P_d can be also used to estimate the penetration factor at a certain time t. Compared to P(t) in Eq. (5), P_d calculated by Eq. (19) ignores the effect of k but adds the time attribute.

4.2.3 Application of concentration model

If taking the indoor compartment as the research object, and also fully considering the situation where C_{out} gradually decreases in the laboratory simulation experiment, Eq. (3) is derived to be

$$\frac{C_{in}(t+\Delta t)-C_{in}(t)}{\Delta t} = aP'C_{out}(t) - aC_{in}(t) - kC_{in}(t) \tag{20}$$

where, Δt represents time interval, and the indoor concentration at "$t+\Delta t$" time is estimated as,

$$C_{in}(t + \Delta t) = C_{in}(t) + \Delta t[aP'C_{out}(t) - aC_{in}(t) - kC_{in}(t)] \tag{21}$$

In this study, the deposition rate k was approximated using the model of Okuyama according to our published work, the value of which is less than 0.25 h^{-1} with a particle size of less than 500 nm [27,34]. The penetration factor P, denoted as $P(t)$, P_{avg}, P_{est} and P_d, respectively, is substituted into Eq. (21), and the optimal P value is discussed and determined by comparing with the observed indoor concentration over time.

4.3 Results

4.3.1 Correction coefficient r

In the experiment, four size segments, 69-100 nm, 100-200 nm, 200-300 nm and 300-500 nm, were divided according to their similar P_{avg} in each segment. Fig. 3 gives the relationship between correction coefficient r and the elapsed time (taking 69-100 nm as an example). These curves are extended indefinitely, and they all finally equal to 1. The larger the AER, the shorter the time.
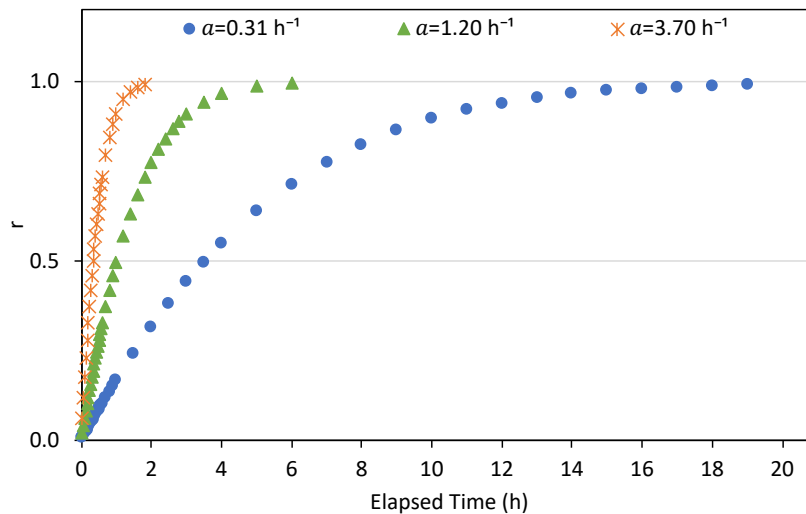
Fig. 3 The relationship between correction coefficient r and elapsed time (taking 69-100 nm as an example)

4.3.2 Values of $P(t)$, P_{avg}, P_{est} and P_d in the four size segments

$P(t)$, P_{avg}, P_{est} and P_d are determined by Eq. (5), Eq. (6), Eq. (16) and Eq. (18), respectively. As displayed in Table 1, each time average value of $P(t)$, P_{avg} and P_d shows a growth trend with the increase of AER, which is consistent with the literature that a high AER corresponds to a high P value when C_{out} is higher than C_{in} [27], but for P_{est}. In addition, the average values of P_{avg} in the four size segments are gradually approaching that of P_{est} as AER is increasing. Moreover, $P(t)$ at an AER of 3.70 h^{-1}, P_d at AERs of more than 1.20 h^{-1} and all the P_{est} values are greater than 1. Comparing with other P values in the four size segments, P_d has a large error while the largest error occurs at $P(t)$ at 3.70 h^{-1}.

Table 1

Time average and standard deviation of $P(t)$, P_{avg}, P_{est} and P_d in four size segments respectively.

AER (h^{-1})	Size segment (nm)	$P(t)$	$\pm SD$	P_{avg}	$\pm SD$	P_{est}	$\pm SD$	P_d	$\pm SD$
0.31	69-100	0.19	0.05	0.20	0.01	4.85	0.14	0.59	0.21
	100-200	0.18	0.05	0.18	0.01	5.53	0.21	0.50	0.25
	200-300	0.20	0.06	0.18	0.01	4.98	0.17	0.70	0.27
	300-500	0.20	0.07	0.20	0.03	4.61	0.46	1.02	0.56
	Total average	0.19	-	0.19	-	4.99	-	0.70	-
1.20	69-100	0.56	0.30	0.45	0.01	3.16	0.05	1.12	0.32
	100-200	0.56	0.30	0.45	0.02	3.04	0.12	1.10	0.34
	200-300	0.54	0.32	0.43	0.01	2.75	0.06	1.05	0.37
	300-500	0.57	0.33	0.46	0.05	2.87	0.29	1.12	0.37
	Total average	0.56	-	0.45	-	2.95	-	1.10	-
3.70	69-100	1.37	0.85	0.75	0.04	1.72	0.08	0.99	0.30
	100-200	1.46	0.86	0.75	0.03	1.94	0.07	1.07	0.32
	200-300	1.52	0.83	0.77	0.03	1.91	0.07	1.13	0.34
	300-500	1.67	1.08	0.77	0.05	1.82	0.11	1.26	0.41
	Total average	1.50	-	0.76	-	1.85	-	1.11	-

4.3.3 Observed and estimated indoor concentration

In Fig. 4, the dotted curves present the observed indoor concentration and the estimated concentrations from $P(t)$, P_{avg}, P_{est} and P_d at 0.31 h^{-1}, 1.20 h^{-1} and 3.70

h^{-1}, respectively. The curve using the P_{est} value clearly deviates from the observed concentration. It means the time-corrected P_{est} has a large error, while the real-time $P(t)$, the size-dependent P_{avg} and the direct-derived P_d are much closer to the expected value. Additionally, the change trend of the curves, growth, maintenance and decline, is summarized in Table 2, referring to $C_{out} > C_{in}$, $C_{out} = C_{in}$ and $C_{out} < C_{in}$, respectively, which are consistent with the results [27].
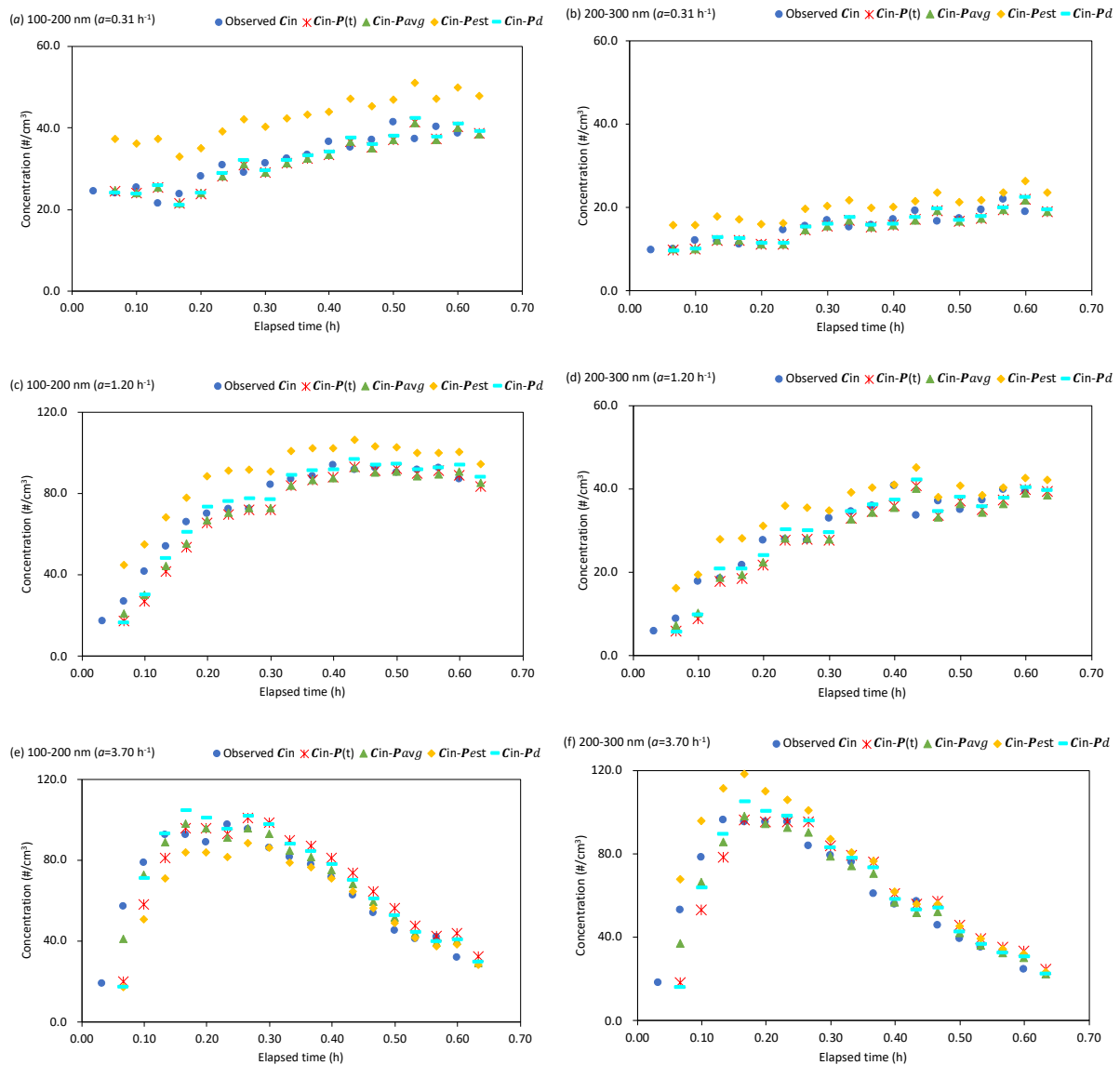
Fig. 4 Comparison of observed indoor concentration and the estimated concentrations from different P values. (a) a = 0.31 h^{-1} for 100-200 nm, (b) a = 0.31 h^{-1} for 200-300 nm, (c) a = 1.20 h^{-1} for 100-200 nm, (d) a = 1.20 h^{-1} for 200-300 nm, (e) a = 3.70 h^{-1} for 100-200 nm and (f) a = 3.70 h^{-1} for 200-300 nm.

Table 2

Change trend of indoor concentration at different AERs

AER (h^{-1})	Growth	Maintenance	Decline
0.31	+	-	-
1.20	+	+	-
3.70	+	+	+

Note: "+" represents yes; "-" represents no.

4.4 Discussion

4.4.1 Correction coefficient r value and its time limit

In the case of $C_{in} \neq 0$, Eq. (16) gives the theory relationship between P_{est} and P_{avg}. Numerically, the two values gradually approach each other as AER increases (see Table 1). In Eq. (16) there are two terms, "$\frac{1}{r}$" and "$\frac{a+k}{a} \cdot \frac{C_{in}(0)}{C_{out}(0)}$". In the laboratory simulation, the initial concentration can be seen as a constant, and the value of "a" ranges from 0.31 h^{-1} to 3.70 h^{-1} with k being negligible compared to the increased AER. Therefore, "$\frac{a+k}{a}$" tends to 1 with the increases of AER and the term "$\frac{a+k}{a} \cdot \frac{C_{in}(0)}{C_{out}(0)}$" has little effect on the value P_{est}. In the term "$\frac{1}{r}$", r plays an important role. As shown in Table 3, the correction coefficient r for different size segment at different AER values will have similar maximum and minimum. Generally, correction coefficient r values are all less than 1, ranging from 0.006 to 0.737. Therefore, the estimated-P_{est} is around 1.37-167 times larger than the size-dependent P_{avg}.

Table 3 The maximum and minimum of correction coefficient **r**

AER (h^{-1})	0.31		1.20		3.70	
Size Range (nm)	Max	Min	Max	Min	Max	Min
69-100	0.103	0.006	0.328	0.021	0.734	0.061
100-200	0.100	0.006	0.325	0.020	0.733	0.061
200-300	0.102	0.006	0.327	0.021	0.734	0.061
300-500	0.110	0.006	0.334	0.021	0.737	0.062

Fig. 3 presents the r value with the size range of 69-100 nm, indicating the larger the AER, the shorter the required time for the "r" value to reach 0.99. Table 4 displays the other size segments. Generally, the averaged required time at each

AER is 18.7 hours (0.31 h^{-1}), 5.7 hours (1.20 h^{-1}), and 2.4 hours (3.70 h^{-1}), respectively. After the required time, r will not play a role between P_{est} and P_{avg}. Eq. (16) changes to,

$$P_{est} = P_{avg} + \frac{a+k}{a} \cdot \frac{C_{in}(0)}{C_{out}(0)} \tag{23}$$

The relationship between P_{est} and P_{avg} is completely related to the term "$\frac{a+k}{a} \cdot \frac{C_{in}(0)}{C_{out}(0)}$", and as the AER value increases, it depends only on the fixed initial concentration. And in the case of C_{in} =0, Eq. (23) changes to

$$P_{est} = P_{avg} \tag{24}$$

Table 4 The time required for r to reach 0.99 (Unit: h)

Size segment (nm)	AER (h^{-1})		
	0.31	1.20	3.70
69-100	19.0	6.0	1.8
100-200	19.6	5.6	2.6
200-300	18.6	5.6	2.6
300-500	17.6	5.6	2.6
Average	18.7	5.7	2.4

Therefore, the time correction under the effect of the correction coefficient r is of little significance due to the simulated ideal experimental conditions in the laboratory, including the good airtightness of the experimental chamber, the mild testing environment, and the controllable particle concentration and ventilation power. In this case, the controllable concentration ratio of the indoor and the outdoor results in the averaged concentrations being similar to the real-time ones. In contrast, it can be speculated that P_{est} could become necessary for the system if the outdoor concentration is much higher than the indoor one, or if there is a large AER (i.e. $a \gg 3.70$ h^{-1}), but further demonstration it still needed.

4.4.2 The estimated indoor concentration at an estimated P value

Fig. 4 gives the comparison between the estimated values at different P and the observed indoor concentration. The concentration model in Eq. (21) is time

dependent. The interval time Δt and the indoor and outdoor concentrations at time t, C_{in} (t) and C_{out} (t), jointly determine the tendency of the concentration change. Visually, the estimated concentrations at P(t), P_{avg}, and P_d are in good agreement with the observed ones compared to the concentration at P_{est}: (1) P(t) is a series of time-dependent values determined by Eq. (5). In the P(t) series, the values corresponding to each time t well reflect the real-time penetration situation, thus obtaining a curve close to the observed concentration; (2) P_{avg} in Eq. (6) is an average value from the time-averaged indoor and outdoor concentrations ($C_{in, avg}$ and $C_{out, avg}$), representing the penetration ratio of each particle size in an average time of 36 minutes. Numerically, it is a series that changes with particle size and does not vary by time. However, the curves in Fig. 4 are fitting well with the actual observed concentrations, illustrating that the average value can reflect the penetration situation in a short-term evaluation of at least 36 minutes. Additionally, outdoor concentration in the laboratory simulation is controlled, the experimental chamber has good air tightness and the AER value is preset. Therefore, there are no drastic changes in concentrations from complex conditions such as turbulence or air leakage. In this case, the error between the average concentration and the real-time concentration is similar so that the fitting results are approximate; (3) P_{est} is the theoretical time-corrected value of P_{avg} because P_{avg} is lacking time-varying characteristics. However, Fig. 4 displays that the estimated concentration has a large error at P_{est}. As described in the previous Sec. 4.1, the error of P_{est} originates from the correction coefficient r. Eq. (15) shows that "r" is a strongly time-dependent parameter, and the minimum action time is 1.8 hours at 69-100 nm with the experimental setting of the maximum AER (3.70 h^{-1}). Therefore, the error of P_{est} exists in the whole experimental process due to the current laboratory simulation only being 36 minutes long. In addition, the P_{avg} value is similar to the expected value, and the time attribute is not significant in this experiment due to the small change in concentrations. In this case, further correction on P_{avg} may bring more errors; (4) P_d in Eq. (18) is

derived visually from the ratio of C_{in}(t) and C_{out}(t), ignoring deposition rate k and introducing real-time t. The ignored k value indicates that the deposition portion is negligible compared to the increased AER in the present laboratory penetration simulation. The result agrees with those in previous studies of the literature [13, 25, 29, 32-36]. Rim et al (2010) found for smaller UFP (d_p < 30 nm) the loss due to deposition is substantially higher than that due to AER, and deposition rate k usually decreases to less than 0.1 h^{-1} at a particle size of more than 100 nm [33]. Additionally, both P(t) and P_{avg} originate from Eq. (4) and this equation has set "C_{in} (0) = 0" as a prerequisite while P_{est} in Eq. (16) and P_d in Eq. (18) include the condition of "C_{in} (0) ≠ 0". It can be considered that P_{est} in Eq. (16) and P_d in Eq. (18) are the corrections of the default item of the initial indoor concentration.

4.4.3 Error analysis and selection of the optimal penetration factor

Table 5 gives the relative errors between the estimated results at different penetration values and the observed indoor concentrations. Generally, the minimal relative errors from P(t), P_{avg} and P_d occur at the AER as 0.31 h^{-1} are approximate. Taking the segment of 100-200 nm as an example, the error ranges (%) are (-15.1 to 18.5) for P(t), (-14.8 to 19.0) for P_{avg} and (-14.3 to 21.4) for P_d, respectively. As the AER increases, the errors from P(t) and P_d increase, for example, (-65.3 to 38.7) for P(t) and (-69.6 to 29.3) for P_d at the AER as 3.70 h^{-1}, and the large errors are mainly concentrated in the early period around 0.233 hours.

In terms of P values, Table 1 shows the average and standard deviation of P(t), P_{avg}, P_{est} and P_d in four size segments, respectively. A large standard deviation indicates that the variation of P value in the size segment fluctuates greatly over 36 minutes, with the largest errors appearing on P(t) at the AER of 3.70 h^{-1}. P(t) in Eq. (5) contains two terms, "$\frac{a+k}{a}$" and "$\frac{C_{in}(t)}{C_{out}(t)}$". For the first term "$\frac{a+k}{a}$", it has reported that deposition rate k usually < 0.1 h^{-1} as d_p > 100 nm and k < 0.25 h^{-1} as

$d_p < 100$nm [33-34], so the term is around 1 to 2 (AER ranges from 0.30 h^{-1} to 3.70 h^{-1}). As we can see in Table 1, the values of P(t) is greater than 1 at a large AER of 3.70 h^{-1} with the term "$\frac{C_{in}(t)}{C_{out}(t)}$" making the main contribution to the value of P(t). Based on the experimental basis [27], the curve of indoor concentration shows three trends during 36 minutes at the three different settings of AERs (Table 2). Before the decline, the curve of growth and maintenance last 0.233 h (first 14 minutes) at the AER of 3.70 h^{-1}, that is, P(t) can only be ensured ranging from 0 to 1 before the occurrence of "$C_{out} < C_{in}$". Additionally, the real-time value is greater than 1, indicating that the indoor concentration is already higher than outdoor and P(t) is no longer applicable for evaluation. Different with P(t), the AER "a" and the time attribute "t", contained in the term "$\frac{1}{at}$", gives the main contribution to the P_d value. As shown in Table 1, P_d indicates a higher value than other three P values at a small AER of less than 1.20 h^{-1}, but the relative errors between the estimated results at P_d and the observed concentrations are similar to P(t) and P_{avg} in Table 5; while in the later period (last 22 minutes) and at a large AER of more than 1.20 h^{-1}, "a" and "t" corrected the deviation caused by the "$\frac{C_{in}(t)}{C_{out}(t)}$" term to some extent, but P_d values are greater than 1. Due to the term "$\frac{C_{in}(t)}{C_{out}(t)}$" being included by P(t) and P_d, the observed indoor concentration at the beginning of the experiment is much lower than the outdoor one, so that both P(t) and P_d values are lower. However, the low penetration values cannot reflect the actual situation of a large number of particles penetrating caused by a large AER and a large concentration difference at the initial time ("$\frac{C_{in}(0)}{C_{out}(0)}$" tends to zero). The concentrations estimated from P(t) and P_d therefore have more significant errors than the actual observed concentration in the early period prior to 0.233 hours, especially when the AER is more than or equal to 1.20 h^{-1} (Table 5). Similarly, P_d in Eq. (18) including the term of "$\frac{C_{in}(0)}{C_{out}(0)}$" has insignificant

correction because the initial indoor concentration tends to zero in this study. Additionally, as described in Eq. (8), "$P_0 = 1$" was assumed under the ideal condition, indicating that those trapped particles do not detach and re-enter the outdoor compartment. However, the errors indicate that the assumed P_0 exists and the value of P_0 is less than 1, implying that detaching and re-entering are inevitable in the actual situation. Therefore, in a 36-minute penetration evaluation, both $P(t)$ and P_d are applicable to conditions where the AER is less than 1.20 h^{-1}, but they cannot be equal due to the different derivations. In addition, $P(t)$ can be also used for the late stage at the AER as 1.20 h^{-1}, and unlike "$\frac{1}{at}$" in P_d, "$\frac{a+k}{a}$" in $P(t)$ has a certain correction effect on the P value under the condition of AER less than 1.20 h^{-1}.

It is worth noting that the estimated result at P_{avg} has small errors among all the P values at each size segment and at each AER in Table 5. Like $P(t)$ in Eq. (5), the "$\frac{a+k}{a}$" term eliminates the effect from AER to some extent, and $C_{in, avg}$ and $C_{out, avg}$ in Eq. (6) eliminates the fluctuation of concentration changes at two adjacent times (i.e. 0.033 h and 0.067 h). Therefore, the estimation at P_{avg} is more stable than other values.

In contrast, the increase of the AER value tends to decrease the error from P_{est}, i.e. from (13.5 to 74.2) at 0.31 h^{-1} to (-69.6 to 21.3) at 3.70 h^{-1}. Correction coefficient r brings a large error to P_{est}, resulting in a change trend that is negatively correlated with AER growth. Similarly, a large AER reduces the action time of the r value. In addition, the overall P_{est} value far exceeding 1 indicates its inapplicability in the 36-minute evaluation. Similar to P_d in Eq. (18), P_{est} in Eq. (16) includes the condition of "$C_{in}(0) \neq 0$" and is insignificant for the correction of P_{avg} due to a low ratio of "$\frac{C_{in}(0)}{C_{out}(0)}$" in this study, and may even cause large errors. Additionally, for systems with large indoor and outdoor concentration changes or an existing large AER (i.e. $a > 3.70$ h^{-1}), whether or not the error caused by P_{est} would decrease still needs further demonstration.

Table 5

Relative errors between estimated results at different penetration values and observed concentrations

Size segment (nm)		100-200				200-300			
t	AER	$P(t)$	P_{avg}	P_{est}	P_d	$P(t)$	P_{avg}	P_{est}	P_d
h	h^{-1}	%	%	%	%	%	%	%	%
0.033		-	-	-	-	-	-	-	-
0.067		2.2	2.8	55.7	1.0	-1.8	-0.9	56.5	-3.1
0.100		-5.7	-5.2	42.8	-5.4	-17.4	-16.7	30.0	-16.6
0.133		18.5	19.0	74.2	21.4	1.5	2.0	49.2	7.4
0.167		-10.1	-9.5	38.4	-11.6	8.1	8.5	55.4	13.9
0.200		-15.1	-14.8	24.8	-14.3	-0.2	0.2	44.7	3.4
0.233		-9.3	-9.2	26.1	-6.5	-24.2	-23.9	10.4	-22.2
0.267		6.6	6.7	44.8	10.2	-4.9	-4.9	27.4	-0.4
0.300		-7.5	-7.3	28.4	-5.5	-9.0	-9.1	19.4	-4.8
0.333	0.31	-3.3	-3.3	30.4	-0.9	11.5	11.2	42.7	16.5
0.367		-2.4	-2.4	30.1	0.0	-2.5	-2.7	27.1	0.9
0.400		-9.1	-9.2	19.9	-7.0	-7.9	-8.1	18.9	-4.9
0.433		4.3	4.1	33.7	7.0	-11.1	-11.4	11.9	-8.1
0.467		-5.3	-5.5	22.0	-3.2	15.1	14.6	41.0	19.0
0.500		-10.2	-10.4	13.5	-8.1	-4.4	-4.6	21.5	-2.0
0.533		11.1	10.7	37.2	13.9	-9.9	-10.2	12.1	-7.6
0.567		-7.5	-7.8	17.1	-5.8	-11.5	-11.9	7.4	-9.1
0.600		4.4	4.1	29.2	6.5	15.4	14.8	38.0	18.4
0.633		-	-	-	-	-	-	-	-
0.033		-	-	-	-	-	-	-	-
0.067		-36.2	-22.9	67.2	-38.7	-33.9	-18.1	80.9	-36.6
0.100		-35.6	-27.5	32.3	-26.7	-49.8	-42.2	9.8	-43.9
0.133		-22.9	-17.9	26.8	-10.5	-4.3	1.0	50.8	12.7
0.167		-18.7	-15.9	18.0	-7.4	-14.8	-10.8	29.7	-3.8
0.200		-6.3	-4.3	26.6	4.8	-21.6	-19.1	11.7	-13.3
0.233		-3.8	-2.3	26.2	5.5	-0.7	0.4	28.8	8.6
0.267		-0.6	0.4	26.6	7.4	0.8	1.5	27.7	8.6
0.300		-14.5	-13.8	7.5	-8.7	-15.7	-15.4	5.4	-10.4
0.333	1.20	-3.8	-3.9	15.5	1.9	-4.9	-5.4	13.1	0.4
0.367		-1.8	-2.2	15.6	3.3	-3.8	-4.7	11.8	0.8
0.400		-6.3	-6.9	8.7	-2.1	-11.8	-13.0	0.2	-8.2
0.433		1.7	0.8	15.9	5.8	20.9	18.7	33.6	25.1
0.467		-1.4	-2.6	11.3	1.8	-9.3	-10.6	2.1	-6.7
0.500		2.1	0.6	13.7	5.0	5.9	3.8	16.2	8.5
0.533		-2.0	-3.3	9.1	0.6	-5.8	-7.7	3.2	-3.9
0.567		-1.8	-3.5	7.8	0.2	-6.4	-8.6	0.9	-4.9
0.600		2.1	4.0	15.1	7.9	1.3	-1.2	8.0	2.7
0.633		-	-	-	-	-	-	-	-
0.033	3.70	-	-	-	-	-	-	-	-

0.067	-65.3	-27.8	-69.6	-69.6	-65.4	-30.0	28.6	-69.7
0.100	-26.1	-7.5	-35.4	-9.4	-32.4	-15.2	22.7	-18.0
0.133	-12.6	-4.1	-23.6	0.4	-18.7	-10.8	15.9	-7.0
0.167	3.6	6.1	-9.3	13.5	0.9	2.7	24.0	10.4
0.200	7.9	7.7	-5.5	13.9	-0.1	-1.2	15.4	5.5
0.233	-4.6	-6.4	-16.3	-2.0	0.2	-2.9	11.0	3.0
0.267	6.0	0.8	-7.1	7.0	13.7	7.9	20.2	14.7
0.300	14.1	7.5	-0.1	13.4	5.4	-0.9	9.3	4.7
0.333	10.2	3.8	-3.5	8.1	4.8	-2.3	6.5	2.8
0.367	11.4	4.4	-2.1	8.2	24.8	16.0	25.9	21.1
0.400	13.2	5.0	-1.1	8.9	9.2	2.0	11.4	5.0
0.433	17.9	9.1	3.2	12.7	-2.5	-9.5	-1.8	-6.9
0.467	19.0	9.7	4.2	13.0	25.5	14.9	22.5	19.1
0.500	24.0	14.0	8.3	17.0	15.8	7.0	15.2	9.3
0.533	15.6	6.9	1.2	8.6	11.9	3.3	11.3	5.1
0.567	1.2	-6.6	-11.5	-5.4	5.9	-2.8	3.9	-0.9
0.600	38.7	25.9	21.3	29.3	36.1	23.8	30.7	26.9
0.633	-	-	-	-	-	-	-	-

4.5 Conclusion

This work proposes four numerical calculations of penetration factor to select the optimal value. In addition, a widely used concentration model is employed to evaluate the penetration process of aerosols from a confined source space to an uncontaminated area within 36 min, and the following conclusions can be applied to the invasion evaluation of virus-containing aerosols.

During the 36-minute penetration process in this study, the proposed correction coefficient r has its own time limit if time-correction is necessary under some non-ideal condition. Moreover, the time limit gets shorter as the AER increases. According to the present experimental design, it ranges averagely from 2.4 h (3.70 h^{-1}) to 18.7 h (0.31 h^{-1}).

Additionally, size-dependent P_{avg} is time-corrected to be P_{est} by the correction coefficient r. However, the time correction is of little significance due to the simulated ideal experimental conditions in the laboratory within the current experimental 36 min. P_{est} was assumed to be necessary for the system if the

confined source space has a much higher initial concentration than the indoor one or there is a large AER (i.e. $a \gg 3.70$ h^{-1}), but it still needs further demonstration.

The error analysis of the real-time $P(t)$ and the direct-derived P_d proves that the assumed P_0 exists and the value of P_0 is less than 1 in the actual situation, indicating that detaching and re-entering are inevitable. Both of them are only suitable for rough evaluation in the case of AER less than 1.20 h^{-1} and $P(t)$ is also applicable to the later stage when the AER is equal to 1.20 h^{-1}. Additionally, the size-dependent P_{avg} is the optimal value among the four under current experimental conditions, due to minimal effect from the AER value and fluctuations in concentration.

References

[1] Morawska, L, Cao, J, 2020. Airborne transmission of SARS-CoV-2: the world should face the reality. Environ. Int. 139, 105730.

[2] Bourouiba, L, 2020. Turbulent gas clouds and respiratory pathogen emissions: potential implications for reducing transmission of COVID-19. JAMA 323 (18), 1837–1838.

[3] Cao, Q, Chen, Y C, Chen, C L, Chiu, C H, 2020. SARS-CoV-2 infection in children: transmission dynamics and clinical characteristics. J. Formos. Med. Assoc. 119 (3), 670–673.

[4] Zhao, B, Liu, Y, Chen, C, 2020. Air purifiers: a supplementary measure to remove airborne SARS-CoV-2. Build. Environ. 177, 106918.

[5] Sobral, M F F, Duarte, G B, da Penha Sobral, A I G, Marinho, M L M, de Souza Melo, A, 2020. Association between climate variables and global transmission of SARS-CoV-2. Sci. Total Environ. 729, 138997.

[6] Correia, G, Rodrigues, L, Gameiro da Silva, M, Gonçalves, T, 2020. Airborne route and bad use of ventilation systems as non-negligible factors in SARS-CoV-2 transmission. Med. Hypotheses 141, 109781.

[7] van Doremalen, N, Bushmaker, T, Morris, D H, et al., 2020. Aerosol and surface stability of SARS-CoV-2 as compared with SARS-CoV-1. N. Engl. J. Med. 382 (16), 1564–1567.

[8] Zhuo, M, Ma, S, Li, G, Yu, Y, An, T, 2019. Chlorinated paraffins in the indoor and outdoor atmospheric particles from the Pearl River Delta: characteristics, sources, and human exposure risks. Sci. Total Environ. 650 (Pt 1), 1041–1049.

[9] Cao, Z, Wang, M, Chen, Q, Zhu, C, Jie, J, Li, X, Dong, X, Miao, Z, Shen, M, Bu, Q, 2019. Spatial, seasonal and particle size dependent variations of PAH contamination in indoor dust and the corresponding human health risk. Sci. Total Environ. 653, 423–430.

[10] Xu, H, Guinot, B, Cao, J, Li, Y, Niu, X, Ho, K F, Shen, Z, Liu, S, Zhang, T, Lei, Y, Zhang, Q, Sun, J, Gao, J, 2018. Source, health risk and composition impact of outdoor very fine particles (VFPs) to school indoor environment in Xi'an, Northwestern China. Sci. Total Environ. 612, 238–246.

[11] Azuma, K, Ikeda, K, Kagi, N, Yanagi, U, Osawa, H, 2018. Physicochemical risk factors for building-related symptoms in air-conditioned office buildings: ambient particles and combined exposure to indoor air pollutants. Sci. Total Environ. 616–617, 1649–1655.

[12] Morawska, L, Ayoko, G A, Bae, G N, Buonanno, G, Chao, C Y H, Clifford, S, Fu, S C, Hanninen, O, He, C, Isaxon, C, Mazaheri, M, Salthammer, T, Waring, M S, Wierzbicka, A, 2017. Airborne particles in indoor environment of homes, schools, offices and aged care facilities: the main routes of exposure. Environ. Int. 108, 75–83.

[13] Chao, C Y H, Wan, M P, Cheng, E C K, 2003. Penetration coefficient and deposition rate as a function of particle size in non-smoking naturally ventilated residences. Atmos. Environ. 37 (30), 4233–4241.

[14] Chatoutsidou, S E, Maskova, L, Ondrackova, L, Ondracek, J, Lazaridis, M, Smolik, J, 2015. Modeling of the aerosol infiltration characteristics in a cultural heritage building: the Baroque Library Hall in Prague. Build. Environ. 89, 253–263.

[15] Cong, X C, Zhao, J J, Jing, Z, Wang, Q G, Ni, P F, 2018. Indoor particle dynamics in a school office: determination of particle concentrations, deposition rates and penetration factors under naturally ventilated conditions. Environ Geochem Hlth 40, 2511–2524.

[16] Hu, Y J, Bao, L J, Huang, C L, Li, S M, Liu, P, Zeng, E Y, 2018. Exposure to air particulate matter with a case study in Guangzhou: is indoor environment a safe haven in China? Atmos. Environ. 191, 351–359.

[17] Hussein, T, 2017. Indoor-to-outdoor relationship of aerosol particles inside a naturally ventilated apartment - a comparison between single-parameter

analysis and indoor aerosol model simulation. Sci. Total Environ. 596, 321–330.

[18] Lai, D, Karava, P, Chen, Q, 2015. Study of outdoor ozone penetration into buildings through ventilation and infiltration. Build. Environ. 93, 112–118.

[19] Liu, C, Yang, J, Ji, S, Lu, Y, Wu, P, Chen, C, 2018. Influence of natural ventilation rate on indoor PM2.5 deposition. Build. Environ. 144, 357–364.

[20] Zhao, H, Gall, E T, Stephens, B, 2019. Measuring the building envelope penetration factor for ambient nitrogen oxides. Environ Sci Technol 53 (16), 9695–9704.

[21] Wang, X, Gao, Z, Yang, J, Yang, X, 2019. In situ investigation on linkage between particle penetration and air exchange through building envelope. Int. J. Vent. 18 (4), 233–245.

[22] Chen, C, Zhao, B, 2017. A modified Brownian force for ultrafine particle penetration through building crack modeling. Atmos. Environ. 170, 143–148.

[23] Lai, A C K, Nazaroff, W W, 2000. Modeling indoor particle deposition from turbulent flow onto smooth surfaces. J. Aerosol Sci. 31 (4), 463–476.

[24] Li, A, Ren, T, Yang, C, Lv, W, Zhang, F, 2017. Study on particle penetration through straight, L, Z and wedge-shaped cracks in buildings. Build. Environ. 114, 333–343.

[25] Liu, D L, Nazaroff, W W, 2001. Modeling pollutant penetration across building envelopes. Atmos. Environ. 35 (26), 4451–4462.

[26] Lv, Y, Wang, H F, Wei, S, Wu, T, Liu, T, Chen, B, 2018. The experimental study on indoor and outdoor penetration coefficient of atmospheric fine particles. Build. Environ. 132, 70–82.

[27] Wang, W, Kato, N, Kimoto, S, Matsui, Y, Yoneda, M, 2020. Simulation and evaluation of sheltering efficiency of houses equipped with ventilation systems. Build. Environ. 168, 106491.

[28] Thatcher, T L, Lunden, M M, Revzan, K L, Sextro, R G, Brown, N J, 2003. A concentration rebound method for measuring particle penetration and

deposition in the indoor environment. Aerosol Sci. Technol. 37 (11), 847–864.

[29] Thornburg, J, Ensor, D S, Rodes, C E, Lawless, P A, Sparks, L E, Mosley, R B, 2001. Penetration of particles into buildings and associated physical factors. Part I: model development and computer simulations. Aerosol Sci. Technol. 34 (3), 284–296.

[30] Nazaroff, W W, 2004. Indoor particle dynamics. Indoor Air 14, 175–183.

[31] Rim, D, Wallace, L A, Persily, A K, 2013. Indoor ultrafine particles of outdoor origin: importance of window opening area and fan operation condition. Environ Sci Technol 47 (4), 1922–1929.

[32] Long, C M, Suh, H H, Catalano, P J, Koutrakis, P, 2001. Using time- and size-resolved particulate data to quantify indoor penetration and deposition behavior. Environ Sci Technol 35 (10), 2089–2099.

[33] Rim, D, Wallace, L, Persily, A, 2010. Infiltration of outdoor ultrafine particles into a test house. Environ. Sci. Technol. 44, 5908–5913.

[34] Okuyama, K, Kousaka, Y, Yamamoto, S, Hosokawa, T, 1986. Particle loss of aerosols with particle diameters between 6 and 2000 nm in stirred tank. J. Colloid Interface Sci. 110, 214–223.

[35] Vette, A F, Rea, A W, Lawless, P A, Rodes, C E, Evans, G, Highsmith, V R, Sheldon, L, 2001. Characterization of indoor-outdoor aerosol concentration relationships during the Fresno PM exposure studies. Aerosol Sci. Technol. 34 (1), 118–126.

[36] Wallace, L A, Emmerich, S J, Howard-Reed, C, 2004. Effect of central fans and in-duct filters on deposition rates of ultrafine and fine particles in an occupied townhouse. Atmos. Environ. 38 (3), 405–413.

Chapter 5. A Review of Indoor Particles: Behavior and Ventilation Technology

Generally, the existence of indoor particles generally has two origins: (1) outdoor source. As mentioned in previous chapters, the particles enter rooms by ventilation, penetration or infiltration; (2) Indoor source. Cooking, smoking, burning, and using candles or incense make the particles present indoors.

5.1 Indoor behavior of aerosol particles

Regardless of whether the particles originate from the outdoors or are generated indoors, the particles in the room typically settle on the ground, adsorb on the surface (walls, ceilings, furniture and other objects), coagulate into large particles or decompose into small particles, and resuspend in the air under a certain condition. In this section, research of deposition and coagulation are reviewed.

5.1.1 Deposition rate

As early as 1940s, Canadian scientists Langstroth and Gillespie used the smoke chamber to study the aging process of ammonium chloride smoke in controlled turbulence and still air, and used hypothetical equations to quantitatively describe the loss of various surfaces, and also analyzed the separation of condensation and surface effects [1].

Based on the experimental result, Corner and Pendlebury theoretically proved the consistency with the empirical constants proposed by Langstroth and Gillespie, and the formula of deposition rate for a cubical vessel was given as [2],

$$\beta = \frac{1}{L}\left[\frac{8\sqrt{k_e D}}{\pi} + v coth\left(\frac{\pi v}{4\sqrt{k_e D}}\right)\right] \tag{1}$$

Hereafter, Crump and Seinfeld (1981) started from the assumption of a sphere, then derived a general formula suitable for an arbitrary vessel by fully considering the boundary layer thickness [3].

$$\beta = \frac{1}{V} \int_{\Sigma} \frac{v\boldsymbol{n}(x)\cdot\boldsymbol{k} \ dA(x)}{exp\left[\dfrac{\pi v\boldsymbol{n}(x)\cdot\boldsymbol{k}}{(n\,sin\frac{\pi}{n})^{n}\sqrt{k_eD^{n-1}}}\right]-1} \tag{2}$$

Actually, (2) is the general formula of (1).

Okuyama et al. (1986) studied deposition loss in a stirred tank under various stirring intensities using three types of monodisperse uncharged particles as research objects, NaCl, DEHS (diethylhexyl sebacate), and polystyrene latex particles [4]. The experiment illustrated that the deposition rate constant of the particles strongly depends on the particle size and turbulence intensity, and in the case of "particle diameter greater than about 0.35 um and energy dissipation rate greater than about 10^3 cm^2 / s^3", the inertia of the particles will increase the deposition rate. In addition, the theory of Crump and Seinfeld (1981) can explain the present study well. Also, the deposition rate constants obtained from batch reactor experiments are suitable for particle loss assessment in continuous stirred tank reactors.

Shimada et al. (1989) further demonstrated the dependence of the deposition rate on particle size and turbulence intensity, and used the model to explain the increase in deposition rate due to particle inertia [5].

Thatcher et al. (2002) used particles with an aerodynamic diameter of 0.5-10 μm as a source to reveal the effect of furniture placement and air velocity on the deposition rate [6]. The indoor surface area increased due to the placement of furniture, increasing the deposition loss rate, especially for small particles. Similarly, increasing the indoor fan speed to increase the air speed has a greater impact on large particles.

14 houses were selected under two different ventilation conditions, and the particle deposition rate and PM2.5 concentration of cooking in the size range of 0.015 to 6mm with time were investigated by He et al. (2005) [7]. The results show that the deposition rate of particles in the size range of 0.2 to 0.3mm is the lowest when the air exchange rate is less than $3.00 \pm 1.23 h^{-1}$. Ventilation conditions have a significant effect on the deposition rate of particles ranging from 0.08 to 1.0 mm. Comparing to the two removal mechanisms of ventilation and deposition, particle coagulation is negligible.

Afshari and Reinhold (2008) revealed surface material has effect on deposition rate, especially for UFP and large particles of 10μm in diameter, while particles with sizes of 0.3-0.5μm showed less deposition. However, the effect of surface properties is less than that of particle size [8].

Lee. et al (2014) estimated the size-resolved ultra-fine and sub-micron particles at the air exchange rate (ACH) of 0.61–1.24 h^{-1} in the non-source period after reaching a steady state for 2 hours after the controlled source period [9]. The results prove that the particle deposition is highly correlated with the size, and the effect of air exchange on the particle deposition is negligible under the enhanced air mixing caused by the fan, but there are still potential effects.

Wang et al. (2017) studied the effect of relative humidity (RH) on the deposition of silica nanoparticles [10]. The results show that both low and high RH generally tend to increase the deposition rate, but the effect of RH on the deposition rate is related to particle size. As the RH increases, the deposition rate of particles with a particle size (d_p) < 70 nm decreases, while the deposition rate of particles with d_p > 70 nm increases.

Kim et al. (2019) illustrates the effects of various factors on indoor PM deposition and removal efficiency, including flow rate, flow direction, and relative humidity (RH) [11]. Experiments show that the highest PM deposition rate is under the conditions of humid and upward wind with the fan RPM of 150.

5.1.2 Coagulation

Xu et al. (1994) utilized a room equipped with an exhaust hood and a high efficiency particulate aerosol (HEPA) filter air cleaner and experimentally investigated the deposition mechanism of tobacco particles indoors at different ventilation rates [12]. The experimental results showed that the coagulation phenomenon occurs when the particle size is less than 0.25um, and large particles with diameters of 0.25-0.5μm can be formed; while the large particles above 0.5um will not coagulate. In addition, calculations conducted during the 10 hours after smoking a cigarette indoors, and it showed that particles with a mass fraction of 22% will be deposited on the surface at 0.03 ACH, 6% at 0.5 ACH, and 3% at 1 ACH.
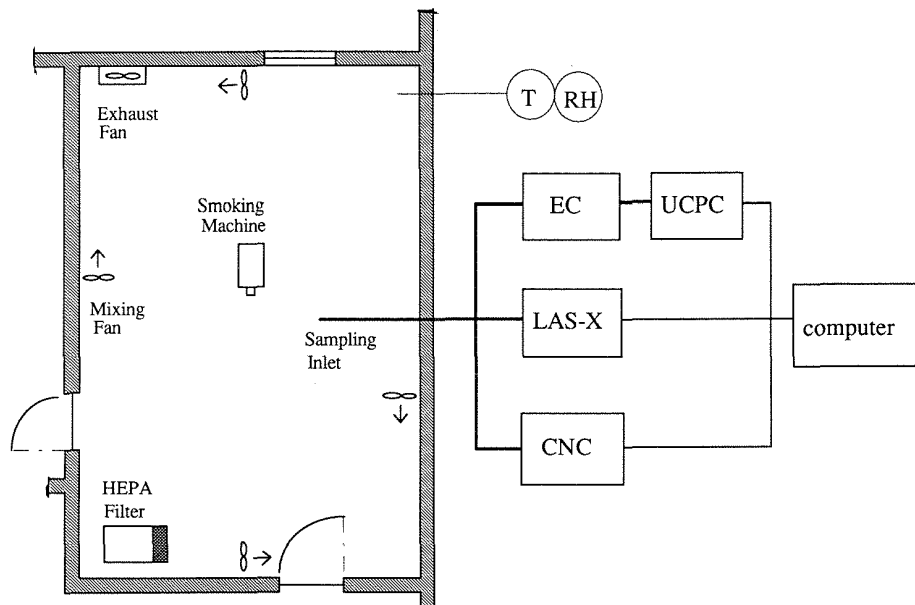
Fig 1. Schematic drawing of the experimental room and measurement system. The room located in a two-floor building has a size of 4.56 x 3.38 x 2.37 m high. T = temperature probe; RH = relative humidity probe; EC = electrostatic classifier; UCPC = ultrafine condensation particle counter; LAS-X = laser aerosol spectrometer; CNC = condensation nucleus counter. The arrows show the fan-driven air flow direction.

Seipenbusch et al. (2008) conducted an environmental chamber to simulate the changing mechanism of nanoparticle aerosols in the workplace from the release to the receptor [13]. The results showed that the nanoparticles changed their size and number concentration by coagulating or by interacting with the background

aerosols. It depends on the concentration, particle size and number concentration of nanoparticles and background aerosols. In addition, due to the different types of aerosol background, there is also the possibility of forming secondary particles through chemical reactions.

Simulation experiments of continuous injection and mixing of particles were established for the study of particle coagulation. A conclusion was given as, the only relevant mechanism for controlling the size distribution is coagulation when particle sizes range from 70 nm to 250 nm [14-15].

Wang et al. (2017) revealed the effect of relative humidity (RH) on the coagulation of silica nanoparticles that low RH will cause electrostatic repulsion between particles, while high humidity increases the coagulation coefficient due to the strong adhesion between the particles [10].

Xiao et al. (2019) investigated the surface deposition and condensation of indoor particles above 0.25μm in diameter using a room-sized chamber at different temperatures [16]. The result showed that deposition rates and coagulation coefficients increase as air temperature and mixing intensity rise. Coagulation shortens the concentration decay time of indoor particles, and particles of 0.25–0.5 μm are more likely to coagulate than those of larger sizes.

5.2 Indoor particles under ventilation mode

Indoor particles will increase the risk of exposure for residents living indoors, especially the risk of respiratory exposure. Ventilation is the main method of removing indoor particles, especially indoor mechanical ventilation in modern society. The Japanese Building Standards Law (BSL) requires the installation of mechanical ventilation equipment and guarantees "24-hour continuous ventilation" to reduce the risk of building syndromes.

In previous literatures, ventilation system usually has two functions, purifying the indoor air and preventing outdoor particles from entering. Park et al. (2014)

had proved that mechanical ventilation is efficient for removal of indoor particles [17].

Additionally, most research on ventilation system are concentrated in removal efficiency by filters. Azimi et al. (2014) collected 194 outdoor particle size distributions (PSD) in the literature to estimate the removal efficiency of HVAC filters for outdoor $PM_{2.5}$ and UFP [18]. The results prove that a positive correlation between MERV and removal efficiency of outdoor $PM_{2.5}$ and UFP. Additionally, outdoor PSD and particle density have little effect on the removal efficiency of $PM_{2.5}$, but outdoor PSD and infiltration factors significantly affect the removal efficiency of UFP.

Chen et al. (2016) investigated indoor and outdoor particles in mechanically ventilated and air-conditioned buildings (ACMV) during and after the 2013 Haze in Singapore. The results indicated that air conditioners and mechanical ventilation systems equipped with MERV 7 filters can effectively improve the removal efficiency of particles larger than about 0.2 μm if I/O ratios are lower. But in extraordinary situations such as haze, it is still difficult to keep people from being exposed to high concentrations indoors.

Lv et al. (2018) used riboflavin particles as the indoor source and conducted a chamber to analyze the removal effect of indoor particles under two typical ventilation modes (ceiling exhaust and slit exhaust) [20]. The results show that the air exchange rate (ACH) is an important factor affecting the indoor particle concentration distribution, and having a linear relationship with the attenuation index. With the increase of ACH, slit exhaust mode on removing coarse particles is more significant.

On this basis, they added the joint influence of the walking behavior of the personnel and the ventilation mode, and further studied the transmission and removal of indoor particles [21]. They found that 1.0-3.0 μm particles have the fastest speed and the largest amount of suspension, while 0.5-1.0 μm particles are

the smallest suspended particles. In addition, the slit exhaust mode is higher than the ceiling ventilation mode.

The latest study from Chen et al. (2019), investigating removal efficiency of UFPs by 47 commercial filter media with 17 filter categories, provided references for selection of filter media and the assessment of human exposure to UFPs [22].

A similar one by Ruan and Rim (2019) selected two cities, Los Angeles and Beijing, to investigate the effect of outdoor ventilation flow and filtration efficiency of office buildings on indoor concentration of $PM_{2.5}$ and ozone [23]. The results show that the combination of the air handling unit filter and the outdoor air filter is more resistant to outdoor $PM_{2.5}$ pollution than a single filter, and the ventilation flow is high. In order to limit indoor $PM_{2.5}$ concentration to less than $35\mu g$ / m^3 in extreme outdoor air pollution in megacities, it is recommended to use high-efficiency filters greater than MERV 11 and reduced flow rate of less than 8.5 L / s per person.

References

[1] G. O. Langstroth and T. Gillespie. Coagulation and surface losses in disperse systems in still and turbulent air. Canadian Journal of Research, 25b (1947) 455-471

[2] J Corner and E D Pendlebury. The Coagulation and Deposition of a Stirred Aerosol. Proc. Phys. Soc. London Sect. B, 64 (1951) 645

[3] J.G Crump, J.H Seinfeld. Turbulent deposition and gravitational sedimentation of an aerosol in a vessel of arbitrary shape. J. Aerosol Sci., 12 (1981) 405

[4] K. Okuyama, Y. Kousaka, S. Yamamoto, T. Hosokawa. Particle loss of aerosols with particle diameters between 6 and 2000 nm in stirred tank. J. Colloid Interface Sci., 110 (1) (1986) 214-223

[5] M. Shimada, K. Okuyama and Y. Kousaka. Influence of particle inertia on aerosol deposition in a stirred turbulent flow field. J. Aerosol Sci., 20 (4) (1989) 419-129

[6] T.L. Thatcher, A.C. Lai, R. Moreno-Jackson, R.G. Sextro, W.W. Nazaroff. Effects of room furnishings and air speed on particle deposition rates indoors. Atmos. Environ., 36 (2002) 1811-1819

[7] C. He, L. Morawska, D. Gilbert. Particle deposition rates in residential houses. Atmos. Environ., 39 (21) (2005) 3891-3899

[8] A. Afshari and C. Reinhold. Deposition of fine and ultrafine particles on indoor surface materials. Indoor Built Environ 17 (2008) 247–251

[9] W. C. Lee, J. M. Wolfson, P. J. Catalano, S. N. Rudnick, and P. Koutrakis. Size-Resolved Deposition Rates for Ultrafine and Submicrometer Particles in a Residential Housing Unit. Environmental Science & Technology. 48 (17) (2014) 10282-10290

[10] Y. Wang, L. Chen, R. Chen, G. Tian, D. Li, C. Chen, X. Ge, G. Ge. Effect of relative humidity on the deposition and coagulation of aerosolized SiO2 nanoparticles. Atmos. Res., 194 (2017) 100-108

[11] J. J. Kim, T. Hann, S.J. Lee. Effect of flow and humidity on indoor deposition of particulate matter. Environ. Pollut., 255 (2019) 113263

[12] M. Xu, M. Nematollahi, R. G. Sextro, A. J. Gadgil, W. W. Nazaroff. Deposition of Tobacco Smoke Particles in a Low Ventilation Room, Aerosol Science and Technology, 20 (1994) 194-206

[13] M. Seipenbusch, A. Binder, G. Kasper. Temporal Evolution of Nanoparticle Aerosols in Workplace Exposure. The Annals of Occupational Hygiene, 52 (2008) 707–716

[14] W. Koch, H. Lödding and G.Pohlmann. A reference aerosol generator based on Brownian coagulation in a continuously fed well stirred tank reactor. Journal of Aerosol Science 49 (2012) 1–8.

[15] S. Anand, Y. S. Mayya, M. Yu, M. Seipenbusch, G. Kasper. A numerical study of coagulation of nanoparticle aerosols injected continuously into a large, well stirred chamber. Journal of Aerosol Science 52 (2012) 18–32.

[16] Y. Xiao, Y. Lv, Y. Zhou, H. Liu, J. Liu. Size-resolved surface deposition and coagulation of indoor particles, International Journal of Environmental Health Research (2019)

[17] J. S. Park, N.-Y. Jee, J.-W. Jeong. Effects of types of ventilation system on indoor particle concentrations in residential buildings. Indoor Air 24 (2014) 629–638

[18] P. Azimi, D. Zhao, B. Stephens. Estimates of HVAC filtration efficiency for fine and ultrafine particles of outdoor origin. Atmos. Environ., 98 (December 2014) 337-346

[19] A. Chen, Q. Cao, J. Zhou, B. Yang, W.C. Chang, W.W. Nazaroff. Indoor and outdoor particles in an air-conditioned building during and after the 2013 haze in Singapore. Build. Environ., 99 (2016) 73-81.

[20] Y. Lv, H. Wang, S. Wei. The transmission characteristics of indoor particles under two ventilation modes. Energy Build., 16 (2018) 1-9.

[21] Y. Lv, H. Wang, Y. Zhou, H. Yoshino, H. Yonekura, R. Takaki, G. Kurihara. The influence of ventilation mode and personnel walking behavior on distribution characteristics of indoor particles. Build. Environ., 149 (2019) 582-591

[22] C. Chen, W. Ji, B. Zhao. Size-dependent efficiencies of ultrafine particle removal of various filter media. Building and Environment 160 (2019) 106171.

[23] T. Ruan and D. Rim. Indoor air pollution in office buildings in mega-cities: Effects of filtration efficiency and outdoor air ventilation rates. Sustainable Cities and Society 49 (2019) 101609.

Chapter 6. Assessment of Air Purification Effect in Sheltering Houses Equipped with Ventilation Systems after Air Pollution Incidents

6.1 Introduction

The air pollutant concentration decreases from a release site by diffusion [1], causing the pollutant plume to spread and pass through cracks in a structure. Some of the particles entering an indoor space are suspended or settled by Brownian motion or gravity depending on the particle sizes if there is no external force interference. The main removal mechanism for airborne particles is sedimentation or settling on the ground, walls, and roofs. Scientists have realized the importance of indoor air quality, because people spend most of their lives indoors [2–3]. A recent report by Kelly and Fussell (2019) mentioned that poor outdoor air quality and the human pursuit of a low-carbon economy have spurred efforts to close indoor spaces [4], increasing the risk of exposure to endogenous indoor air pollutants [5]. Therefore, the development of indoor air purification technologies and the corresponding studies on indoor particles are highly desired [4–10].

Particle deposition has been investigated. The indoor particle concentration decreases gradually over time [11–16]. Xu et al. (2019) investigated the particle deposition characteristics using a particle deposition model with a random function method. They found small particles have a strong thermal motion, and a temperature difference can increase the average deposition efficiency of 1.0-µm particles, while simultaneously decreasing that of 7.0-µm ones [17]. For both forced and natural ventilation, AER is the key factor for the value of deposition rate [18–20]. Nomura et al. (1997) demonstrated that particles are more efficiently removed at a high AER due to the combination of ventilation and increased turbulent deposition [14]. Although five particle sizes (15–2000 nm)

show the same general trend where the deposition rate increases linearly with AER, significant particle removal with different d_p (except 15 nm) was not observed. Liu et al. (2018) conducted field measurements in two classrooms to study the influence of the natural ventilation rate on indoor $PM_{2.5}$ deposition. The indoor $PM_{2.5}$ deposition rate increases with the natural ventilation rate [21]. Similarly, Ruan and Rim (2019) revealed that high AERs severely affect the indoor air quality [22]. Additionally, changes in particle motion due to the use of electric fans also plays an important role [12, 23–24]. Wang et al. (2018) reported that providing a more homogeneous distribution of indoor air with a lower temperature difference may reduce dust deposition [25]. The deposition rate is extremely dependent on the particle diameter [26–28]. Even for extremely small particles with 5–6-nm diameters, coagulation can occur for indoor sources at a concentration around 2.0×10^4 /cm^3 [29–32]. This differs from the value of 1.0×10^6 /cm^3 for diameters larger than 0.1 μm [33]. Chapter 3 had reported that window frames made of plastic coupled with an AER less than or equal to 1.20 h^{-1} can prevent the penetration of most particles, because external particles gradually disperse and the concentrations decrease to less than that of indoors. Hence, increasing AER of the ventilation system may be an effective method to purify indoor air. However, the research did not determine the removal characteristics corresponding to a specific particle size or an AER value [34]. Consequently, the size-dependent deposition rate under controllable conditions should be further examined to understand the deposition and removal behaviors of nanosized particles at different AERs.

Previous studies have shown that the deposition rate is affected by three movements: Brownian motion (the thermal effect), gravity settlement, and turbulent motion (the kinematic effect) [35]. The deposition rate is subject to the interaction of a certain kind of motion or multiple movements due to the nature of the particle diameter, external factors (such as fan operation or ventilation), and charge contribution [36–38]. All these models assumed well-mixed indoor

air coupled with turbulent diffusion, the gravity effect, and Brownian motion. Considering the three effects of eddy diffusion, the deposition rate has been estimated by the Crump and Seinfeld model (1981) [39]. The calculation model, which includes the deposition velocity K(θ), is expressed as

$$\beta = \left[\sum_{\theta=0}^{2\pi} K(\theta)\{S_T(\theta) + S_S(\theta)\}\right] / V_T \tag{1}$$

In this regard, the deposition rate involves the calculation of K(θ) and the discussion of K_e (turbulent intensity parameter). Nomura et al. (1997) [14] compared two models: Crump and Seinfeld (1981) and Beneš and Holub (1996) [40]. Both models illustrate that the deposition rate is proportional to K_e. However, few studies have focused on the effect of introducing particles in mixed states. Moreover, it is unclear whether the activities of different sized particles, which are expressed as the deposition rate, change when a charge interaction is also present.

In recent years, as more places of residence have become equipped with forced ventilation systems, a reasonable ventilation strategy for indoor air purification has become a key issue. Zhou et al. (2017) concentrated on the dispersion and deposition of fine particles due to a combination of the inlet velocity and floor temperature. Particles deposited on the floor decrease as the inlet velocity and floor temperature increase [41]. Lv et al. (2019) analyzed the removal effect of indoor particulate matter (0.5–3.0 μm) by two different ventilation modes. They employed an environmental chamber for simulations and considered walking behavior. The results showed that 1.0–3.0-μm particles are more easily suspended than 0.5–1.0-μm particles. The ventilation effect of the slit exhaust mode is higher than that of the ceiling ventilation mode [42]. However, a reasonable strategy for removing smaller particles (for example, d_p < 0.5 μm) via a ventilation system has yet to be determined.

Every year, various environmental emergencies related to air pollution occur in different regions of the world. Examples include the leakage or the explosion of chemicals during transportation or in a factory incident. Additionally, air pollution can be caused by extreme weather such as floating dust or haze. Pollutant plumes containing aerosol particles enter houses during migration and diffusion. These particles are suspended in indoor air or deposited on the ground, walls, and roofs, increasing exposure risks for residents sheltering in houses. To prepare for these and similar incidents, effective evacuation plans and related data are urgently required, not only for the government to centrally manage and resettle people in emergencies but also for any industrial plants that utilize toxic chemicals.

As part of the research on emergency evacuations, a closed test chamber to simulate a sheltering house, including indoor and outdoor environments, was used in this work. The determination and estimation of the deposition rate of aerosol particles under the action of the ventilation system should provide important basis to improve indoor air quality. This study aims to elucidate: (1) the AER application scope of a forced ventilation system based on the relationship between actual and set values, (2) general rules under ideal conditions by confirming the relationship between the deposition rate and particle diameter (uncharged and pre-mixed particles at full scoped AERs), (3) general rules under non-ideal conditions (well-mixed and unmixed, uncharged and neutralized particles for select AERs), (4) the turbulent state caused by the ventilation system at a certain AER by using the experimental data to query the optimal K_e in the β-K_e diagram plotted by two estimation models, and (5) a reasonable ventilation strategy for indoor air purification in the later stage of an air pollution accident or similar incident.

This study provides a reference to improve the indoor air quality in the event of an air pollution accident. It also provides effective information for general household air purification. Additionally, it can support the construction of

shelters in areas and countries prone to air pollution accidents or floating dust/hazy weather.

6.2 Methodology

6.2.1 Experimental methodology

6.2.1.1 Experimental chamber

Fig. 1 shows the experimental system used to measure the deposition rate. A fully enclosed chamber, including two compartments, which each had interior dimensions of 1.01 m×0.80m×0.80m, simulated the indoor and outdoor spaces where people live. In this experiment, only the indoor compartment (right side of the chamber) was used, and a fixed-speed household fan was installed to premix particles thoroughly and maximize their uniform distribution. A plain aluminum sliding window that remained closed was embedded in the middle of the two sections. The ventilation system was the main structure in the simulation environment. Its main body was a power-adjustable vacuum pump located outside the indoor compartment. The chamber system was placed in a windowless laboratory, which was maintained at 25 °C, to avoid airflow interference from the external environment.
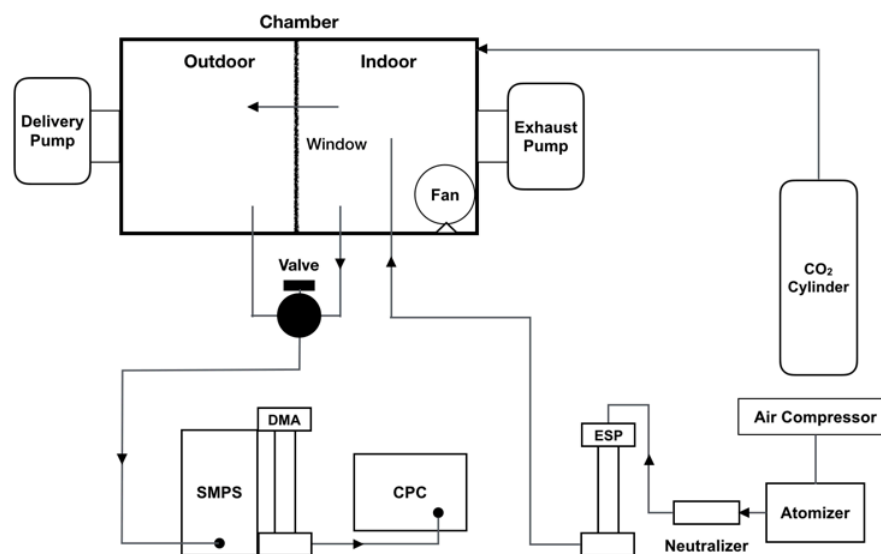
Fig. 1. Experimental system for the deposition rate of aerosol particles

6.2.1.2 Sampling and measurements

Polydisperse sodium chloride aerosols (10% NaCl in pure water) were generated by a six-jet atomizer (TSI model 3706). Ultrafine and fine particles (17.5-532.8 nm) passed through a dryer, a neutralizer (Am241, 3MBq), and an electrostatic precipitator (ESP, self-product). The ESP can be switched on/off to realize uncharged /neutralized particles before entering the indoor compartment. Here, 'neutralized' means the particles have a bipolar equilibrium charge distribution, while 'uncharged' indicates that the surface charge has been removed from the neutralized ones.

The particles were measured with a scanning mobility particles sizer (SMPS, TSI model 3938), and an electrostatic classifier (TSI model 3082) was used with a long differential mobility analyzer (DMA, TSI model 3081A). A condensation particle counter (CPC, TSI model 3776) was configured to read the particle concentration in the chamber. The operating specifications for the measuring instruments are shown in Table 1.

Table 1

Specifications for the measuring instruments.

	Specifications	This study
Sheath flow	2-30 L/ min ± 2 % of reading	3.0 L/ min
Aerosol flow	0.3 ± 0.015 L/ min	0.3 L/ min
Particle size range	10-1000 nm	17.2-542.5 nm
Sizing accuracy	±1 % at 100 nm for 10:1 sheath/ aerosol flow ratio	
DMA voltage	10-10000 VDC ± 0.5 % over full range	
Particle resolution	64 channels/ Decade	
Particle concentration accuracy	±10%	

In this experiment, the introduced concentration was controlled initially to be around 1.00×10^4 particles/cm^3 because the concentration of real aerosols in the air is around several thousand to ten thousand per cm^3. The actual concentration was measured in real-time for 36 minutes.

To measure the AER value, the operated AERs in this experiment were set to 0.16 h^{-1}, 0.30 h^{-1}, 0.70 h^{-1}, 1.07 h^{-1}, 1.50 h^{-1}, 2.00 h^{-1}, or 3.00 h^{-1} in advance. The indoor compartment was filled with carbon dioxide gas (CO_2, 99.999%) at a concentration of less than 5.0×10^3 ppm, and the decay of the CO_2 concentration was measured over time to determine the application scope of AER.

To ensure the effective background value of the indoor data and that the outdoor did not contribute to the indoor environment, the chamber was flushed continuously at a high power with dry purified air by the delivery pump outside the outdoor compartment until the total concentration was less than 5.0 particles/cm^3 at the end of each measurement. Moreover, the instruments used in this experiment were regularly maintained, and particle size distribution tests were performed before each measurement. The errors for AER under mixed conditions were less than 10% on average, but for unmixed conditions the maximum was 34%. Additionally, under non-ideal conditions, especially in case of unmixed condition, the particles are unevenly dispersed under the influence of various factors, which makes measurement difficult. Consequently, the effects from the mixing differences and instrument drift were minimized by conducting multiple measurements under the same conditions, and the corresponding averages are used for rough estimation.

6.2.2 Experimental determination of the deposition rate

Assuming that the source concentration in this air-tight chamber was constant and there was no release of other sources, the particle concentration C (t) should decay with time 't' as

$$C(t) = C(0)exp\,(-\lambda t) \tag{2}$$

Where C (0) is the initial concentration (#/cm^3), t is the elapsed time from C (0) to C (t), and λ is the particle decay rate, which reflects the total loss such as diffusion loss, gravitational settling loss, and any other loss caused by external

forces [43]. In this work, losses by the ventilation system at different AERs and by the wall or floor deposition were considered. In addition, the concentrations within 36 min were collected directly by CPC. Therefore, if 'a' represents the air exchange rate, a series of size-resolved deposition rate 'β' are obtained experimentally through a simple calculation as

$$\beta = \lambda - \alpha \tag{3}$$

In this study, the experimental data was used to determine deposition rate under both ideal and non-ideal conditions, in order to provide a basis for inferring turbulent states. The corresponding concentration was used to obtain the particle removal time under different conditions, so as to provide a reference for determining an effective ventilation strategy.

6.2.3 Assessment of the deposition rate

The influencing factors are very singular and regular in a laminar flow. When the particle concentration is uniformly dispersed in a test chamber, it tends to have a regular linear change as a function of time regardless of special conditions such as the influence of the boundary layer thickness. Thus, the formula describing the deposition rate in a laminar flow due to Brownian motion and gravitational sedimentation was approximated by Okuyama et al. (1986) as [24]

$$\beta = \left(\frac{S_T}{V_T}\right)\left(\frac{D}{\delta}\right) + \frac{u_t}{H} \tag{4}$$

In this study, the deposition rate in a laminar flow was used as the reference object to compare with the results of different turbulent states. The detailed representation is shown in the Appendix.

Kinematic factors were expressed as the results of various movements between particles due to mechanical external forces except for Brownian motion. For instance, the effect of the greater velocity gradient arising from the droplets

emitted from the spray nozzles of the atomizer was significantly reflected in the experimental conditions where the particles were not mixed. Therefore, three mechanisms may be operating simultaneously: a direct kinematic effect (produced by the spray droplets and the ventilator), gravitational settling (produced by the precipitation of the large spray droplets), and a thermal effect (produced among the particles, even with dust). As described above, various fluctuation factors exist in the deposition rate of particles in a turbulent flow. Corner and Pendlebury (1951) evaluated the theoretical deposition rate of particles in a sealed rectangular container by consider the mechanisms as turbulent diffusion, gravity sedimentation, and Brownian movement [35]. Crump and Seinfeld (1981) then derived Eq. (1) under the influence of these three forces in a sealed container with an arbitrary shape as [39]

$$\beta = \frac{K(0)S_T(0) + K(\pi)S_T(\pi) + K(\frac{\pi}{2})S_T(\frac{\pi}{2})}{V_T} \tag{5}$$

where $S_T(0)$, $S_T(\pi)$, and $S_T(\frac{\pi}{2})$ indicate the surface areas of the upper, lower, and side walls of the indoor compartment, respectively, and $K(0), K(\pi), and\ K(\frac{\pi}{2})$ are the corresponding K(θ). θ is the angle of the chamber surface with respect to the vertical direction. In this study, Eq. (5) was used to estimate the deposition rate. However, the surface areas of the fans were ignored because the indoor compartment volume greatly exceeds that of a household fan.

The simulation of the particles deposited in the chamber under turbulent flow conditions is much closer to the actual situation. Eq. (5) was described by Okuyama et al. (1986) [24]. Crump and Seinfeld (1981) expressed the deposition velocity K(θ) as the ratio of the amount deposited on the surfaces and the particle number concentration above the surface [39]. Specifically, the derivation is

$$K(\theta) = \cfrac{u_t \cos\theta}{exp\left[\cfrac{\pi u_t \cos\theta}{(m\sin(\frac{\pi}{m}))^m \sqrt{K_e D^{m-1}}}\right]-1} \tag{6}$$

where K_e is the turbulent intensity parameter. K_e is related to the physical properties of the fluid and characterizes the turbulence intensity. Okuyama et al. (1986) ever discussed K_e values from 0–269.4 s^{-1} using a stirred tank with a total volume of 2.61×10^{-3} m^3 [24]. To estimate the deposition rate in this study, a K_e value of 1.19 s^{-1} was assumed. By comparing the estimated results with the experimental data, the rationality of K_e selection can be determined. Moreover, while using the experimental data to query the β-K_e diagram proposed in this work, the actual turbulence state can be inferred.

By introducing the experimental constant κ=0.3 (used for the calculation of Eq. (4), see Appendix) and m=2.7 along with considering the slip correction factor C_m expressed by Lee and Liu (1980) [44], Eq. (6) is derived as

$$K(\theta) = \frac{B' \cos\theta\, d_p^{1.5}}{exp\,(F' \cos\theta\, d_p^{2.44})-1} \tag{7}$$

Where, $C_m = 3.69\left(\lambda/d_p\right)^{1/2}$ (8)

$$F' = \frac{AB'}{C^{0.63}} \tag{9}$$

$$A = \frac{\pi}{2.7\sin\left(\frac{\pi}{2.7}\right)K_e^{\frac{1}{2.7}}} \tag{10}$$

$$B' = \frac{g(\rho_p-\rho_f)(3.69\lambda^{0.5})}{18\mu} \tag{11}$$

$$C = \frac{\kappa T(3.69\lambda^{0.5})}{3\pi\mu} \tag{12}$$

6.3 Results and discussion

6.3.1 Determination of the application scope of AER

The AER range of the experimental chamber was evaluated due to the actual operating conditions of the ventilation. Table 2 presents the actual AER values based on the operated AER under various conditions. The first group named 'uncharged and mixed' represents the ideal condition. It tends to increase (decrease) for the actual (operated) AER, except for the operated AER at 0.16 h^{-1}. The presence of an outlier indicates that the minimum limit of the ventilation system in this experiment is exceeded. Thus, the full scoped-AER from 0.32 h^{-1} to 4.22 h^{-1} corresponds to the operated AER from 0.30 h^{-1} to 3.00 h^{-1}. In addition, the measurement without a ventilation system (operated AER at 0.00 h^{-1}) was also performed. It corresponds to an AER of 0.25 h^{-1}, which represents natural settlement due to gravity. Table 2 shows the correction of the actual AER values of the particles with different charging states under different mixing conditions. The obtained experimental conditions are used in later sections.

Table 2

Operated AER and actual AER

Operated AER (h^{-1})	Actual AER (h^{-1})				Averaged AER (h^{-1})
	Uncharged and mixed	Uncharged and unmixed	Neutralized and mixed	Neutralized and unmixed	
0	0.25±0.01	-	0.24±0.01	-	0.24
0.16	0.38±0.01	0.23±0.11	0.35±0.02	0.15±0.12	0.28
0.30	0.32±0.01	0.50±0.34	0.31±0.01	0.18±0.09	0.33
0.70	0.82±0.03	0.48±0.11	0.83±0.02	0.60±0.26	0.68
1.07	1.19±0.04	0.92±0.17	1.20±0.05	0.78±0.22	1.02
1.50	1.82±0.04	-	-	-	-
2.00	2.54±0.07	-	-	-	-
3.00	4.22±0.19	-	-	-	-

6.3.2 Size-resolved deposition rate under ideal conditions

The deposition rate experiment was performed simultaneously with the correction of the actual AER under ideal conditions. For comparison, representative AER values as 0.25 h^{-1} (without ventilation), 0.32 h^{-1}, 1.19 h^{-1}, 1.82 h^{-1}, 2.54 h^{-1}, 4.22 h^{-1} were chosen. Brownian motion and turbulent diffusion are the reported dominant mechanisms for particles with diameters less than 100 nm, while gravity begins to function for particles with diameters above 1000 nm. However, the above mechanisms are not predominant for particle diameters between 100–1000 nm, which are called cumulative mode particles [45].

This work further refines the particle size division. To discuss the characteristics of different segments, three representative points (d_p, β) were selected. As shown in Fig. 2, their coordinates are (53.3, 0.01), which is the maximum of the diameter less than 100 nm in the portion of 'sudden drop area-1' for a deposition rate less than 0.12 h^{-1}, (113.4, 0.12), which is the 'V-shape' bottom point, and (371.8, 0.14), which is the minimum of the diameter larger than 200 nm in the portion of 'sudden drop area-2' at a deposition rate less than 0.16 h^{-1}. Here, the 'sudden drop' areas are defined according to the value of the 4.22 h^{-1} group. For the anticipated 'V-shape' area with a stable distribution between 53.3–371.8 nm, the decreasing portion is from 53.3–113.4 nm, while the increasing is from 113.4–371.8 nm. Similarly, 113.4 nm is the key point to distinguish the two parts of the mechanisms.
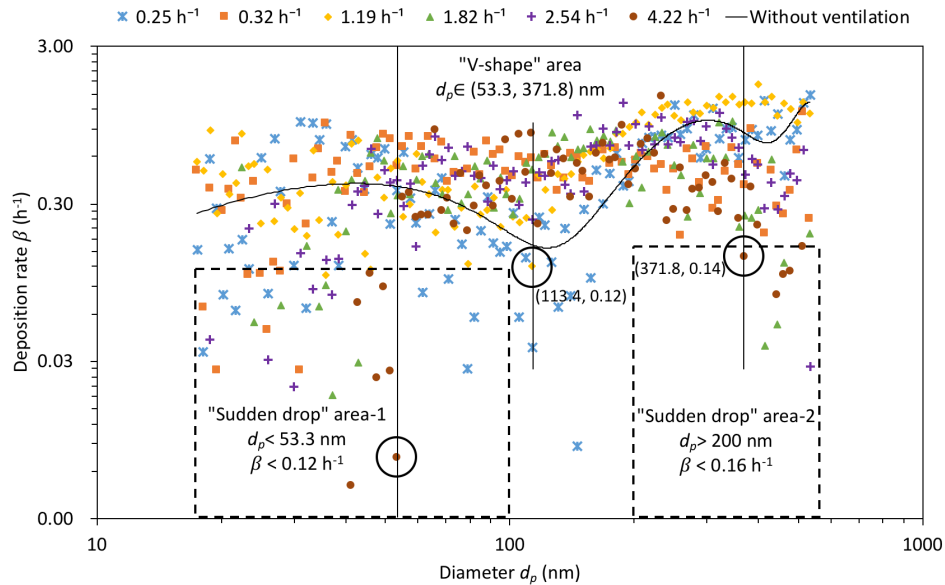
Fig. 2 Deposition rate as a function of diameter (uncharged and mixed conditions)

In addition, it is generally believed that the cumulative mode particles have a higher exposure risk due to their long suspension time in air [45]. Thus, this area is usually the main target in most studies. However, the value of the deposition rate that suddenly drops outside the range of 53.3–371.8 nm under ventilation conditions is worth considering. For particles with diameters less than 53.3 nm, the deposition rate values sharply trend toward zero as the actual AER increases, especially more than 1.19 h^{-1}. When the actual AER increases to 4.22 h^{-1}, the values of these particles are mostly zero. This indicates that particles smaller than 53.3 nm are more sensitive to the external forces provided by the ventilation system. Consequently, they are much easier to suspend in the air than cumulative mode particles if the ventilation system is turned on at a certain frequency because their extremely small gravity can be overcome easily by other external forces.

Similarly, for particle sizes larger than 371.8 nm, gravity starts to occupy a dominant position. Although it can overcome a certain resistance of mechanical forces, it is much less than the turbulence diffusion provided by the ventilation system for particle sizes less than 2000 nm [46]. Thus, the 'sudden drop' amount is less than the part with small diameters. Meanwhile, the concentration ranging from 53.3–371.8 nm is high enough to increase the possibility of a collision and

has various effects when stably operated. As shown in Fig. A.$_1$, the contribution of the segment concentration values is given. Since the particle size distribution exhibits a normal distribution, the particle concentration in the region of 53.3–371.8 nm is higher than that in the outer range, which also explains why the deposition rate in this region is a stable V-shape.

6.3.3 Total concentration with time

  Fig. 3 shows the particle concentration decay as a function of time under different ventilation conditions. The straight lines on the logarithmic scale indicate that the 36-min averaged concentration in the indoor compartment follows a single exponential decay. As the actual AER value increases, the decay rate increases (Table 3). As mentioned in the previous section, the background value should be controlled at less than 5.0 particles/cm^3.

  In this case, the time required for the indoor air quality to reach the 'standard' can be calculated. When the ventilation system is turned off, the removal mechanism of natural sedimentation requires 12.96 h to reduce the concentration of suspended airborne particles below 5.0 particles/cm^3. Once the ventilation system is turned on, the time is greatly reduced. When the actual AER is 0.32 h$^-$^{1}, the time is reduced to 9.16 h. When the actual AER is increased to 4.22 h^{-1}, the suspended particles can be 'cleaned' in 1.73 h.
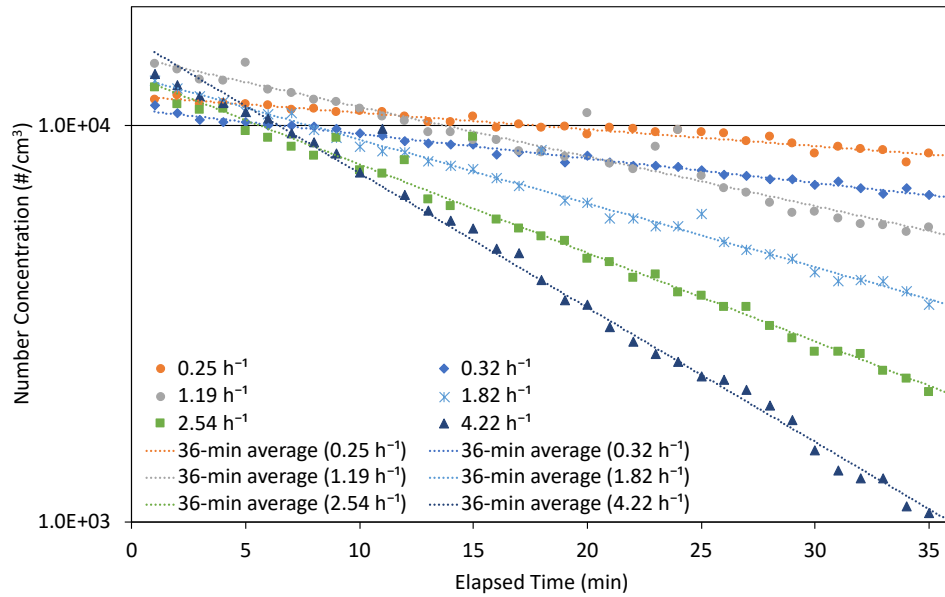
Fig. 3. Decay of the particle concentration as a function of time for different ventilation conditions

Table 3

Results of exponential regression

Actual AER	Exponential regression			
	Equation	r^2	λ	$t_{c=5.0}$
h^{-1}	-	-	min^{-1}	h
0.25	$y=11887e^{-0.010x}$	0.957	0.010	12.96
0.32	$y=10984e^{-0.014x}$	0.989	0.014	9.16
1.19	$y=14881e^{-0.029x}$	0.940	0.029	4.60
1.87	$y=13371e^{-0.037x}$	0.984	0.037	3.55
2.54	$y=13362e^{-0.051x}$	0.978	0.051	2.58
4.42	$y=16562e^{-0.078x}$	0.991	0.078	1.73

The concentration decay does not equal ventilation effectiveness because the decay rate λ is the sum of the deposition rate β and AER a under ventilation conditions (Eq. (3)). Fig. 4 shows the contribution ratio of the ventilation and deposition in decay rate (Data is shown in Table A.₁.) When the diameter is less than 113.4 nm, the contribution of the actual AER to the concentration decay mostly exceeds 0.5. As the diameter increases, the proportion of sedimentation increases gradually, further demonstrating that gravity begins to work from 113.4–371.8 nm. In addition, 1.19 h⁻¹ could be a cut-off value. When the actual

AER is greater than 1.19 h^{-1}, the contribution value of the ventilation part is basically greater than 0.5. In this case, the decay of the indoor particle concentration is mainly due to the replacement of indoor particles by the ventilation system, instead of being deposited indoors. Hence, the indoor air quality is improved.
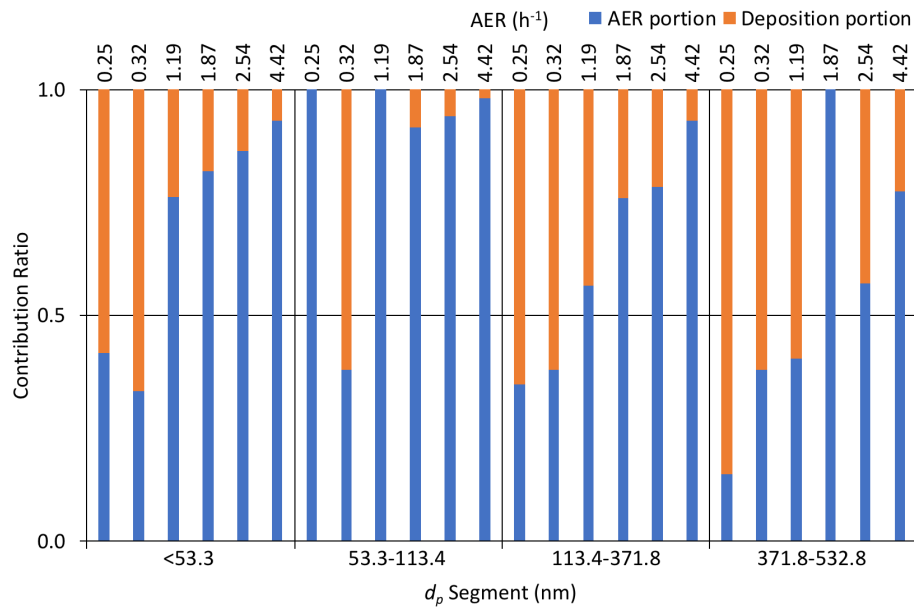
Fig. 4. Contribution ratio of ventilation and deposition in the decay rate

6.3.4 Size-resolved deposition rate under non-ideal conditions

Based on the conclusion above, the averaged AERs (operated AERs) of 0.33 h^{-1} (0.30 h^{-1}), 0.68 h^{-1} (0.70 h^{-1}), and 1.02 h^{-1} (1.07 h^{-1}) were selected to compare conditions. This study considered various mixing and charging combinations. One factor that may greatly impact the distribution of the particles in the room is whether or not the particles are mixed prior to the measurement. Similarly, the distinction between uncharged and neutralized electrification may also affect the deposition of the particles from the perspective of electrostatic force.

Figs. 5 (a) and (b) present deposition rate β as a function of diameter with forced ventilation (averaged AER ≤1.02 h^{-1}) under mixed and unmixed conditions, respectively. Both conditions exhibit the same V-shape. For a given actual AER value, the deposition rate under the unmixed condition is slightly higher than that

under the mixed condition, regardless of the charging state. This is especially obvious for uncharged particles with diameters less than 113.4 nm. Under the condition where the uncharged particles are uniformly mixed beforehand, non-cumulative mode particles correspond more to the sudden drop in the deposition rate value, indicating that it is more susceptible to suspension by external forces. On the other hand, the unmixed particles do not show significant features. From the perspective of experimental operations, mixed particles are more easily collected due to the uniform distribution and the relatively stable data.
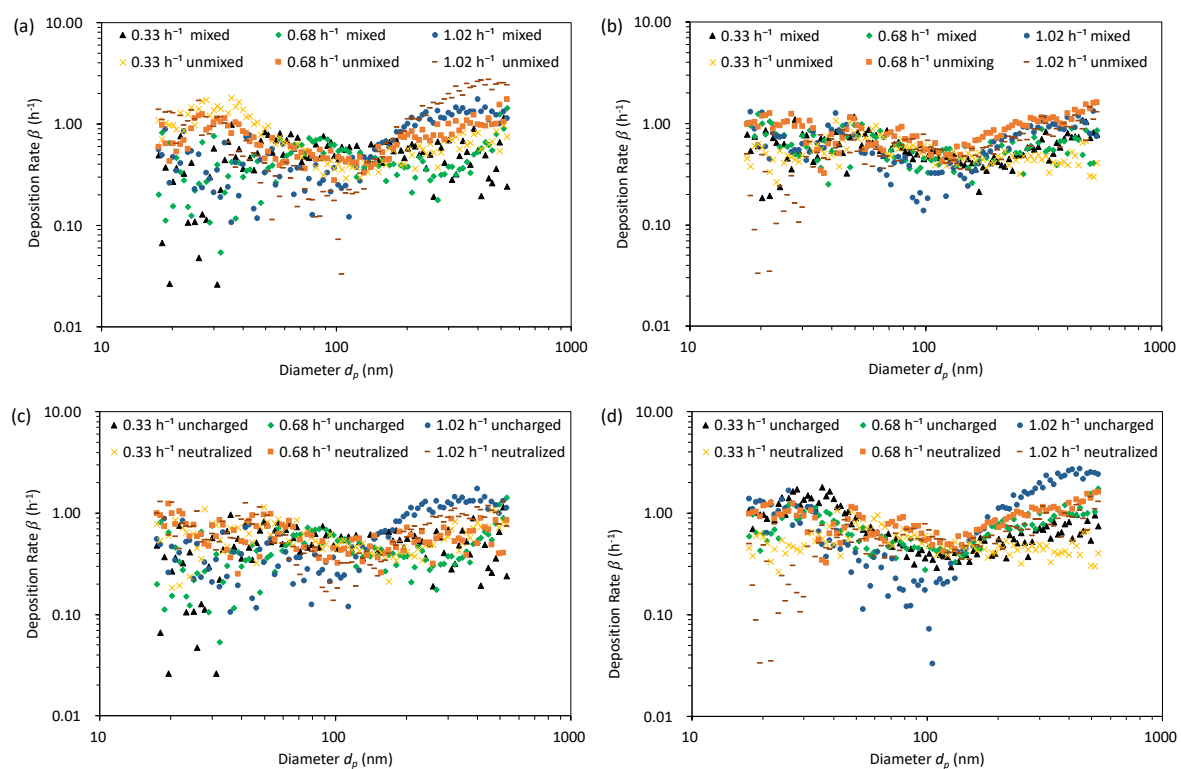
Fig. 5. Deposition rate β as a function of diameter d_p with forced ventilation (actual AER ≤ 1.02 h^{-1}). (a) Uncharged particles: mixed versus unmixed, (b) Neutralized particles: mixed versus unmixed, (c) Mixed: Uncharged versus Neutralized, and (d) Unmixed: Uncharged versus Neutralized.

Figs. 5 (c) and (d) present the deposition rate as a function of diameter with forced ventilation (averaged AER ≤ 1.02 h^{-1}) between uncharged and neutralized particles, respectively. Combined with Fig. 5 (b), the neutralized particles pose more regular characteristics than the uncharged ones. This is probably due to the electrostatic effects from the particle-particle and particle-surface like a wall, floor, or roof. Such an electrostatic action significantly limits particle movements,

making deposition the primary removal mechanism for particles in indoor air. However, it should be noted that the deposition-based removal mechanism increases the risk of indoor exposure, making it difficult to improve the indoor air quality. Furthermore, Figs. 5 (b) and (d) show that neutralized particles less than 100 nm without being pre-mixed can be resuspended or even removed, if the compartment is subject to an averaged AER of 1.02 h^{-1} or higher. For other particle sizes, the present actual AERs are ineffective.

6.3.5 Comparison with the estimation results

K_e, which is the turbulent intensity parameter included in Eq. (6) that characterizes the turbulence intensity, is related to the physical properties of the fluid. Fig. 6 (a) gives β-K_e diagram, which reflects the relationship between the size-resolved deposition rate and K_e value at the average level. In the case where the experimental conditions are fixed, the larger the value of K_e selected, the larger the corresponding deposition rate. Table A.$_2$ shows the t-test results of the difference between the estimation models that varied by K_e. Significant differences ($p < 0.05$, paired-groups t-test) are observed between every group (Laminar and Eq. (5) & Eq. (6), Laminar and Eq. (5) & Eq. (7), Eq. (5) & Eq. (6), and Eq. (5) & Eq. (7)). Data by Eq. (5) & Eq. (6) show higher average values than those using Eq. (5) & Eq. (7) due to the consideration of C_m in Eq. (7). Moreover, the theoretical result in the laminar flow as the background value displays the smallest deposition rate, which corresponds to the minimal K_e (is less or equals to 0.10). In terms of the specific particle size, as shown visually in Fig. 6 (b), the deposition rate value obtained by Eq. (5) & Eq. (6) is higher than Eq. (5) & Eq. (7) when the particle size is less than approximately 100 nm. Between 100–131 nm, the two methods provide similar values. Above 131 nm, the results from Eq. (5) & Eq. (7) become slightly higher than Eq. (5) & Eq. (6). This also illustrates that Eq. (7) with the parameter C_m has a significant effect on the calculated

deposition rate of ultrafine particles (particle size <100 nm), which differs from the range of 100–1000 nm reported by Lee and Liu (1980) [44].
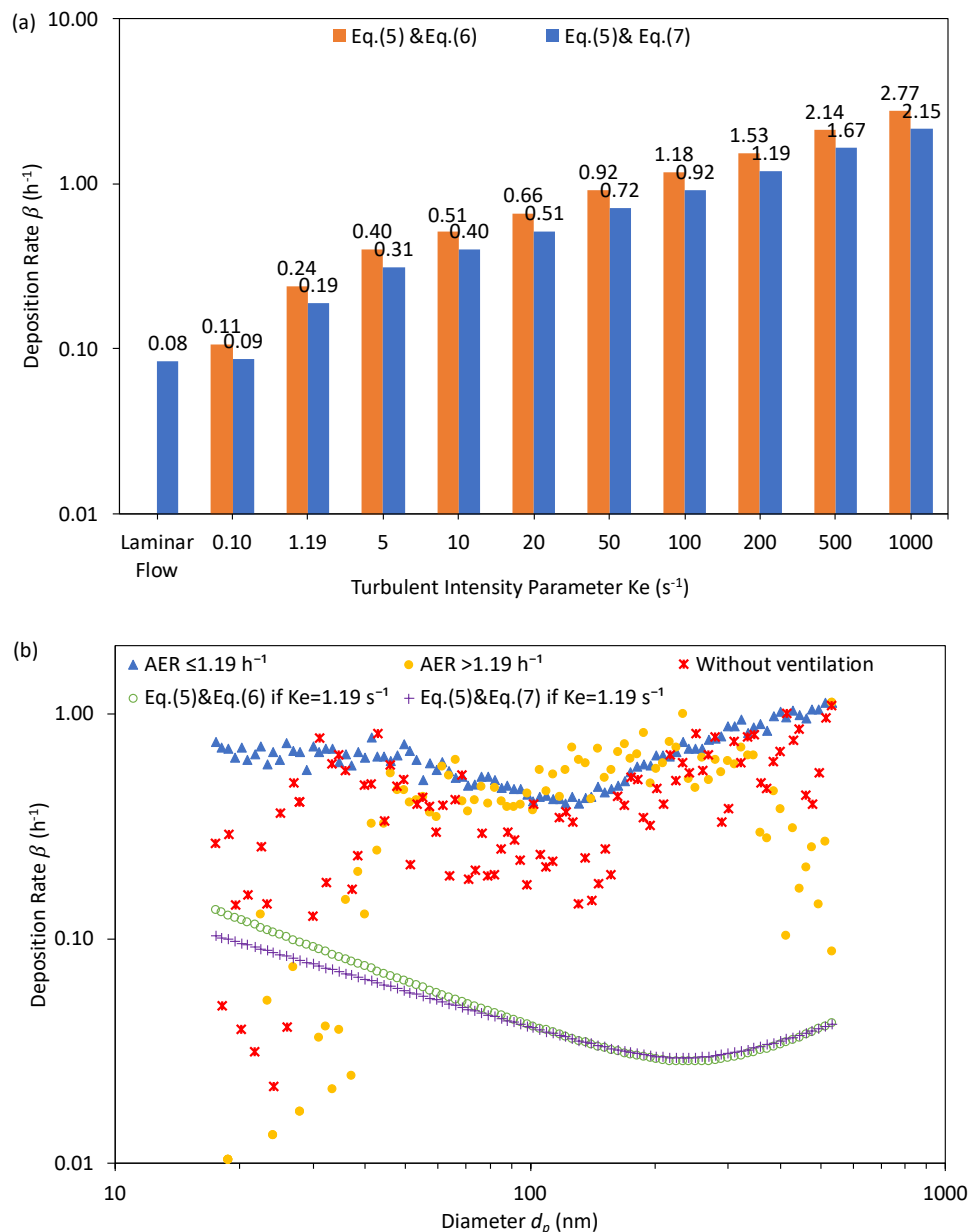
Fig. 6. Comparison of the deposition rate using two estimation models. (a) β-K_e diagram by two estimation models under different K_e values in the turbulent flow. Bar of the measurement result in the laminar flow is used as a reference, and the ten selected K_e values range from 0.10–1000 s^{-1} and (b) deposition rate from the two estimation models (K_e=1.19 s^{-1}) and the experiment.

By referring to Okuyama et al. (1986), the estimation assumed that K_e=1.19 s^{-1}. Fig. 6 (b) compares the estimation results and experimental data of the size-resolved deposition rate. The experimental deposition rate is higher than the estimation. Regardless of these values in the sudden drop under the conditions of

'averaged AER >1.19 h^{-1}' and 'without ventilation', the averaged-deposition rates in the V-shape (40.0, 346.0) are approximately 0.53 h^{-1} and 0.40 h^{-1}, respectively. These values correspond to K_e as 10 s^{-1} and 5 s^{-1} (excluding C_m) or 20 s^{-1} and 10 s^{-1} (including C_m), which can be reversely checked in β-K_e diagram. A higher K_e value represents a greater degree of turbulence during the ventilation process, especially at a higher AER. The higher turbulence may be due to the fact that the main body of the ventilation system is a high-powered vacuum pump that provides a strong suction force, causing a large turbulent diffusion. For the 'without ventilation' condition, correction parameter C_m may be necessary due to the high deposition rate value.

Additionally, other factors may also affect the deposition rate. Okuyama et al. (1986) conducted a study using uncharged NaCl, DEHS, and PSL as the sources and a vessel with four baffles and a total stirred tank volume of 2.61×10^{-3} m^3 [24]. The K_e values ranged from 0 s^{-1} to 269.4 s^{-1} (only two sets of data are shown in Fig. 7). The large volume of the test body usually corresponds to a small value of a deposition rate (K_e value), which is consistent with the results of Nomura et al. (1997) [14] but not with Cheng (1997) due to the differences in physical and chemical properties of the particle sources (metal and polymeric materials). Cheng (1997) conducted an experiment in a 161-liter spherical aluminum chamber with a turbine impeller and a fan inside [23]. They used silver aerosols and polystyrene latex (PSL) particles, and minimized the electricity effects by grounding. Their study assumed K_e values of 0.094 s^{-1}, 0.496 s^{-1}, and 1.046 s^{-1}, which were coupled with three rotational speeds. Xu et al. (1994) reported the lowest values in the literature (Fig. 7). They used environmental tobacco smoke (ETS) particles in a 36.5-m^3 room size with a fan, exhaust hood, and air cleaner. Using selected K_e values of 0.026 s^{-1} (fan off) and 0.451 s^{-1} (3070 rpm), they fitted the theoretical result (Fig. 6 (a)). They also revealed that a higher turbulence intensity may accompany a higher AER [12].

As shown above, multiple factors impact the results, including the enclosure volume, particle density and diameters, texture/roughness of the deposition surface, etc. These should be analyzed on a case-by-case basis. In addition, a background comparison is necessary ('without ventilation' in this study) since a higher value usually provides information about the properties of the experimental body itself.
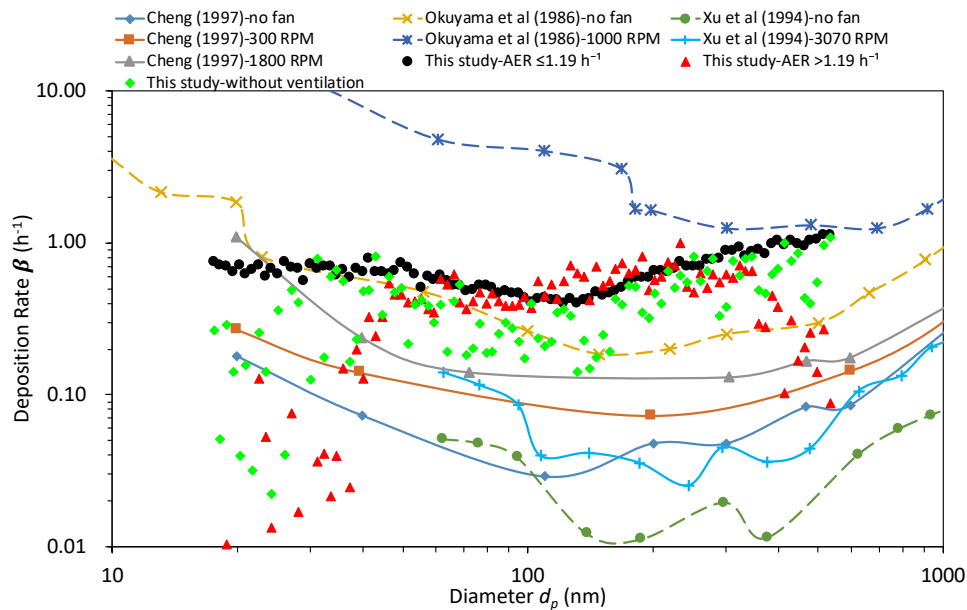

Fig. 7. Comparison of the particle deposition rates in different studies

6.4 Conclusion

The range of cumulative mode particles is redefined as 53.3–371.8 nm in this study. When the actual AER value of the ventilation system is set to 1.19 h^{-1} or less, the corresponding particle deposition rate is relatively stable in this range, revealing the potential of a higher exposure risk. When the actual AER value is set above 1.19 h^{-1}, the particles outside this range exhibit a sudden drop. The smaller the particle size, the closer the deposition rate value is to zero. That is, mechanical removal is the predominant mechanism. From the perspective of concentration decay under ventilation conditions, the decay rate in the particle concentration in the air increases as the AER value gradually increases from 1.19 h^{-1}, indicating that the air purification efficiency increases.

For non-ideal conditions, neutralized particles exhibit stable and regular 'V-shape' features in the cumulative mode region due to electrostatic force, making them more difficult to remove. However, unmixed neutralized particles may be suspended and removed at an average AER value of 1.02 h^{-1}. Thus, premixing increases the probability of a collision between particles, which may make it more difficult to improve air quality.

To infer the turbulent state caused by the ventilation system at a certain AER, the β-K_e diagram is proposed. The turbulence status of particles can be roughly estimated by querying the optimal K_e in the β-K_e diagram. Additionally, the corresponding high K_e values show that the high-power exhaust pump of the ventilation system in the sheltering house may induce a great degree of turbulence, which may be the main cause of the 'sudden drop' in the deposition rate values. However, a suitable particle removal method in the cumulative mode remains a challenge.

In the later stage of an air pollution accident or in the case where outdoor particles do not contribute indoors, turning off other stirrers/fans and increasing the AER value of the ventilation system to more than 1.19 h^{-1} is a reasonable ventilation strategy to achieve the desired air purification effect. One limitation of this study is that the sensitivity of the nanoparticles to external factors may result in large errors in the present measurement. Consequently, the result based on the regularity of particle motion is only a rough estimate, and further tests are necessary to determine the contribution of external forces on particle behavior.

References

[1] Evaluating Exposures to Toxic Air Pollutants: A Citizen's Guide. USEPA, 450/3-90-023 (1991).

[2] N. E. Klepeis, W. C. Nelson, W. R. Ott, J. P. Robinson, A. M. Tsang, P. Switzer, J. V. Behar, S. C. Hern, W. H. Engelmann, The National Human Activity Pattern Survey (NHAPS): a resource for assessing exposure to environmental pollutants, J Expo Sci Env Epid. 11 (3) (2001) 231.

[3] P. L. Jenkins, T. J. Phillips, E. J. Mulberg, S. P. Hui, Activity patterns of Californians: use of and proximity to indoor pollutant sources, Atmos Environ. Part A. General Topics, 26 (12) (1992) 2141-2148.

[4] F. J. Kelly, J. C. Fussell, Improving indoor air quality, health and performance within environments where people live, travel, learn and work, Atmos Environ. 200 (2019) 90-109.

[5] Y. Yang, B. Zhang, Q. Feng, H. Cai, M. Jiang, K. Zhou, F. Li, S. Liu, X. Li, Towards locating time-varying indoor particle sources: Development of two multi-robot olfaction methods based on whale optimization algorithm, Build Environ. 166 (2019) 106413.

[6] P. J. Landrigan. Air pollution and health, The Lancet Public Health, 2 (1) (2017) e4-e5.

[7] Y. Guo, H. Zeng, R. Zheng, S. Li, A. G. Barnett, S. Zhang, X. Zou, R. Huxley, W. Chen, G. Williams, The association between lung cancer incidence and ambient air pollution in China: a spatiotemporal analysis, Environ Res. 144 (2016) 60-65.

[8] F. Dominici, R. D. Peng, M. L. Bell, L. Pham, A. McDermott, S. L. Zeger, J. M. Samet, Fine particulate air pollution and hospital admission for cardiovascular and respiratory diseases, Jama, 295 (10) (2006) 1127-1134.

[9] E.V. Bräuner, L. Forchhammer, P. Møller, J. Simonsen, M. Glasius, P. Wåhlin, O. Raaschou-Nielsen, S. Loft, Exposure to ultrafine particles from

ambient air and oxidative stress–induced DNA damage, Environ. Health Perspect. 115 (8) (2007) 1177-1182.

[10] M. Brauer, G. Hoek, H. Smit, J. De Jongste, J. Gerritsen, D. S. Postma, M. Kerkhof, B. Brunekreef, Air pollution and development of asthma, allergy and infections in a birth cohort, Eur Respir J. 29 (5) (2007) 879-888.

[11] B. Zhao, J. Wu, Particle deposition in indoor environments: analysis of influencing factors, J Hazard Mater. 147 (1-2) (2007) 439-448.

[12] M. Xu, M. Nematollahi, R. G. Sextro, A. J. Gadgil, W. W. Nazaroff, Deposition of tobacco smoke particles in a low ventilation room, Aerosol Sci Tech. 20 (2) (1994) 194-206.

[13] J. Smolík, M. Lazaridis, P. Moravec, J. Schwarz, S. K. Zaripov, V. Ždímal, Indoor aerosol particle deposition in an empty office, Water Air Soil Pollut. 165 (1-4) (2005) 301-312.

[14] Y. Nomura, P. Hopke, B. Fitzgerald, B. Mesbah, Deposition of particles in a chamber as a function of ventilation rate, Aerosol Sci Tech. 27 (1) (1997) 62-72.

[15] T. Hussein, A. Hruška, P. Dohányosov, L. Džumbová, J. Hemerka, M. Kulmala, J. Smolík, Deposition rates on smooth surfaces and coagulation of aerosol particles inside a test chamber, Atmos Environ. 43 (4) (2009) 905-914.

[16] S. El Hamdani, K. Limam, M. Abadie, A. Bendou, Deposition of fine particles on building internal surfaces, Atmos Environ. 42 (39) (2008) 8893-8901.

[17] Z. Xu, A. Sun, Z. Han, X. Yu, Y. Zhang. Simulation of particle deposition in a plate-fin heat exchanger using a particle deposition model with a random function method, Power Technology 355 (2019) 145-156.

[18] W. Huang, X. Xie, X. Qi, J. Huang, F. Li, Determination of Particle Penetration Coefficient, Particle Deposition Rate and Air Infiltration Rate in

Classrooms Based on Monitored Indoor and Outdoor Concentration Levels of Particle and Carbon Dioxide, Procedia Eng. 205 (2017) 3123-3129.

[19] C. H. Halios, C. G. Helmis, K. Deligianni, S. Vratolis, K. Eleftheriadis, Determining the ventilation and aerosol deposition rates from routine indoor-air measurements, Environ Monit Assess. 186 (1) (2014) 151-63.

[20] W. C. Lee, J. M. Wolfson, P. J. Catalano, S. N. Rudnick, P. Koutrakis, Size-resolved deposition rates for ultrafine and submicrometer particles in a residential housing unit, Environ Sci Tech. 48 (17) (2014) 10282-10290.

[21] C. Liu, J. Yang, S. Ji, Y. Lu, P. Wu, C. Chen, Influence of natural ventilation rate on indoor PM2.5 deposition. Build Environ. 144 (2018) 357-364.

[22] T. Ruan, D. Rim. Indoor air pollution in office buildings in mega-cities: Effects of filtration efficiency and outdoor air ventilation rates. Sustain Cities Soc. 49 (2019) 101609.

[23] Y. S. Cheng, Wall Deposition of Radon Progeny and Particles in a Spherical Chamber, Aerosol Sci Tech. 27 (2) (1997) 131-146.

[24] K. Okuyama, Y. Kousaka, S. Yamamoto, T. Hosokawa, Particle loss of aerosols with particle diameters between 6 and 2000 nm in stirred tank, J Colloid Interf Sci. 110 (1) (1986) 214-223.

[25] Y. Wang, W. Zheng, Q. Tong, B. Li, Reducing dust deposition and temperature fluctuations in the laying hen houses of Northwest China using a surge chamber, Biosyst Eng. 175 (2018) 206-218.

[26] C. He, L. Morawska, D. Gilbert, Particle deposition rates in residential houses, Atmos Environ. 39 (21) (2005) 3891-3899.

[27] M. Yu, A. J. Koivisto, K. Hämeri, M. Seipenbusch, Size dependence of the ratio of aerosol coagulation to deposition rates for indoor aerosols, Aerosol Sci Tech. 47 (4) (2013) 427-434.

[28] P, Pluschke, H. Schleibinger, Indoor air pollut. Springer, (2018) Vol. 64.

[29] L. A. Wallace, S. J. Emmerich, C. Howard-Reed, Source strengths of ultrafine and fine particles due to cooking with a gas stove, Environ Sci Tech. 38 (8) (2004) 2304-2311.

[30] D. Rim, L. Wallace, A. Persily. Infiltration of outdoor ultrafine particles into a test house. Environ Sci Tech. 44 (15) (2010) 5908-5913.

[31] D. Rim, L. A. Wallace, A. K. Persily, Indoor ultrafine particles of outdoor origin: importance of window opening area and fan operation condition, Environ Sci Tech. 47 (4) (2013) 1922-1929.

[32] L. Wallace, F. Wang, C. Howard-Reed, A. Persily, Contribution of gas and electric stoves to residential ultrafine particle concentrations between 2 and 64 nm: size distributions and emission and coagulation rates, Environ Sci Tech. 42 (23) (2008) 8641-8647.

[33] W. C. Hinds, Aerosol technology: properties, behavior, and measurement of airborne particles, John Wiley & Sons. 2012.

[34] W. Wang, N. Kato, S. Kimoto, Y. Matsui, M. Yoneda. Simulation and evaluation of sheltering efficiency of houses equipped with ventilation systems. Build Environ. 168 (2020) 106491.

[35] J. Corner, E. Pendlebury, The coagulation and deposition of a stirred aerosol, Proc. Phys. Soc. Sec. B. 64 (8) (1951) 645.

[36] E. Ma, T. Ouahbi, H. Wang, N. D. Ahfir, A. Alem, A. Hammadi, Modeling of the transport and deposition of polydispersed particles: Effects of hydrodynamics and spatiotemporal evolution of the deposition rate, Environ Pollut. 237 (2018) 1011-1022.

[37] K. P. Yu, H. C. Shih, Y. C Chen, X. E. Yang, Effect of turbulence intensity and particle characteristics on the deposition of submicron particles enhanced by the ionic air purifier, Build Environ. 114 (2017) 166-177.

[38] C. Zhu, D. Wang, C. H. Lin, Jet dispersion and deposition of charged particles in confined chambers, Particuology, 8 (1) (2010) 28-36.

[39] J. G. Crump, J. H. Seinfeld, Turbulent deposition and gravitational sedimentation of an aerosol in a vessel of arbitrary shape, J Aerosol Sci. 12 (5) (1981) 405-415.

[40] M. Beneš, R. F. Holub, Aerosol wall deposition in enclosures investigated by means of a stagnant layer, Environ Int. 22 (1996) 883-889.

[41] Y. Zhou, Y. Deng, P. Wu, S. Cao, The effects of ventilation and floor heating systems on the dispersion and deposition offine particles in an enclosed environment, Build Environ. 125 (2017) 192-205.

[42] Y. Lv, H. Wang, Y. Zhou, H. Yoshino, H. Yonekura, R. Takaki, G. Kurihara, The influence of ventilation mode and personnel walking behavior on distribution characteristics of indoor particles, Build Environ. 149 (2019) 582-591.

[43] A. C. K. Lai, Particle deposition and decay in a chamber and the implications to exposure assessment, Water Air Soil Pollut. 175 (2006) 323.

[44] K. Lee, B. Liu, On the minimum efficiency and the most penetrating particle size for fibrous filters, J Air Pollut Control Assoc. 30 (4) (1980) 377-381.

[45] A. C. K. Lai. Particle deposition indoors: a review. Indoor Air. 4 (12) (2002) 211-214.

[46] F. Chen, S. C. M. Yu, A. C. K. Lai, Modeling particle distribution and deposition in indoor environments with a new drift–flux model. Atmos Environ. 40 (2) (2006) 357-367.

[47] J. H. Kim, G. W. Mulholland, S. R. Kukuck, D. Y. Pui, Slip correction measurements of certified PSL nanoparticles using a nanometer differential mobility analyzer (nano-DMA) for Knudsen number from 0.5 to 83, J Res NIST. 110 (1) (2005) 31.

Chapter 7. Conclusions and Perspectives

7.1 Main results and conclusions

The series of experiments and work in this thesis are prepared for environmental emergency. It began researching the sheltering efficiency of houses by determining the penetration factor. This involved using a test chamber to simulate the process of outdoor particles passing through cracks of a household sliding window and elucidating the most effective sheltering configuration of houses in air pollution emergencies. The results illustrate that a high air exchange rate corresponds to a high penetration factor, and the concentration difference between outdoor and indoor affects ventilation efficiency. For universal household sliding windows, frames made of plastic coupled with an air exchange rate less than or equal to 1.20 h^{-1} can prevent particle penetration more effectively in air pollution emergencies. As the external particles gradually disperse and the concentration decreases, a ventilation system with a large air exchange rate may effectively purify the indoor air. However, UFPs of less than 69 nm are able to undergo penetrate in a large amount, especially when the air exchange rate is lower than 1.20 h^{-1}. Therefore, effective housing sheltering is still a challenge if the external source is primarily UFPs. In addition, laboratory simulations may overestimate/ underestimate the penetration factor and the ventilation efficiency if the particles with a one charging state are the only source.

Then, evaluating the optimal penetration factor of the virus-containing aerosols was performed for preventing and controlling the spread of the epidemic. This study proposed four numerical calculations of penetration factor to select the optimal value, and a widely used concentration model was applied for the evaluation of a 36-min-penetration process of aerosols from a confined source space.

First of all, size-dependent P_{avg} is time-corrected to be P_{est} by a proposed correction coefficient r. During the 36 minutes penetration process in this study, proposed correction coefficient r has its own time limit if time-correction is necessary under some non-ideal condition. Moreover, the time limit gets shorter as the AER increases. According to the present experimental design, it ranges averagely from 2.4 h ($3.70 \ h^{-1}$) to 18.7 h ($0.31 \ h^{-1}$). However, the time correction is of little significance due to the simulated ideal experimental conditions in laboratory within the current experimental 36 min. P_{est} was assumed to be necessary for the system if the confined source space has a much higher initial concentration than the indoor one or there is a large AER (i.e. a »$3.70 \ h^{-1}$), but it still needs further demonstration.

And then, the error analysis of the real-time $P(t)$ and the direct-derived P_d proved the existent of assumed P_0, indicating that detaching and re-entering are inevitable. Both of them are only suitable for rough evaluation under certain conditions, $P(t)$ for the case of AER less than $1.20 \ h^{-1}$ and P_d for later stage. Additionally, the size-dependent P_{avg} is the optimal value among the four under current experimental conditions, due to minimal effect from AER value and fluctuations in concentration.

Additionally, this thesis also investigates a reasonable ventilation strategy for indoor air purification in the later stage of an air pollution accident. Firstly, the range of cumulative mode particles is redefined as 53.3–371.8 nm. When the actual AER value of the ventilation system is set to $1.19 \ h^{-1}$ or less, the potential of a higher exposure risk was revealed; When the actual AER value is set above $1.19 \ h^{-1}$, the exhibition of a sudden drop outside this range with "the smaller the particle size, the closer the deposition rate value is to zero" indicates that mechanical removal is the predominant mechanism. In addition, air purification efficiency increases as the AER value gradually increases from $1.19 \ h^{-1}$.

Secondly, neutralized particles are more difficult to be removed due to electrostatic force, but unmixed of which may be suspended and removed at an

average AER value of 1.02 h^{-1}. That is, premixing increases the probability of a collision between particles, making it more difficult to improve air quality.

Then, the β-K$_e$ diagram is proposed to infer the turbulent state caused by the ventilation system at a certain AER. The corresponding high K$_e$ values show that the high-power exhaust pump of the ventilation system in the sheltering house may induce a great degree of turbulence, which may be the main cause of the 'sudden drop' in the deposition rate values. However, a suitable particle removal method in the cumulative mode remains a challenge.

Therefore, in the later stage of an air pollution accident or in the case where outdoor particles do not contribute indoors, turning off other stirrers/fans and increasing the AER value of the ventilation system to more than 1.19 h^{-1} is a reasonable ventilation strategy to achieve the desired air purification effect.

7.2 Limitations and perspectives

The limitation of this study is that the sensitivity of the nanoparticles to external factors, such as the number of charges, may result in large errors in the present measurement. Consequently, some results based on the regularity of particle motion are only for rough estimates, and further tests are necessary to determine the contribution of external forces on particle behavior.

Moreover, the relationship between the wind speed / volume of the fan and the dimension of the room is one of the factors that cause the turbulence. It should be as a separated factor requiring further studies.

Additionally, temperatures, humidity and some other environmental conditions are caused by climate change or human factors, resulting in the change of particle behaviors, thereby bringing positive or negative effects to human exposure. All these issues require further investigations.

Appendix

Appendix 1

Table A.$_1$

Penetration factor change by actual average AER and the comparison of the relevant factors

Actual Averaged AER	10%					0.10%				
(h^{-1})	Uncharged	±SD	Neutralized	±SD	Averaged P Value	Uncharged	±SD	Neutralized	±SD	Averaged P Value
0.46	0.23	0.01	0.24	0.01	0.24	0.14	0.01	0.14	0.01	0.14
0.85	0.37	0.01	0.36	0.01	0.37	0.24	0.02	0.24	0.01	0.24
1.20	0.45	0.01	0.45	0.01	0.45	0.32	0.03	0.34	0.02	0.33
1.79	0.59	0.02	0.52	0.05	0.56	0.43	0.09	0.40	0.03	0.42
2.43	0.67	0.03	0.63	0.03	0.65	0.57	0.04	0.52	0.03	0.55
3.70	0.75	0.03	0.73	0.03	0.74	0.64	0.05	0.59	0.03	0.62

Table A.$_2$

Effect of particle concentrations on the penetration factor using two kinds of window frame materials

Concentration	Actual Averaged AER		Plastic		Aluminum	
	h^{-1}	±SE	P	±SE	P	±SE
10%	0.46	0.03	0.19	0.01	0.23	0.01
0.1%			0.13	0.01	0.14	0.01
10%	0.85	0.07	0.28	0.01	0.37	0.01
0.1%			0.24	0.02	0.24	0.02
10%	1.20	0.03	0.46	0.01	0.45	0.01
0.1%			0.32	0.02	0.32	0.03
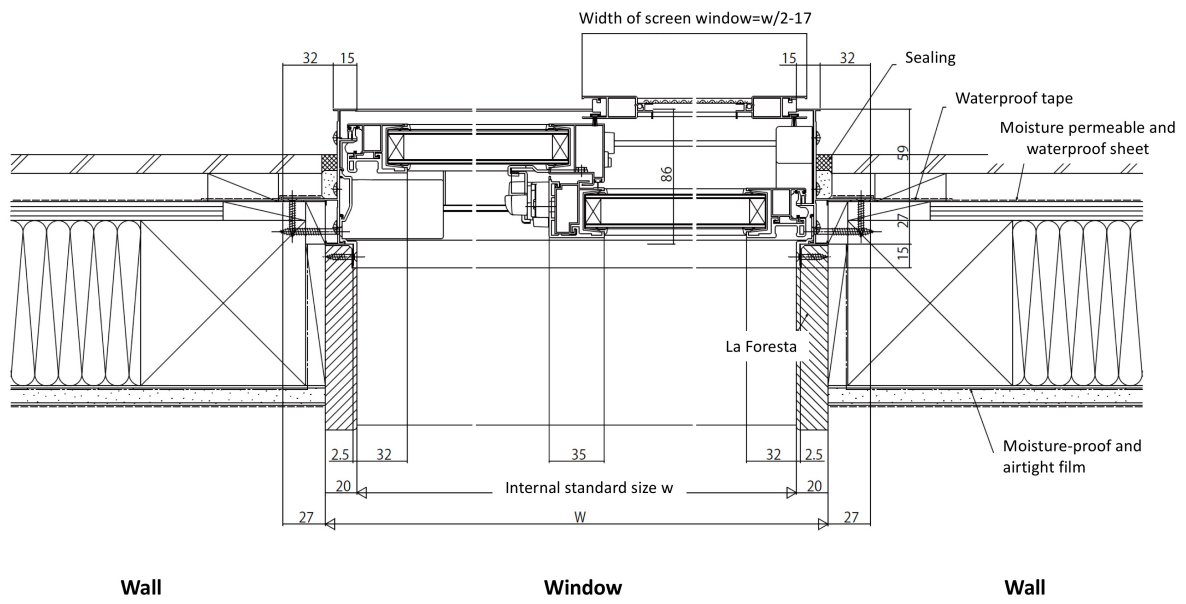
Fig. A.₁ Cross-sectional view of the sliding window and the walls (Window type: Semi-external type / Angle integrated frame)

(a) Outdoor, 10% (w/w) uncharged, AER=0.31 h⁻¹

(b) Indoor, 10% (w/w) uncharged, AER=0.31 h⁻¹

(c) Outdoor, 10% (w/w) uncharged, AER=1.20 h⁻¹

(d) Indoor, 10% (w/w) uncharged, AER=1.20 h⁻¹

(e) Outdoor, 10% (w/w) uncharged, AER=3.70 h⁻¹

(f) Indoor, 10% (w/w) uncharged, AER=3.70 h⁻¹
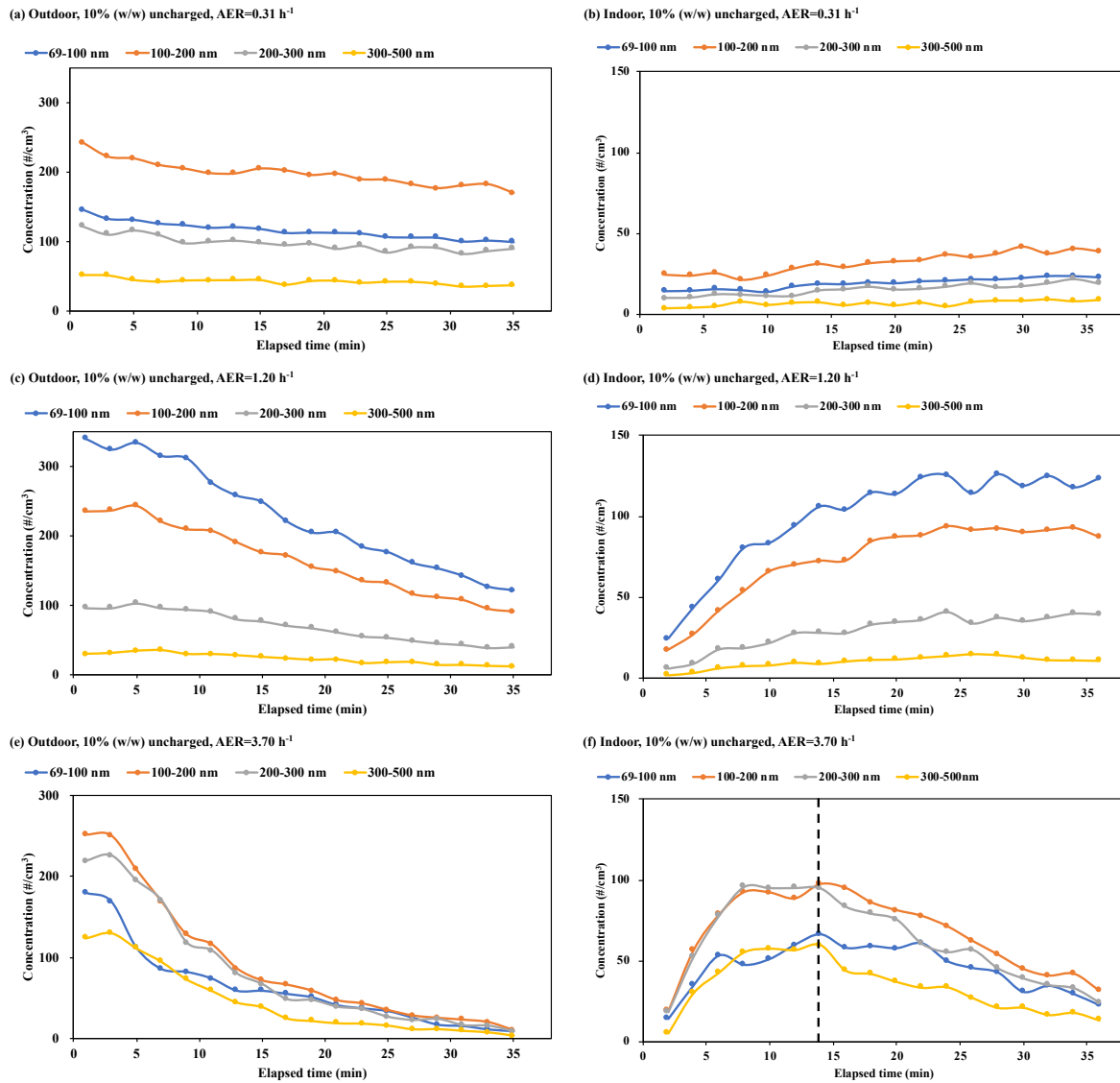
Fig. A.₂ Concentration of indoors and outdoors as a function of elapsed time, and the comparison of the relevant factors (10%(w/w) uncharged particles)
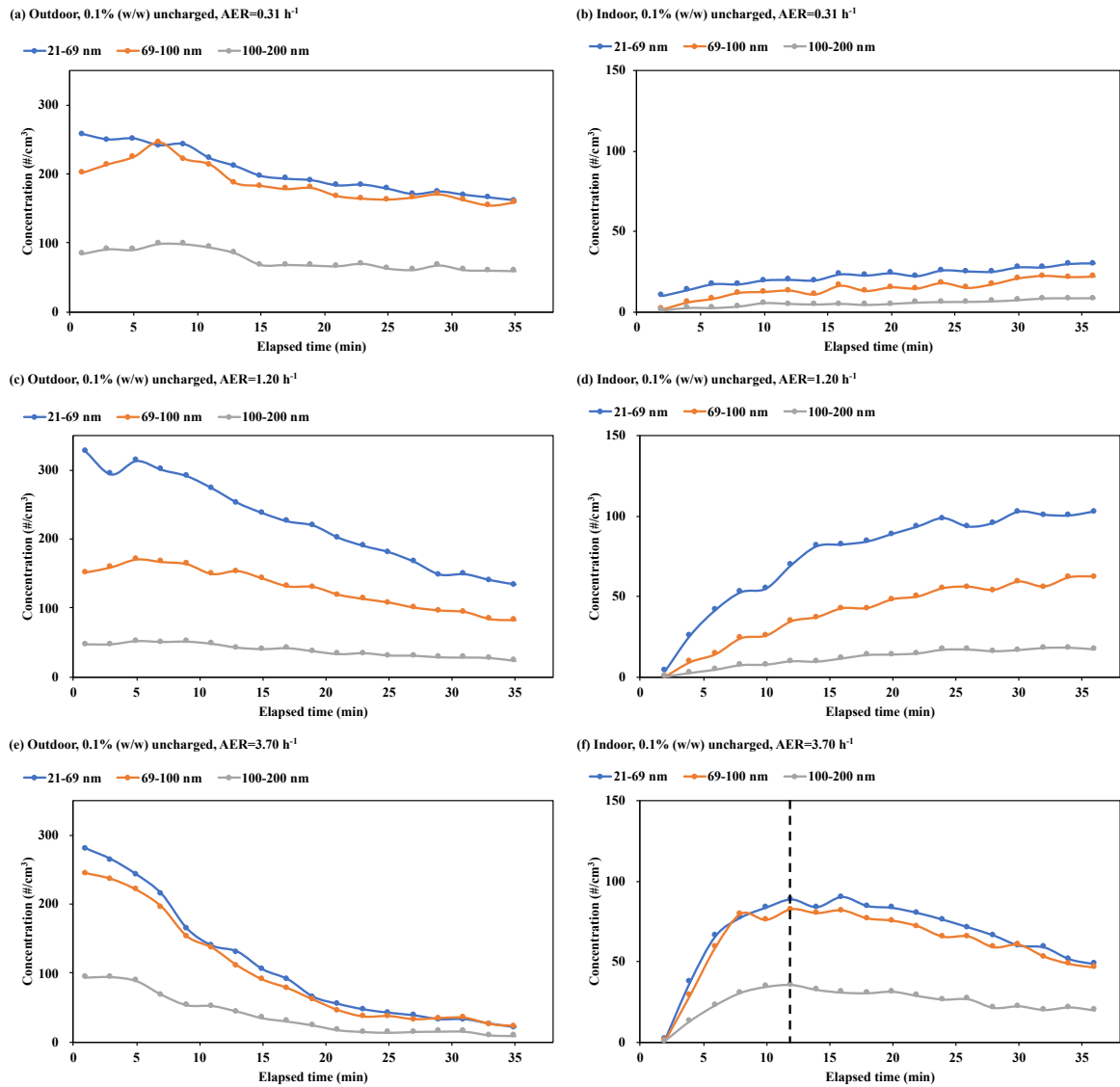
Fig. A.3 Concentration of indoors and outdoors as a function of elapsed time, and the comparison of the relevant factors (0.1%(w/w) uncharged particles)
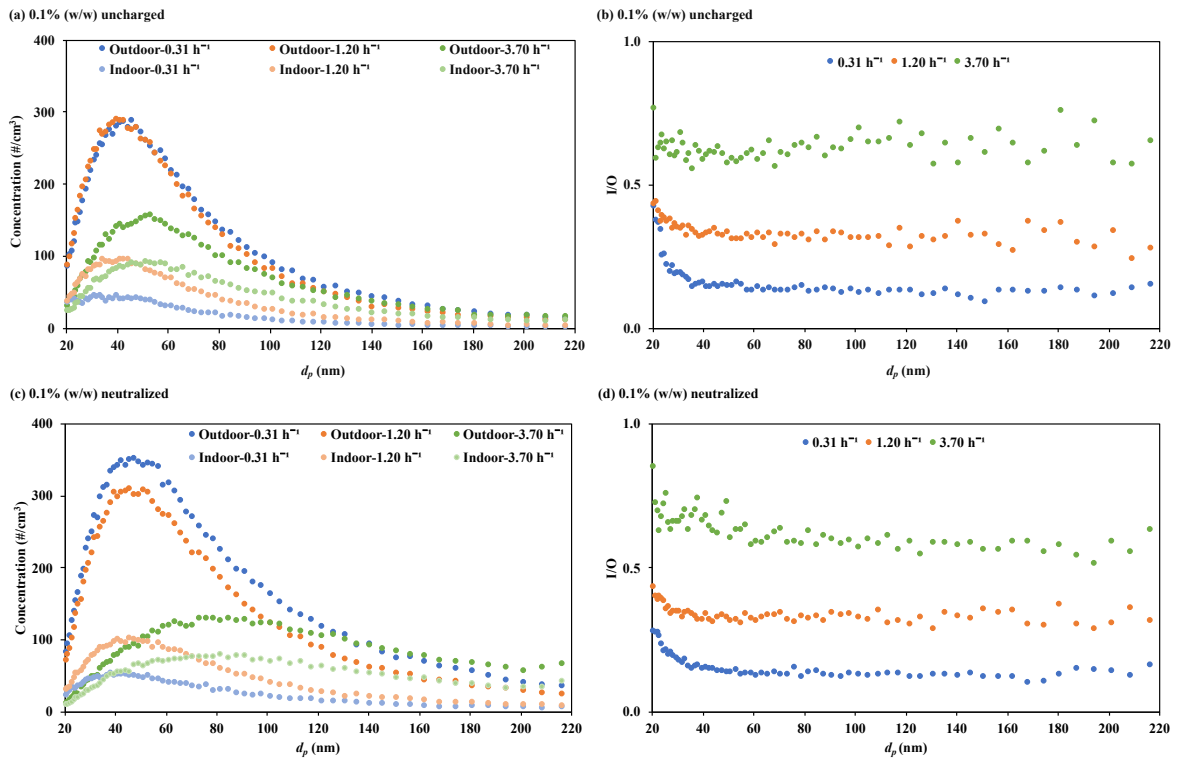
Fig. A.4 Experimental data size distribution of particle number concentration (indoor and outdoor compartments) and I/O ratios with the comparison of the relevant factors (0.1%(w/w) solution)

Appendix 2

Calculation of the deposition rate in a laminar flow

The formula describing β in a laminar flow due to Brownian motion and gravitational sedimentation was approximated by Okuyama et al. (1986) as

$$\beta = \left(\frac{S_T}{V_T}\right)\left(\frac{D}{\delta}\right) + \frac{u_t}{H}$$

Where, δ, the boundary layer thickness, is given as $\delta = 2.884 D^{\frac{1}{3}}$ cm

D, Brownian diffusion coefficient, $D = \frac{C_m \kappa T}{3\pi\mu d_p}$ cm^2/s

u_t, Gravitational settling velocity, $u_t = \frac{C_m(\rho_p - \rho_f)d_p^2 g}{18\mu}$ cm/s

With C_m, Slip correction factor, $C_m = 1 + K_n\left[A + Bexp(-\frac{C}{K_n})\right]$

With K_n, Knudsen number, $K_n = \frac{2\lambda}{d_p}$

λ= 67.3 nm, the mean free path of gas molecules

A=1.165, B=0.483, C=0.997 [1]
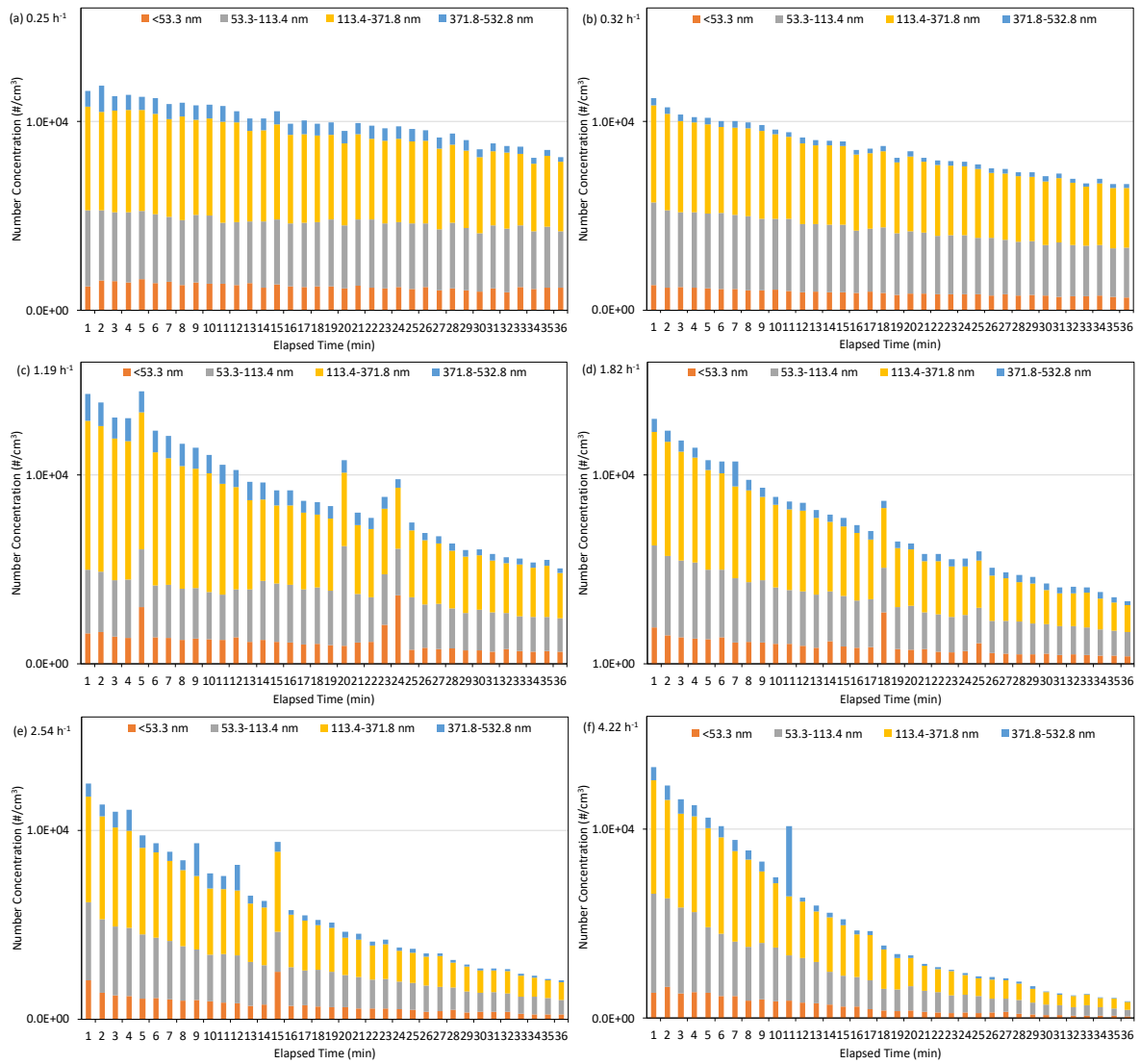
Fig. A.₁ Contribution of segment concentration values under different ventilation conditions

Table A.1

Contribution ratio of the ventilation and deposition in the decay rate

d_p Segment (nm)	AER portion	Deposition portion
<53.3	0.42	0.58
	0.33	0.67
	0.76	0.24
	0.82	0.18
	0.86	0.14
	0.93	0.07
53.3-113.4	1.00	0.00
	0.38	0.62
	1.00	0.00
	0.92	0.08
	0.94	0.06
	0.98	0.02
113.4-371.8	0.35	0.65
	0.38	0.62
	0.57	0.43
	0.76	0.24
	0.78	0.22
	0.93	0.07
371.8-532.8	0.15	0.85
	0.38	0.62
	0.40	0.60
	1.00	0.00
	0.57	0.43
	0.78	0.22

Table A.₂

t-Test results of the difference on the theoretical calculation for different K_e values in a turbulent flow

K_e	Paired-Group Name	Laminar Eq.(5)&Eq.(6)	Laminar Eq.(5)&Eq.(7)	Eq.(5)&Eq.(6) Eq.(5)&Eq.(7)
0.01	Correlation coefficient	0.994	0.992	0.990
	p	2.5E-96	5.8E-91	1.5E-85
1.19	Correlation coefficient	0.964	0.953	0.995
	p	8.3E-59	3.1E-53	4.1E-103
5	Correlation Coefficient	0.952	0.933	0.995
	p	6.5E-53	1.2E-45	7.7E-101
10	Correlation Coefficient	0.949	0.926	0.995
	p	3.1E-51	1.4E-43	9.3E-100
20	Correlation Coefficient	0.945	0.920	0.995
	p	5.0E-50	4.2E-42	7.1E-99
50	Correlation Coefficient	0.943	0.915	0.994
	p	6.1E-49	9.0E-41	5.3E-98
100	Correlation Coefficient	0.941	0.912	0.994
	p	2.1E-48	4.1E-40	1.5E-97
200	Correlation Coefficient	0.940	0.910	0.994
	p	5.0E-48	1.2E-39	3.3E-97
500	Correlation Coefficient	0.939	0.908	0.994
	p	1.0E-47	2.8E-39	6.3E-97
1000	Correlation Coefficient	0.939	0.908	0.994
	p	1.4E-47	4.1E-39	8.4E-97

Significant differences ($p<0.05$, paired-groups t-test) were observed between the two groups.

Appendix 3

Abbreviations in Chapter 3 and Chapter 4

P, Penetration factor; a, Air exchange rate (AER), h^{-1}; $\Delta C_{(CO2)}$, CO_2 concentration difference over time, ppm; t, Time, min or s; T, Temperature, K; k, Deposition rate constant, h^{-1}; λ, Exponential decay rate of particles, min^{-1} or h^{-1}; $C(0)$, Initial concentration of indoor particles at the start of the measurement, $particles/cm^3$ or $\#/cm^3$; $C(t)$, Indoor concentration of particles at time t, $particles/cm^3$ or $\#/cm^3$; C_{in}, Indoor particle number concentration, $particles/cm^3$ or $\#/cm^3$; C_{out}, Outdoor particle number concentration, $particles/cm^3$ or $\#/cm^3$; d_p, Diameter or particle size, nm; S_T, Total inner surface area of the chamber, cm^2; V_T, Volume of the chamber, cm^3; u_t, Gravitational settling velocity, $cm \cdot s^{-1}$; C_{max}, Maximum concentration, $particles/cm^3$ or $\#/cm^3$; C_{min}, Minimum concentration, $particles/cm^3$ or $\#/cm^3$; H, Height of the chamber, cm; δ, Boundary layer thickness, cm; g, Acceleration of gravity, cm/s^2; D, Brownian diffusion coefficient, $cm^2 \cdot s^{-1}$; μ, Viscosity of gas, $g/cm \cdot s$; k, Boltzmann's constant, dyne.cm/K; C_c, Cunningham correction factor; ρ_p, Particle density, g/cm^3; ρ_f, Gas density, g/cm^3; K_n, Knudsen number; λ_m, Mean free path of gas molecules, cm; w/w, Ratio of the mass concentration; n, Number of samples; UFPs, Ultrafine particles; FPs, Fine particles.

Abbreviations in Chapter 6

β, deposition rate, h^{-1}; AER or a, air exchange rate, h^{-1}; S_T, the total inner surface area, cm^2; d_p, Diameter or particle size, nm; H, chamber height, cm; , gravitational settling velocity, cm/s; ρ_p, particle density, g/cm^3; ρ_f, density of gas, g/cm^3; δ, boundary layer thickness, cm; D, Brownian diffusion coefficient, cm^2/s; g, acceleration of gravity, cm/s^2; k, Boltzmann's constant, dyne.cm/K; μ, viscosity of gas, $g/cm \cdot s$; T, temperature, K; C_m, slip correction factor; K_n, Knudsen number; λ, mean free path of gas molecules, nm; A, B, C, constant; K_e, turbulent intensity parameter, s^{-1}.

Acknowledgement

List of Publications

1. W. Wang, N. Kato, S. Kimoto, Y. Matsui, M. Yoneda, Simulation and evaluation of sheltering efficiency of houses equipped with ventilation systems, Build Environ. 168 (2020) 106491.
   DOI: 10.1016/j.buildenv.2019.106491

2. W. Wang, S. Kimoto, N. Kato, N. T. Thuong, Y. Matsui, M. Yoneda. Assessment of air purification effect in sheltering houses equipped with ventilation systems after air pollution incidents. Build Environ. 172 (2020) 106701.
   DOI: 10.1016/j.buildenv.2020.106701

3. W. Wang, M. Yoneda. Determination of the Optimal Penetration Factor for Evaluating the Invasion Process of Aerosols from a Confined Source Space to an Uncontaminated Area, Sci Total Environ. 740 (2020) 140113.
   DOI: 10.1016/j.scitotenv.2020.140113